Max-Planck-Institut
für Meteorologie

MAX-PLANCK-GESELLSCHAFT

International Max Planck Research School
on Earth System Modelling

Integrated Assessment of Climate Tipping Points

Mariia Belaia

Hamburg 2017

Berichte zur Erdsystemforschung
Reports on Earth System Science

192
2017

Hinweis

Die Berichte zur Erdsystemforschung werden vom Max-Planck-Institut für Meteorologie in Hamburg in unregelmäßiger Abfolge herausgegeben.

Sie enthalten wissenschaftliche und technische Beiträge, inklusive Dissertationen.

Die Beiträge geben nicht notwendigerweise die Auffassung des Instituts wieder.

Die "Berichte zur Erdsystemforschung" führen die vorherigen Reihen "Reports" und "Examensarbeiten" weiter.

Notice

The Reports on Earth System Science are published by the Max Planck Institute for Meteorology in Hamburg. They appear in irregular intervals.

They contain scientific and technical contributions, including Ph. D. theses.

The Reports do not necessarily reflect the opinion of the Institute.

The "Reports on Earth System Science" continue the former "Reports" and "Examensarbeiten" of the Max Planck Institute.

Anschrift / Address

Max-Planck-Institut für Meteorologie
Bundesstrasse 53
20146 Hamburg
Deutschland

Tel./Phone: +49 (0)40 4 11 73 - 0
Fax: +49 (0)40 4 11 73 - 298

name.surname@mpimet.mpg.de
www.mpimet.mpg.de

Layout

Bettina Diallo and Norbert P. Noreiks
Communication

Copyright

Integrated Assessment of Climate Tipping Points

Dissertation zur Erlangung des akademischen Grades
Doktor der Wirtschafts- und Sozialwissenschaften (Dr. rer. pol.)
des Fachbereichs Wirtschaftswissenschaften
der Universität Hamburg

submitted by

Mariia Belaia
aus Petrozawodsk

Hamburg 2017

Mariia Belaia

Max-Planck-Institut für Meteorologie
The International Max Planck Research School on Earth System Modelling
(IMPRS-ESM)
Bundesstrasse 53
20146 Hamburg

Universität Hamburg
Fakultät für Wirtschafts- und Sozialwissenschaften
Fachbereich Volkswirtschaftslehre
Makroökonomie und Quantitative Wirtschaftspolitik
Von-Melle-Park 5
20146 Hamburg

Tag der Disputation: 09.05.2017

Folgende Gutachter empfehlen die Annahme der Dissertation:

Prof. Dr. Michael Funke
Prof. Dr. Uwe Schneider

Berichte zur Erdsystemforschung / Max-Planck-Institut für Meteorologie 192
Reports on Earth System Science / Max Planck Institute for Meteorology 2017

ISSN 1614-1199

Summary

Earth's climate is changing, threatening the welfare of humankind. The extent of future changes will depend on the implemented climate policy. Therefore, climate policy has a key role in discussions of sustainable development, which is defined as the *development that meets the needs of the present without compromising the ability of future generations to meet their own needs.* What is the optimal climate policy response to achieve this balance? The first step to address this question, from an economics perspective, is to recognize that climate change is a global externality, characterized by a long-term timescale and large uncertainties. The first attempt to internalize the greenhouse gas externality was conducted by William Nordhaus in 1991, followed by the development of the dynamic integrated model of climate and the economy (DICE). The DICE model belongs to a class of an integrated assessment models (IAM), which are designed to explore synergies and trade-offs between economic growth and climate change. However, it is important to acknowledge the limitations of existing IAMs. Even the most advanced IAMs have difficulties in dealing with the roles of governance, culture, the heterogeneity and non-linearity of human and natural systems. In particular, DICE and its regional version, RICE, model the economic impacts of climate change as smooth, gradual reductions in economic output as temperature increases.

The objective of this thesis is to improve our understanding of the economic consequences of anthropogenic-induced climate change and to derive associated policy implications. I emphasize that changes in the climate system under anthropogenic forcing need not be smooth and gradual. For example, a small increase in the temperature may trigger breakdown of the Atlantic thermohaline circulation (THC) and a small increase in aerosol concentration over Indian peninsula may weaken the ISM circulation. The two systems, THC and ISM, share one common feature: a small change implies a big difference. This characteristic is described by the term *tipping point* – the critical point at which a transition to a different state of the system is triggered. In the present thesis, using DICE and RICE as a starting point, I explore the policy implications of the economic risks related to the THC and ISM.

Thermohaline circulation is a part of ocean circulation that is driven by density gradients, which depends on water temperature (hence, "'thermo") and salinity (hence, "haline"). The THC plays an important role in transporting heat to the polar regions. In particular, THC is the primary reason that Western Europe is so temperate. The breakdown of the THC under global warming is a low-probability high-impact risk. The associated impacts include: (i) sea level rise of about 1 m in parts of the North Atlantic, including about 0.5 m along the Atlantic coasts of North America and Europe; (ii) changes in the tropical precipitation pattern; and (iii) declining phytoplankton population. Chapter 1 finds that discounting and negligence of the inertia in climate and the economic systems limit the possibility to account for the risk of the THC breakdown. Therefore, the derived climate policies should be interpreted accordingly.

The monsoons are large-scale seasonal winds, which are driven by the temperature difference betwen the land and ocean. The ISM affects the Indian subcontinent, bringing moist air towards land. In fact, it accounts for 80% per cent of annual rainfall. The ISM system exists at a global-regional policy nexus: both India's and global climate policy alter the system. Projected changes in the ISM rainfall under anthropogenic interference are of particular concern for India as its economy is closely tied to the ISM-rainfall strength. Chapter 2 explores the ability of India to limit an increase in the frequency of ISM-rainfall extremes through mitigation. The integrated assessment modelling exercise indicates that global efforts on combatting climate change slightly reduce the ISM rainfall –related risk relative to the business-as-usual policy. Yet, an increased frequency and intensity of extreme ISM rainfall in the future is inevitable as more stringent policies, which could reduce the risk of ISM rainfall extremes even further, do not pass the cost-benefit test in many regions. Hence, India's particular interest in reaching a climate policy agreement and the importance of domestic adaptation to ISM-rainfall extremes. This result motivates the next question – what is the optimal adaptation-mitigation mix for India? Chapter 3 addresses this question. I find that the optimal policy mix includes both mitigation and adaptation efforts. However, adaptation plays a greater role in regional welfare. First, benefits are enjoyed locally, irrespectively of the actions of other countries. Second, adaptation allows for stronger mitigation efforts due to greater economic output available for investment.

Overall, by providing a detailed view of the impacts related to selected tipping elements in the Earth's system, this thesis serves as further reminder of the existing interplay between system complexity and model simplicity, and between realism and understanding.

Zusammenfassung

Das Klima der Erde verändert sich und bedroht das langfristige Wohlergehen der Menschheit. Das Ausmaß der künftigen Veränderungen hängt von der umgesetzten Klimapolitik ab. Deshalb spielt die Klimapolitik für eine nachhaltige wirtschaftliche Entwicklung eine zentrale und wichtige Rolle. Die Herausforderung besteht dabei darin, *aktuelle Herausforderungen und Probleme so zu bewältigen, dass künftige Generationen keine Nachteile erleiden*. Wie muss eine Klimapolitik ausgestaltet sein, die diesen Anspruch erfüllt? Der erste Schritt, um diese Frage aus ökonomischer Perspektive zu beantworten, besteht in der Erkenntnis, dass der erwartete Klimawandel ein globales Phänomen ist, welches aufgrund der sehr langen Zeiträume durch eine erhebliche Prognoseunsicherheit charakterisiert ist.

Der erste Versuch, die Treibhausgas-Externalität zu internalisieren, wurde von William Nordhaus im Jahre 1991 durchgeführt. Dies führte zur Entwicklung des „Dynamic Integrated Climate-Economy“ (DICE) Modells, welches das Klimasystem, die wirtschaftliche Entwicklung sowie deren wechselseitige Abhängigkeit modelliert. Im DICE-Modell wird die wirtschaftliche Entwicklung vom Bevölkerungswachstum, der Kapitalakkumulation und dem exogen technischen Fortschritt getrieben. Ferner wird die wirtschaftliche Entwicklung vom Klimawandel und der Klimapolitik beeinflusst. Das Klimasystem wird mittels des CO2-Kreislaufs beschrieben, während die Kosten von Klimaschäden als fiktive Reduktion der Produktion dargestellt werden. Wie in ökonomischen Modellen üblich, werden rational handelnde Akteure unterstellt, die eine intertemporale Wohlfahrtsfunktion maximieren. Eine Weiterentwicklung des DICE-Modells ist das „Regional Integrated Climate-Economy (RICE) Modell, in dem eine Aufgliederung des aggregierten Modells in einzelne Weltregionen erfolgt.

Das Ziel dieser Dissertation ist, unser Verständnis der Konsequenzen des anthropogen-induzierten Klimawandels unter besonderer Berücksichtigung von sogenannten „tipping points“ zu verbessern, an denen das Klima schlagartig umschlagen kann. Die beiden betrachteten Problemzonen des globalen Klimasystems sind dabei die ozeanische Zirkulation im

Nordatlantik sowie das Indische Monsun-Regime. Die Nordatlantikströmung wird auch als „thermohaline Zirkulation“ (THC) bezeichnet. Der Motor der THC ist das Absinken von kaltem und salzreichem Wasser im Nordatlantik. Im Atlantik strömt warmes und salzreiches Oberflächenwasser über den Äquator und den Golf von Mexiko bis in das Gebiet zwischen Grönland, Island und Norwegen. Diese als Golfstrom bekannte Meeresströmung transportiert enorme Energiemengen, die zu einem großen Teil an die Atmosphäre abgegeben werden. Dadurch wird das außerordentlich milde Klima in nordöstlichen Nordwesteuropa erzeugt. Das indische Monsun-Regime besteht aus einem System von jahreszeitlich wechselnden Winden. Der Grund ist die unterschiedlich starke Aufheizung von großen Land- und Meeresflächen. Der Indische Sommermonsun ist eine Zirkulation mit Südwestwinden in Bodennähe, die durch die starke Aufheizung des Kontinents in den Sommermonaten entsteht. Der vom Meer über das Land wehende Sommermonsun nimmt über dem Indischen Ozean viel Feuchtigkeit auf und bringt hohe Niederschläge mit sich. Vom Einsetzen des Sommermonsuns, seiner Dauer und der Niederschlagsverteilung hängen vor allem die landwirtschaftliche Erträge Indiens ab. Ein schwacher Sommermonsun ist häufig mit Dürren verbunden. Stärkere Monsunniederschläge als gewöhnlich können umgekehrt zu Überschwemmungen führen. Die Frage ist nun, wie sich die Klimaerwärmung auf das Indische Monsunregime auswirkt und ob ein „tipping point“ mit solchen verstärkten Extremwetterlagen auftreten kann. In den vorliegenden drei Papieren der Dissertation wird – der DICE- bzw. RICE-Modellierungstradition folgend - die Wechselwirkung von ökonomischen Entscheidungen und zukünftigenr Klimaveränderung an diesen beiden „Klima-Hotspots“ untersucht. Dabei werden jeweils ökonomische und physikalische Modelle gekoppelt.

Insgesamt liefern die modelltheoretischen Betrachtungen der beiden ausgewählten Kippelemente im Erdsystem ein vertieftes Verständnis des sehr komplexen Zusammenspiels von naturwissenschaftlichen und ökonomischen Modellbausteinen sowie daraus abgeleiteten Politikempfehlungen.

Table of contents

List of figures

List of tables

Introduction

The overwhelming quantity of independent scientific evidence points to the existence of human-made climate change. After UN General Assembly [9], the term climate change refers to "a change of climate which is attributed directly or indirectly to human activity that alters the composition of the global atmosphere and which is in addition to natural climate variability observed over comparable time periods". This definition is deliberately broad and inclusive. Among the already detected changes are (i) surface and ocean temperature change; (ii) sea level rise; (iii) ocean acidification; (iv) precipitation pattern; (v) sea pressure pattern; (vi) increased frequency of the most intense tropical cyclones; and (vii) reduction in Nothern Hemisphere sea ice extent (Bindoff et al. [1]).

Climate change is a truly global issue, with impacts experienced by economies worldwide. The United Nations Development Programme (UNDP) has estimated that economic losses exceed 125 billion USD per year and growth rates of global GDP have been reduced by 0.23 percent due to already occurring changes (Global Humanitarian Forum [2]). These impacts are determined by both the levels of the climate-related changes and the vulnerability to these changes. Hence, two general forms of response are identified – mitigation and adaptation. Yet, there is no consensus on what is the optimal policy response.

Over the past few decades, Integrated assessment models (IAM) have emerged as a widely used tool to analyse alternative climate change policies. IAMs offer a unique perspective on both scientific and socioeconomic aspects of climate change, reflecting the inter-relations over space and time of how economic activity alters the environment, and how the environment, in turn, feeds back onto the economy. There are over 20 IAMs, which vary widely in several key aspects: (i) degree of focus on economic issues vis-à-vis climate processes; (ii) geographic scope, (iii) sectoral coverage, etc. IAMs are categorized into two broad classes: policy evaluation and policy optimization (Weyant [11]). Policy-evaluation models explore changes in climate and economic systems under pre-specified policy options. Policy-optimization models determine optimal policy either by weighing costs and benefits or by minimising the

costs of achieving a specified goal. The present dissertation follows the latter approach.

To date, some studies have argued for gradual emissions reductions (e.g. Nordhaus and Yang [7], Tol [8]), while others have called for more drastic near-term mitigation efforts (Moore and Diaz [5]). One of the key reasons for the disagreements is the presence of deep uncertainties about the economic impacts of climate change. Specifically, the current literature offers little empirical evidence on what a climate change damage function should look like. Therefore, the results of cost-benefit analysis, which rely upon assumptions about the welfare impacts of increased temperatures, can differ greatly and are often met with strong criticism (e.g. Weitzman [10]). In particular, the highly aggregated damage functions in IAMs, such as DICE, fail to reflect that changes related to global warming are likely to be abrupt and unpredictable. As such, they neglect the possibility of reaching tipping points – abrupt and, in some cases, even irreversible transitions in the state of major components of the Earth.

Lenton et al. [4] identified a set of tipping elements in the Earth's climate system, which are parts of climate system that may pass an element-specific tipping point. The tipping elements include: Arctic summer sea-ice, Greenland ice sheet, west Antarctic ice sheet, Atlantic thermohaline circulation (THC), El Nino-Southern Oscillation (ENSO), Indian summer monsoon (ISM), Sahara/Sahel and West African monsoon, Amazon rainforest, and boreal forest. They differ according to control parameters and critical values, the level of warming that induces changes and transition timescale, as well as the resulting climate impacts. Understanding the economic risk from, and thus the optimal policy response to climate change would ideally include a thorough assessment of each tipping element with respect to: (i) climate impacts and associated economic damages followed by tipping; (ii) regions affected; (iii) reversability of the tipping; and (iv) uncertainties in both economic and climate systems evolution.

The present thesis introduces two tipping elements, THC and ISM, into a policy-optimization analysis using a well-known IAM, the DICE model by Nordhaus [6]. It investigates the policy implications of including the risk of possible economic impacts from crossing these thresholds in such an analysis. Chapter 1 focuses on the risks related to the THC breakdown. Chapter 2 elaborates on the risk of increased frequency of ISM-rainfall extremes under anthropogenic interference, focusing on the role of international cooperation in mitigating climate change. Chapter 3 evaluates India's alternative policy responses – mitigation and adaptation – to the increased frequency of the ISM-rainfall extremes.

Thesis Outline

The breakdown of the THC under global warming is referred to as a low-probability high-impact risk. The non-linear behaviour of the THC suggests the existence of multiple equilibria and thresholds. Once the circulation breaks down, the associated damage costs may be locked in for dozens of years to come. The first chapter of the thesis examines how well IAMs address this particular risk. For this, the DICE model by Nordhaus [6] is fully coupled to the simple conceptual model of the THC. Further, the Epstein-Zin utility specification is used to disentangle the coefficient of risk aversion from the time preferences, allowing to demonstrate the insensitivity of the near-term climate policy to the risk aversion of a decision maker. The critical aspects of IAMs, such as DICE, which limit the success of addressing this risk, include: (i) discounting excludes long-term risks from welfare calculation, (ii) the presence of exogenous technological development provokes delaying an action, and (iii) disregarding socio-economic and technological inertia allows for a sudden increase in emissions control in future. The bottom line is that low-probability high-impact nonlinear risks in a distant future are currently underrepresented in climate policy. This Chapter is written in cooperation with Michael Funke and Nicole Glanemann.

Chapter 2 deals with the threat of an increased frequency of extreme ISM-rainfall events – extensive droughts and floods – under global warming and local aerosol pollution. While the ISM rainfall is a crucial factor for India's economic welfare, its future changes are dependent upon both regional and global policy. This puts forward a question as to whether India can prevent a projected increase in summer monsoon extremes. To tackle the question, a fully coupled regional IAM is developed. The model extends the IAM by Ikefuji et al. [3], which is based on the RICE model by Nordhaus and Yang [7], by explicitly representing inter-annual ISM rainfall variability and accounting for drought- and flood-related damage costs for India's economy. The two scenarios are contrasted: cooperative, where Negishi-weighted welfare is maximized, and non-cooperative, which is modelled through an open-loop Nash equilibirum. Overall, the study finds significant evidence in favour of stringent environmental policy in India. Yet, even joint global efforts may not be sufficient to fully eliminate the risk of increased extremes as: (i) changes may already be locked in due to inertia in climate and socio-economic systems, and (ii) the discrepancy in costs and benefits among regions give rise to a conflict of interests. This Chapter is written in cooperation with Nicole Glanemann.

Chapter 3 elaborates on the relative importance of investments in adaptation and mitigation in view of the risk of increased frequency of ISM-rainfall extremes. This study provides a long-term context to decisions regarding India's mitigation and adaptation efforts. In

line with current literature, I find that the optimal policy mix includes both mitigation and adaptation efforts. Also, I stress the particular importance of adaptation for regional welfare. First, the effectiveness of mitigation is limited by the efforts of the rest of the world and thereby some of the impacts are locked-in. Second, the benefits from adaptation are enjoyed locally, irrespective of the actions of the other countries. Third, adaptation allows for stronger mitigation efforts due to greater output available for investments.

Publications

Chapter 1 was submitted individually to a journal. The final version is available at Springer:

Mariia Belaia, Michael Funke and Nicole Glanemann (2017). Global Warming and a Potential Tipping Point in the Atlantic Thermohaline Circulation: The Role of Risk Aversion. Environmental and Resource Economics, 67 (1), pp.93-125; http://dx.doi.org/10.1007/s10640-015-9978-x.

References

[1] Bindoff, N., Stott, P., Achuta-Rao, K., M.R., A., Gillett, N., Gutzler, D., Hansingo, K., Hegerl, G., Hu, Y., S., J., Mokhov, I., Overland, J., Perlwitz, J., Sebbari, R., Zhang, X., 2013. Detection and attribution of climate change: from global to regional. In: Climate Change 2013: The Physical Science Basis. Contribution of Working Group I to the Fifth Assessment Report of the Intergovernmental Panel on Climate Change. Cambridge University Press, Cambridge, United Kingdom and New York, NY, USA.

[2] Global Humanitarian Forum (Ed.), 2009. Human Impact Report: Climate Change - The Anatomy of a Silent Crisis.

[3] Ikefuji, M., Magnus, J. R., Sakamoto, H., 2014. The effect of health benefits on climate change mitigation policies. Climatic Change 126 (1-2), pp 229-243.

[4] Lenton, T., Held, H., Kriegler, E., Hall, J. W., Lucht, W., Rahmstorf, S., Schellnhuber, H. J., 2008. Tipping elements in the earth's climate system. Proceedings of the National Academy of Sciences 105 (6), pp 1786–1793.

[5] Moore, F. C., Diaz, D. B., Feb. 2015. Temperature impacts on economic growth warrant stringent mitigation policy. Nature Clim. Change 5 (2), pp 127–131.

[6] Nordhaus, W. D., Boyer, J., 2000. Warming the World: Economic Models of Global Warming. MIT Press, Cambridge Mass.

[7] Nordhaus, W. D., Yang, Z., 1996. A regional dynamic general-equilibrium model of alternative climate-change strategies. The American Economic Review 86 (4), pp 741–765.

[8] Tol, R. S., 2013. Targets for global climate policy: An overview. Journal of Economic Dynamics and Control 37 (5), pp 911–928.

[9] UN General Assembly, 1992. United nations framework convention on climate change: resolution / adopted by the general assembly.

[10] Weitzman, M., 2010. What is the "damages function" for global warming – and what difference might it make? Climate Change Economics.

[11] Weyant, J. e. a., 1996. Climate Change 1995: Economic and Social Dimensions of Climate Change: Contribution of Working Group III to the Second Assessment Report of the Intergovernmental Panel on Climate Change. Cambridge University Press, Cambridge, UK, Ch. Integrated Assessment of Climate Change: An Overview and Comparison of Approaches and Results., pp. 367–398.

Chapter 1

Global Warming and a Potential Tipping Point in the Atlantic Thermohaline Circulation: The Role of Risk Aversion

1.1 Introduction

A stable climate system in the future is a valuable international public good. Like a stable world financial system, its benefits are largely taken for granted until they are lost. National authorities and international institutions are the guardians of this public good. Their responsibility is to implement climate policies that preserve it. The possibility of large-scale climate risk in the distant future poses a particular challenge to climate policy assessment. In this respect, special attention is paid to tipping points, which define abrupt and in some cases even irreversible transitions in the state of a major component of the Earth (Lenton et.al. [45]). An example of a tipping element is the Atlantic thermohaline circulation (THC), which is responsible for about one-third of the global northward heat transport and thus an important guarantor of the heat supply in the North Atlantic region (Ganachaud and Wunsch [19] and Trenberth and Caron [75]). According to the IPCC [28], the ongoing warming of the Atlantic is very likely to lead to a slowdown in the THC during the 21st century, which raises concerns about a shutdown of the heat supply in the next century.[1] Actions over a long

[1]Long-run predictions about the THC, however, involve tremendous uncertainties and the estimates of future circulation strength are therefore somewhat speculative (Matei et al. [51]). As reviewed by Lenton and Ciscar [44], the expert elicitation study by Kriegler et al. [39] and the IPCC [28] suggest that rather high temperatures (>4 °C) are needed to push the THC towards collapse. However, these models are criticised for being biased towards the stability of the THC dynamics (Drijfhout et al. [15] and Hofmann and Rahmstorf [26]) and observations indicate a higher vulnerability of the THC (Drijfhout et al. [15] and Hawkins et al. [25]). A recent probabilistic assessment of different representative concentration pathways (RCPs) by Schleussner et al.

period of time thus affect the likelihood of such a tipping point happening. Consequently, climate policy assessment must be equipped with methods that adequately treat such long periods of time and the involved risks.

Lately, most of the integrated assessment models (IAMs) used for climate policy recommendations have faced increasing criticism that they appear greatly to underestimate these risks (e.g. Stern [69]). The main arguments put forward are, inter alia, that they do not encompass sufficient modelling of the ubiquitous uncertainties involved (e.g. Pindyck [62]), that the risks of climate catastrophes are not satisfactorily accounted for (e.g. Lenton and Ciscar [44]), and that the climate damage functions are not reconcilable with current research on the impacts of climate change (e.g. Ackerman et al. [2] and Kopp et al. [37]). Another main point of criticism is that the assumptions implicitly made by the commonly used concept of intertemporally additive expected utility, such as the constant relative risk aversion utility function (CRRA), provide a contorted representation of a decision maker's preferences. More precisely, the coefficient of relative risk aversion and the inverse of the elasticity of intertemporal substitution are merged as one parameter. An increase in this parameter could be attributed to a change in the preference of the time and interpreted as greater aversion to a transfer of wealth from the present to the future. As a result, the social discount rate also increases and policy is less concerned about climate change. The bias of the concept, however, is caused when the decision maker becomes more risk averse. Then the coefficient also increases, which, as already argued, leads to less abatement. Accordingly, the application of such a utility concept leads to counterintuitive results concerning the role of risk and risk aversion. By utilising a more realistic preference specification, this paper aims to reexamine the optimal policy response to risk, in particular to the risk of a THC collapse, and investigates the role of risk aversion in the stringency of the optimal policy response.

The limitations of the parsimonious and easily tractable intertemporally additive expected utility functions were first identified in finance by demonstrating the 'equity premium puzzle' (Mehra and Prescott [55]). This puzzle illustrates the difficulties in explaining why the rates on return are rather high in terms of equity and rather low in relation to risk-free assets. Although it has not been possible to resolve this problem so far, possible explanations for this puzzle could be provided and it has resulted in some fundamental concepts being questioned.[2] An intuitively appealing approach is pursued by the 'generalized expected utility' concept proposed by Epstein and Zin [17, 18], and Kreps and Porteus [38], which

[67] shows that a significant slowdown of the THC is within the likely range, in particular for the unmitigated climate change scenario.

[2] For a recent survey see DeLong and Magin [12].

allows a separate preference specification for risk and time in a recursive utility model. Since then, the Epstein-Zin preferences have gained in importance and found many applications. It is not the goal of this paper to give a literature review of these applications, but some striking examples of the contribution of this concept should be mentioned. For instance, the Epstein-Zin preferences are found to illuminate many patterns of asset pricing, especially in the case of long-term risk (e.g. Bansal and Yaron [4]). An important contribution to macroeconomics is exemplified by Tallarini [72], showing that the Epstein-Zin preferences significantly increase the welfare costs of the business cycle by providing refined model predictions for the asset market.

In climate economics, most of the IAMs, such as the famous DICE [58], FUND [74] and PAGE [27], rely on the CRRA utility specification. The equivalent of the equity premium puzzle given by a 'negative risk premium on high climate change outcomes' (Nordhaus [58]) in DICE is attributed to the preference specification and to the absence of fat-tailed uncertainty about climate catastrophes in the model (Kaufman [31]).[3] Recent advances in accounting for Epstein-Zin preferences and for fat-tailed risk indicate a significant understatement of the optimal emission reduction rates in DICE (e.g. Ackerman et al. [3], Cai et al. [8], Crost and Traeger [11], Jensen and Traeger [30], Kaufman [31], Lemoine and Traeger [42]). Of particular importance to this paper is the study by Ackerman et al. [3]. Ackerman et al. [3] report the results generated by their 'EZ-DICE' model to be rather insensitive to risk aversion and only to show meaningful effects owing to the intertemporal elasticity of substitution. Ackerman et al. [3] capture climate risk by accounting for a fat-tailed climate sensitivity distribution, where the decision maker knows that the true climate sensitivity value will be disclosed in the year 2075. At this point in time, however, DICE allows for jumping to 100% abatement at a relatively low cost, which can completely prevent temperatures from escalating. Consequently, irrespective of the level of risk aversion, it is always beneficial to respond to the risk only after the true state of nature is revealed and then to act accordingly. A more realistic modelling of the abatement options and of the climate risks is surmised to provide a stronger risk aversion effect (Ackerman et al. [3]). A strong effect is also supported by the simple, albeit reduced-form, framework in Barro [5]. Our research tackles the question 'Is risk aversion irrelevant to climate policy?' raised by Ackerman et al. [3] and develops an enhanced version of the EZ-DICE model that satisfies these features towards building a more realistic modelling framework.

[3] The benchmark study by Weitzman [81] reveals that, as a result of plausible values of uncertain parameters, the probability of extreme losses is much larger than predicted by, for instance, normal distribution. Particularly, as shown by Urban and Keller [78] for Atlantic meridional overturning circulation, the policy-relevant projections are strongly linked to tail-area parameter estimates.

In our model, uncertainty about climate sensitivity translates into uncertainty about a slow-down of the THC.[4] We consider modelling climate risk in terms of the potential for a THC collapse as particularly interesting because the dynamics involved lag behind the emission of greenhouse gases by several decades and also, as mentioned above, because it exhibits an abrupt transition to a complete shut-down. Accordingly, once the true climate sensitivity value is identified, it may be too late to prevent with certainty the THC from collapsing. Risk aversion may then play a more meaningful role for climate policy.

The literature incorporating a more or less refined representation of the THC dynamics into an IAM is rich and may be categorised according to the representation of oceanographic dynamics. The more refined representations are given by the two-box Stommel model (Stommel [71]) or extensions of the same e.g. the Simple Climate Demonstrator by Schneider and Thompson [68] and a four-box model by Zickfeld et al. [86], in which the heat transport is explicitly given. To our knowledge, none of the IAMs that are coupled with such a box model account for the more realistic Epstein-Zin preferences. However, this strand of research acknowledges the problem of accounting for a risky event in the far future. Mastrandrea and Schneider [50] demonstrate the importance of choosing a more realistic discounting by opting for hyperbolic discounting as otherwise the damages from a THC collapse vanish from today's welfare calculus. To avoid discounting the impacts altogether, other studies (e.g. Zickfeld and Bruckner [83] and Zickfeld and Bruckner [84]) employ cost effectiveness analysis in which only policies that (almost certainly) prevent the THC from collapsing are permitted. At the other end of the spectrum, the idea of simplifying analysis is to ignore transient dynamics and to derive a THC threshold representation on the basis of data from other studies. On the one hand, this approach harbours the potential of neglecting some of the internal feedback processes between the economy and the THC (Mastrandrea and Schneider[33]). On the other hand, it saves significantly on computational costs and thus offers the opportunity to easily expand the model in many ways. One example of such a representation of the threat of a THC collapse is given by hazard rates (e.g. Lontzek et al. [47] and Nal and Oppenheimer [60]). Lontzek et al. [47] calibrate this hazard rate on the basis of elicitation studies by Kriegler et al. [39] and Zickfeld et al. [85]. Following this idea, Cai et al. [8] adopt this simplistic concept to model (unspecified) tipping points and

[4] It must be noted, that while the simplified treatment of uncertainty serves the purpose of our study well, in reality uncertainty about a potential THC collapse is likely not to be resolved even if the climate sensitivity value is perfectly known. In fact, the projections of a THC collapse depend on many more uncertain parameters, some of which are correlated. Accordingly, Urban and Keller [78] propose the concept that breaks important new ground in risk analysis. The authors use the nonparametric Bayesian inversion approach to derive probabilistic projections of a THC collapse by accounting for the tail areas of the parameter probability distributions and for more observational constraints of relevance.

can also account for Epstein-Zin preferences. Again, Epstein-Zin preferences are shown to increase the stringency of optimal climate policy. Another example falling into this category of modelling the THC threshold is derived by Keller et al. [34]. Using ocean model results by Stocker and Schmittner [70], the authors derive a critical value of atmospheric CO_2 concentration beyond which a THC collapse is irreversibly triggered. The clarity of this threshold representation allows investigating complex research questions that address the interaction of the threshold response with multifaceted and deep uncertainty and learning (Hall et al. [24], Keller et al. [32], Lempert et al. [43], McInerney and Keller [53], McInerney et al. [54]). Keller et al. [32] find that parameter uncertainty about the threshold-specific damages and the CO_2 level triggering a threshold may lead to a decrease in near-term abatement. Combining the model by Keller et al. [32] with a stochastic global optimisation algorithm, Lempert et al. [43] explore multiple equilibria generated by different policy paths. The identified equilibria belong to abatement paths that are almost identical for the first hundred years and diverge only later. This result thus suggests that the policy maker is not offered a set of alternative, optimal near-term policy choices. McInerney and Keller [53] revisit the study by Keller et al. [32] by accounting for uncertainty in four parameters crucial to the uncertain system response. They show that an emissions reduction of 25% (relative to the business-as-usual scenario) at the end of the century is optimal. This policy path is, however, not stringent enough to significantly reduce the odds of a THC collapse – only a complete and fast decarbonisation would. Just like our study, Hall et al. [24] and McInerney et al. [54] direct attention to the expected utility maximisation with the CRRA utility function. However, different from our study, they are concerned with the performance of this decision criterion in the face of deep uncertainty because the abatement strategies implied lack robustness. They propose two alternative decision criteria, based on the idea of minimising the worst-case performance while maximising the expected CRRA utility, and prove them to be more robust. Our study is thus not the first to explore solutions to the problems caused by relying on the CRRA utility function in the context of a non-convex optimal growth problem with the THC. Yet, the role of risk aversion has not been addressed in such a setting.

We believe that our research question on the role of risk aversion benefits from the more precise modelling of the THC provided by the box models. Thus, we build a climate model with geophysical microfoundations that then, as an emergent property, exhibits multiple steady states and transition dynamics. As argued above, the explicitly modelled transition dynamics and in particular the characteristic of the THC significantly lagging behind temperature evolution may play an important role in the effects of risk aversion and are thus better modelled by a fully fledged box model.

Coupling an EZ-DICE model with a dynamic THC model expands on previous work not only by exploring the effects of risk aversion on near-term policy. It is also improves on the existing optimal growth literature that incorporates THC box models by drawing on a utility function that provides a clear and disentangled preference specification.

In a nutshell, our model is a fully coupled continuous-time EZ-THC-DICE model. More precisely, it combines the continuous-time DICE version by Cai et al. [6] with the continuous-time four-box THC model by Zickfeld et al. [86]. As in Ackerman et al. [3], the 'Epstein-Zin policy maker' needs to decide on an optimal policy path while facing a fat-tailed probability distribution for the true climate sensitivity parameter. In the interest of comparability we also adopt the assumption that uncertainty is resolved fully in the year 2075 and the policy path can be adjusted. For this specific set-up, we aim to clarify whether the climate policy path until 2075 is significantly affected by the risk of a THC collapse and, more importantly, by the policy maker's attitude towards this risk. A sensitivity analysis will clarify the extent to which the results are affected by the calibration of important, uncertain parameters, e.g. the damage costs caused by the critical weakening of the THC and the year of learning. We also investigate how restrictions on the policy adjustment affect our results. Despite ever advancing technology, ceasing to emit instantaneously might still be impossible in the middle of the second half of the century. Apart from technological limitations, it is also conceivable that policy inertia or inertia in the economic system will slow emission reduction efforts down (Grübler et al. [21], Ha-Duong et al. [22], Lecocq et al. [41], Waisman et al. [80]).

The paper is structured as follows. Section 1.2 elucidates how the two models are coupled and provides detail about new and less well-known parts. Section 1.3 describes the calibration of the model and presents the resulting simulations together with an analysis. Section 1.4 draws conclusions based on the findings.

1.2 The Model

To represent the interaction between the economy, the climate, and the THC, we choose to couple fully a version of the original DICE-2007 model (Nordhaus [58]) and the continuous-time four-box THC model by Zickfeld et al. [86]. To guarantee the consistency of the time steps in the two sub-models, we choose to keep the continuous-time formulation of the THC model and to adopt the continuous-time version of DICE-2007 (DICE-CJL) by Cai

et al. [6].[5] A rough illustration of our model is provided in Figure 1.1, which highlights the changes to DICE-CJL and how the two models are coupled. DICE-CJL in itself links a Ramsey-type optimal growth model of the global economy, which produces emissions, with a simplified climate model, which describes the effect of the emissions on the increase in global mean temperature ΔT. The THC model then takes the global mean temperature increase ΔT as input to generate an assessment concerning the strength of the THC overturning m. This value discloses whether the THC is slowing down or whether it has already collapsed, thus incurring additional climate damage costs. To account for these costs, we develop an alternative formulation for the damage cost function that increases with global warming ΔT and with a lower overturning strength m.

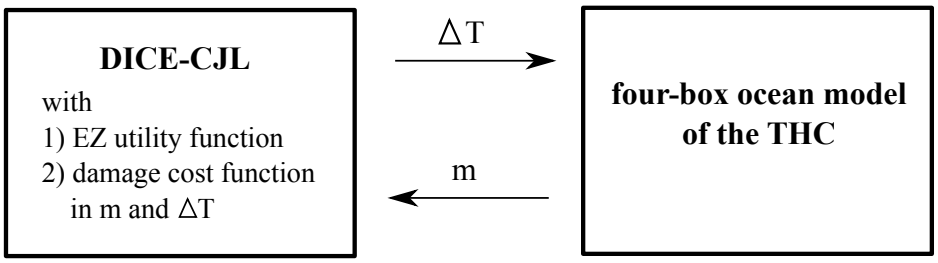

Fig. 1.1 Illustration of the coupling of the modified DICE-CJL (with the EZ utility function and an alternative damage cost function) with the THC model by Zickfeld et al. [86]. The global mean temperature increase ΔT is used as input for the THC model, while the THC model computes the overturning strength m. The new damage cost function comprises the impacts of both ΔT and m

The remainder of this section explains in detail the parts of the model that are new or less well known. As DICE is presumably the most frequently applied IAM in climate economics, we avoid giving a detailed decription of DICE and instead proceed directly to explaining the changes to this model. To ensure clarity, we also point out the most important equations in the THC model.

The first alteration to DICE replaces the commonly used CRRA utility function

$$U(c_t, l_t) = \frac{\left(\frac{c_t}{l_t}\right)^{1-\gamma}}{1-\gamma} l_t, \tag{1.1}$$

[5] The most important modifications to DICE-2007 implemented by Cai et al. [6] involve recalibrations of the parameters owing to the different time units. In addition, the atmospheric temperature response function is adjusted to rule out warming being affected by future atmospheric carbon concentrations. Note that 'continuous' refers to a time-discretization of one-year time steps.

where c_t is the optimised consumption path over time and l_t specifies the exogenously evolving labour supply over time. The motivation for dismissing the CRRA utility function can be explained by directing attention towards γ, which is referred to as the coefficient of relative risk aversion. Through the calibration of γ the curvature of the utility is configured and thereby the decision maker's attitude towards risk. The larger this parameter, the more risk averse the decision maker, who will refrain from gambling on uncertain outcomes. Assuming a different attitude towards risk also affects the 'Ramsey equation' (Cass [9], Koopmans [36], Ramsey [64]) in which γ also appears. This states that for optimal intertemporal allocation the social discount rate r equals

$$r = \delta + \gamma g, \tag{1.2}$$

where δ is the rate of pure time preference and g is the rate of growth of per capita consumption. In this context, γ is referred to as the elasticity of the marginal utility of consumption or the inverse of the intertemporal elasticity of substitution. When assuming a more risk-averse climate policy maker, γ increases, which leads to a more concave utility function in equation (1.1) and a higher social discount rate r in equation (1.2). Consequently, future damage costs receive less weight in the welfare assessment, leading to less concern about future risks. The CRRA utility function thus cannot mirror concerns about risk without implying time preferences. In doing so, only two preference specifications are allowed: less concern for the future and greater concern for current risks or high concern for the future and less concern for current risks. Disentangling time preferences and risk aversion is achieved by the recursive utility function, provided by Epstein and Zin [17, 18], which derives utility at time t, U_t by drawing on current consumption and the certainty equivalent of the utility in the future,

$$U_t = \left((1-\beta) \frac{\left(\frac{c_t}{l_t}\right)^{1-\psi}}{1-\psi} l_t + \beta \left(\mathbb{E}_t \left[U_{t+1}^{1-\alpha} \right] \right)^{\frac{1-\psi}{1-\alpha}} \right)^{\frac{1}{1-\psi}}, \tag{1.3}$$

where β is the discount factor for utility and relates to the rate of pure time preferences by $\delta = \frac{1-\beta}{\beta}$. The expectation operator at time t is described by $\mathbb{E}_t$. The inverse of the intertemporal elasticity of substitution is now given by ψ and α is the risk aversion parameter. For $\psi = \alpha$, equation (1.3) would collapse into a time separable specification as in equation (1.1). However, Bansal and Yaron [4] point out that this case would be rather unrealistic.

The recursive structure of the Epstein-Zin utility specification causes great analytical and computational costs. To compute current utility, not only current consumption but also the expected value of the next period's utility must be known. The next period's utility, in turn,

depends on the expected utility of the following period and so on. Therefore, current utility requires computation of the full branching tree of all possible futures. The implementation of equation (1.3) in IAMs has been accomplished by reducing complexity in one way or another: (i) Crost and Traeger [11] opt to give a more stylised version of the climate dynamics to transform the problem into a Bellman equation; (ii) Ha-Duong and Treich [23] and Kaufman [31] reduce the number of branches by accounting for only a few periods; and (iii) Ackerman et al. [3] thin out the tree by limiting the number of possible values for the uncertain parameter. We choose to follow closely the method used by Ackerman et al. [3] for two reasons. Firstly, as our research addresses the research question posed by Ackerman et al [3], we will ensure comparability of the results. Secondly, we consider this method rather advantageous compared to the other approaches as it retains the long time horizon structure in climate change decision problems. In addition, it allows us to implement additional dynamics given by the THC and thus even to increase model complexity. Following Ackerman et al. [3], we assume that five climate sensitivity values are possible candidates for being the true state of nature. Each climate sensitivity value is assigned a different probability.[6] We also adopt the assumption that this uncertainty persists until the middle of the second half of the century. The decision maker is required to decide on one policy path factoring in the uncertainty concerning all five climate sensitivity values. In 2075, uncertainty is fully resolved and the policy maker is then allowed to adjust policy accordingly.[7]

This design makes it possible to consider a tree that exhibits one branch until 2075, which goes out only once into five branches. The Epstein-Zin utility function for the first branch draws on current consumption and on the expected value of the utility after 2075. The expected value comprises the five different utilities that relate to the realisation of one of the possible 'worlds' or branches. These five utility functions are deterministic and reflect the present value over the remaining time. The recursive structure of the problem is therefore only given for the time until 2075. This simplified and stylised representation of uncertainty

[6]The next section describes in detail how these values and their probabilities are derived.

[7]Note that it is not within the scope of this paper to explore the learning process itself. The assumptions regarding the learning process are made for the mere reason to keep the analysis tractable and to limit computational costs. In reality, learning about climate sensitivity will most likely happen gradually as observations of the temperature evolution and/or research findings provide more information. For an overview of studies assessing the learning time-scales and for a recent approach to exploring them, see Urban et al. [76]. Ackerman et al. [3] have chosen learning to take place in a meaningful time interval: the period of uncertainty must be long enough to rule out the dominance of the wait-and-see strategy and short enough to grant learning and particularly acting after learning some importance. Indeed, this way of modelling learning is not uncommon in the literature (e.g. Hall et al. [24], Iverson and Perrings [29], McInerney et al. [54], Neubersch et al. [57]). In the next section, we shall undertake a robustness analysis to test for the sensitivity of our results. For further information on learning about a threshold in the THC, see Keller and McInerney [33]. For a general survey of learning-related questions, see O'Neill et al. [61].

allows us to expand the IAM used by Ackerman et al. [3] and also to account for a detailed representation of the THC.

The conceptual four-box model we implement is designed to reproduce key processes such as the possibility of a sudden collapse and the driving mechanisms of the overturning. Figure 1.2 provides a schematic representation of the model. The Atlantic is partitioned into the South Atlantic (box 1), the North Atlantic (box 2), and the Tropics (box 3 stands for the ocean surface and box 4 is associated with the deep ocean). The bold arrows indicate the direction of water circulation, which is determined by global density gradients generated by surface heat and freshwater fluxes. In the South Atlantic, the water is warmed and flows northward, where it cools en route, sinks down, and then flows back towards the South, where it warms again. The double arrows depict the heat exchange with the atmosphere in the different regions. In particular, the double arrow above box 2 describes the warmth provided by the THC to the North Atlantic region. The temperatures T_i^*, $i \in \{1,2,3\}$ are referred to as the 'restoring temperatures'. The curved arrows hint at the atmospheric water vapour transport F_1 and F_2 determining the degree of salinity in the surface boxes. The third curved arrow, which is not connected to any of the other boxes, indicates an additional freshwater flux F_2^{MW} provided by the meltwater runoff from the Greenland ice sheet and the meltwater from the Arctic sea ice.

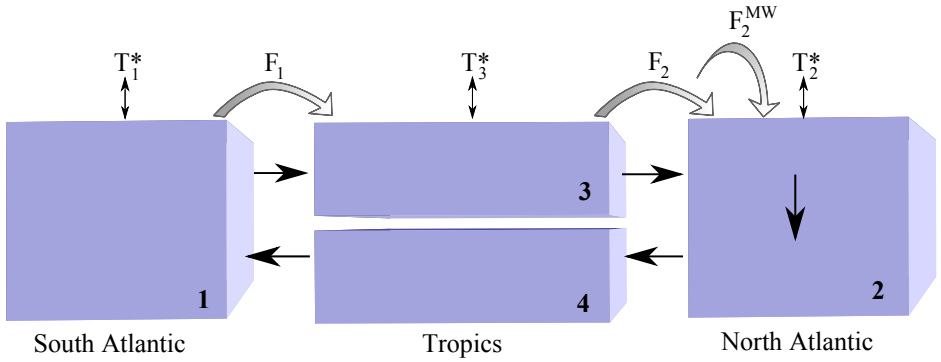

Fig. 1.2 Schematic representation of the THC box model

The global mean temperature ΔT provided by DICE affects the THC model through two channels. The global temperature increase can be scaled to derive the regional restoring temperatures:

$$\Delta T_i^*(t) = p_i \Delta T(t), \qquad i \in \{1,2,3\}, \tag{1.4}$$

where p_i are regional temperature constants. In addition, the freshwater forcing evolves according to ΔT:

$$\Delta F_1(t) = h_1 p_{SH} \Delta T(t), \tag{1.5}$$

$$\Delta F_2^{tot} = \Delta F_2(t) + \Delta F_2^{MW}(t) = \left(h_2 + h_2^{MW}\right) p_{NH} \Delta T(t) \equiv h_2^{tot} p_{NH} \Delta T(t), \tag{1.6}$$

where p_{SH} and p_{NH} are temperature constants for the Southern and Northern Hemispheres, respectively, and h_1, h_2, and h_2^{MW} are hydrological sensitivity parameters. We define h_2^{tot} as the sum of the two hydrological sensitivity parameters h_2 and h_2^{MW}.

Water temperature T_i, $i \in \{1,\ldots,4\}$ in the boxes is influenced by the restoring temperatures T_i^* and the temperature of the water that flows into the box i, as indicated by the bold arrows in Figure 1.2. More specifically,

$$\dot{T}_1 = \frac{m}{V_1}(T_4 - T_1) + \lambda_1 (T_1^* - T_1), \tag{1.7}$$

$$\dot{T}_2 = \frac{m}{V_2}(T_3 - T_2) + \lambda_2 (T_2^* - T_2), \tag{1.8}$$

$$\dot{T}_3 = \frac{m}{V_3}(T_1 - T_3) + \lambda_3 (T_3^* - T_3), \tag{1.9}$$

$$\dot{T}_4 = \frac{m}{V_4}(T_2 - T_4), \tag{1.10}$$

where V_i are the box volumes, λ_i thermal coupling constants and m the above-mentioned meridional volume transport. The dot over the variable is used to denote the time derivative.

The salinity levels in the boxes S_i^{THC}, $i \in \{1,\ldots,4\}$ are determined by the freshwater fluxes F_1 and F_2^{tot} and the salinity level of the water flowing into the box i.

$$\dot{S}_1^{THC} = \frac{m}{V_1}\left(S_4^{THC} - S_1^{THC}\right) + \frac{S_0 F_1}{V_1}, \tag{1.11}$$

$$\dot{S}_2^{THC} = \frac{m}{V_2}\left(S_3^{THC} - S_2^{THC}\right) + \frac{S_0 F_2^{tot}}{V_2}, \tag{1.12}$$

$$\dot{S}_3^{THC} = \frac{m}{V_3}\left(S_1^{THC} - S_3^{THC}\right) + \frac{S_0\left(F_1 - F_2^{tot}\right)}{V_3}, \tag{1.13}$$

$$\dot{S}_4^{THC} = \frac{m}{V_4}\left(S_2^{THC} - S_4^{THC}\right), \tag{1.14}$$

where F_1 and F_2^{tot} are multiplied by S_0 for conversion to a salt flux.

The meridional volume transport m evolves according to the north-south temperature gradient and salinity gradient:

$$m(t) = k\left(\beta\left(S_2^{THC}(t) - S_1^{THC}(t)\right) - \zeta\left(T_2(t) - T_1(t)\right)\right), \tag{1.15}$$

where ζ and β are thermal and haline expansion coefficients and k is a hydraulic constant. Note that the system of differential equations (1.7)–(1.14) is non-linear, because m also depends on temperature and salinity.

All parameters of the THC model, which is here presented in a condensed form, are derived by Zickfeld et al. [86] from simulations with an Earth-system model of intermediate complexity.

The variable that the THC model hands over to DICE, the meridonial volume transport m, is an essential part of the new climate damage function. In this model, the damage cost function consists of two parts: the first part relates to the (non-catastrophic) damages caused by global warming and the second and new part refers to the costs incurred by a substantial slowdown of the THC. For the first part, we adopt the same quadratic functional form as in DICE. Note that the commonly used cost function in DICE only encapsulates the impacts by increasing temperatures, but it is also specified to capture all resulting losses comprising those of the non-catastrophic and the catastrophic impacts. As our model framework already accounts for one of these catastrophes explicitly, we choose to recalibrate the damage function in DICE according to the non-catastrophic damage estimates given by Cline [10]. After employing a two-point fit to these estimates, we obtain the following damage cost function:

$$D(\Delta T, m) = 0.000976(\Delta T)^2 + f_{THC}(m) \tag{1.16}$$

as a fraction of global GDP, where $f_{THC}(m)$ refers to the yet unspecified damage cost function of a slowdown in the THC.

As with all climate damage functions, developing $f_{THC}(m)$ is a challenging task, leaving us no other option but to adopt some stylised assumptions. Firstly, we refrain from postulating that only a collapse would incur costs. In fact, Link and Tol [46] demonstrate rather similar costs for a circulation that has 'strongly weakened'. Secondly, we assume that the cost development exhibits some sudden increase, as it is sometimes assumed for abrupt climate change processes crossing some threshold (e.g. see Nordhaus [59]). Thirdly, we presume that this sudden increase in the damage costs occurs in the proximity of a

significant slowdown, in a point we denote as m_{crit}. A specification complying with the above description is the following 'sharp' logistic function:

$$f_{THC}(m) = \frac{d_m}{\pi}\left(\frac{\pi}{2} + ArcTan[100(m_{crit} + 0.5 - m)]\right) \tag{1.17}$$

where π is the mathematical constant ≈ 3.14159. Figure 1.3 illustrates this specific function for the yet to be calibrated values d_m and m_{crit}. Duly noted, it is critical to find good estimates for m_{crit} and for d_m. How we choose to calibrate these values is explained in the next section.

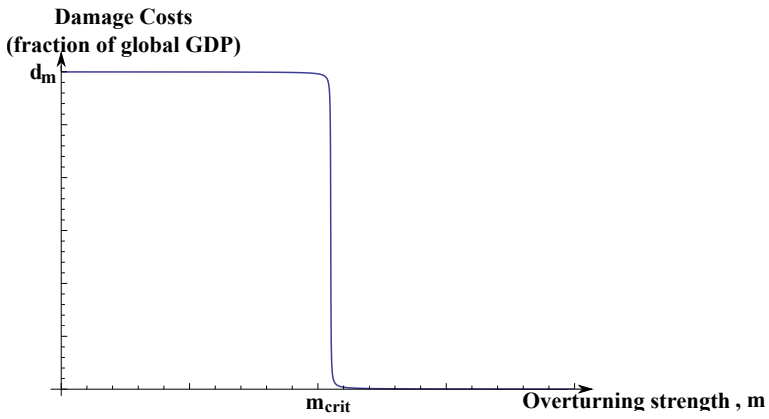

Fig. 1.3 The damage cost function $f_{THC}(m)$ for m_{crit} and d_m.

As the weakening of the THC not only depends on temperature levels but also on the rate of temperature change, the climate damage cost function in equation (1.17) is also determined by the rate of climate change, which is not captured by the commonly used damage function in DICE-2007 and DICE-CJL.[8]

As the analytical solution is not available for this welfare optimisation problem, the solution is numerically approximated using the General Algebraic Modeling System (GAMS, McCarl [52]). Please refer to the Appendix 1.B for further information.

In the next section, we turn to investigate this model and its implications concerning the decision maker's risk preferences.

[8] Of course, there are also other extensions of the DICE model that replace the original damage function by a rate-dependent version, for example Goes et al. [20].

1.3 Numerical Simulation

Before investigating the simulations of the model described above, we direct special attention to the calibration of some crucial parameters. Firstly, we specify the exact nature of the modelled uncertainty concerning the climate sensitivity value. We proceed with giving details of how we calibrate equation (1.17), which describes the damage costs of a THC weakening. Moreover we specify how the value of the North Atlantic hydrological sensitivity, h_2^{tot}, is chosen. Afterwards, we explain our choices for the rate of pure time preference and the intertemporal elasticity of substitution. After providing a thorough analysis of the baseline case and a comprehensive sensitivity analysis, we direct our attention to the effects of not having unlimited abatement options. Further information is provided in the Appendix. Appendix 1 A tests whether our model can reproduce the simulations undertaken by Ackerman et al. [3] and shows the differences between these models. Appendix 1 B discusses the caveats of the numerical solution of the problem. Appendix 1 C summarises the entire calibration.

The five possible states of nature are given by a selection of climate sensitivity values and their associated probabilities. Figure 1.4 illustrates the proposal of Ackerman et al. [3] for how these values can be derived. Assuming the probability distribution function (PDF) given by Roe and Baker [66], they partition the cumulative distribution function (CDF) into five unequal intervals spanning 50, 40, 5, 3, and 2 per cent of the whole interval, respectively. The five states of nature are then derived by taking the midpoints of these intervals as the percentiles of the distribution. For instance, the midpoint of the 50 per cent interval is 25 per cent, the 25th percentile climate sensitivity value is 2.43. The probability of 2.43 being the true state of nature is then assumed to be given by the length of the interval, i.e. 50 per cent. Taking everything together, the following climate sensitivity values evolve as the possible states of nature S with a probability p: $S_1 = 2.43$, $p_1 = 0.5$; $S_2 = 3.76$, $p_2 = 0.4$; $S_3 = 6.05$, $p_3 = 0.05$; $S_4 = 8.2$, $p_4 = 0.03$; $S_5 = 16.15$, $p_5 = 0.02$.
The assessments of the potential costs, d_m, are an area of active research and mainly include changes in regional temperatures and in precipitation patterns, a reduced carbon uptake in the Atlantic, and a rise in sea level. However, they ignore several other possible impacts, such as a deterioration of food quality (Kuhlbrodt et al. [40] and Zickfeld et al. [85]). Furthermore, only few monetised estimates are available in the literature. Only accounting for the effects on regional temperatures, Tol [73] finds that the losses may range from 0 to 3 per cent of global GDP. More recently, however, Link and Tol [46] provide an estimate of 0.5 per cent of global GDP. The partial coverage of the impacts may systematically underestimate the actual costs. Accordingly, significantly higher cost estimates cannot be ruled out due to further consequences such as strain resulting from geopolitical tensions (Mastrandrea

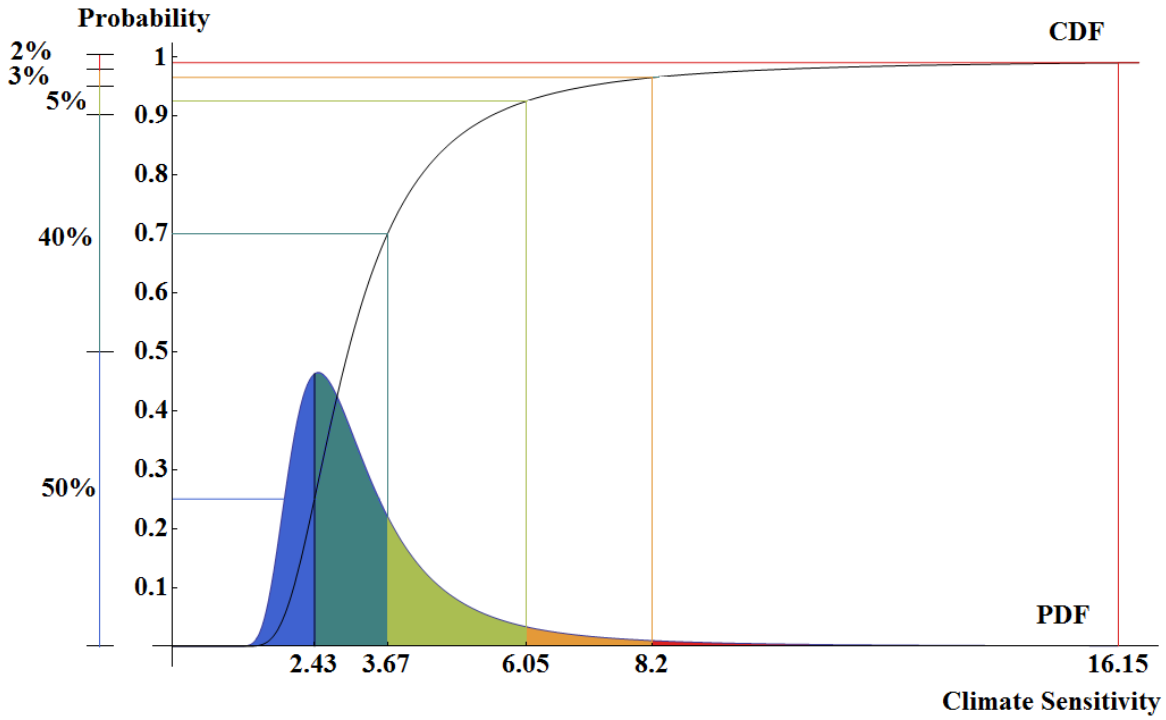

Fig. 1.4 Partitioning of the probability distribution for climate sensitivity

and Schneider [50]). On the basis of these studies, we consider a baseline calibration of $d_m = 0.03$ a reasonable choice and test the sensitivity of the results with respect to d_m being 0.015 and 0.045 later on.

The damage costs are often assumed to diverge from zero as the circulation shuts down altogether i.e. $m_{crit} = 0$ (e.g. e.g. Keller et al [32] and McInerney et al. [54]). However, as mentioned in section 3.2, we postulate that a significant slowdown is sufficient to cause costs, thus $m_{crit} > 0$. The exact calibration of m_{crit} is not clear, though. Simulations using the FUND model in Link and Tol [46] indicate that the point of such a strong weakening inducing significant costs might be about half of today's value of the overturning strength, which corresponds to 22.6 Sv in our model. As assessments of such a critical weakening are sparse, we may also consult some tipping point estimates. Although m_{crit} and a tipping point cannot be considered to be the same, this estimate might give us a better sense of a range of values that signify a strong weakening. Using the four-box model, Zickfeld and Bruckner (2003) and Zickfeld et al. (2004) provide an assessment of a critical flow strength that is less than half of today's value. More specifically, Zickfeld and Bruckner (2003) and Zickfeld et al. (2004) also account for transient effects and conclude that 10 Sv is a good estimate when accounting for a reasonable range of crucial parameter values. Motivated by

the aforementioned studies, we adopt this value for m_{crit}. Note that although the choice of calibrating m_{crit} is inter alia based on an estimate of the bifurcation point, the model does not equate the tipping point with the point at which the damage costs diverge considerably from zero. The bifurcation point is determined endogenously by the model, while m_{crit} is exogenously imposed. In other words, this choice does not imply that crossing m_{crit} would lead to a collapse in the model. It is simply assumed that crossing m_{crit} signifies a slowdown that is sufficient to cause costs. Dependent on the rate of temperature change and on the value of hydrological sensitivity, it could be the case that the THC reaches a point at which costs are incurred but the bifurcation point has not been transgressed. At such a point it cannot be ruled out that the THC recovers after some time and the associated damage costs fall. If, in contrast, the system is tipped, the THC damage costs might add up to a magnitude that influences policy. Yet, it goes without saying that the uncertainty involved in calibrating m_{crit} must be addressed by a sensitivity analysis, as provided in Appendix 1 D.[9]

The North Atlantic hydrological sensitivity, h_2^{tot}, is one of the factors that determines the magnitude of the changes in m. As explained by equation (1.6), the hydrological sensitivity h_2^{tot} measures the additional increase in freshwater for a warming of one degree Celsius, including the meltwater runoff from the Greenland ice sheet and the meltwater from the Arctic sea ice. The quantification of h_2^{tot} involves great uncertainties as it rests on largely differing estimates of evaporation, precipitation, river runoff, and meltwater volumes (Rahmstorf and Ganopolski [63] and Zickfeld et al. [86]). The identified estimates for h_2 range from 0.01 Sv $°C^{-1}$ to 0.053 Sv $°C^{-1}$ (Manabe and Stouffer [48] and Zickfeld et al. [86]). The contribution of the Greenland ice sheet to h_2^{MW} is found to be between 0.002 Sv $°C^{-1}$ and 0.01 Sv $°C^{-1}$ and the melting of the sea ice adds approximately 0.0125 Sv $°C^{-1}$ (Zickfeld [86]). Taking all these estimates into account, we choose to set h_2 to 0.03 Sv $°C^{-1}$ and h_2^{MW} to 0.0225 Sv $°C^{-1}$, adding up to h_2^{tot} at 0.0525 Sv $°C^{-1}$. With the diverging estimates in mind, Zickfeld et al. [86] also test the THC dynamics for alternative values ranging from 0.013 Sv $°C^{-1}$ up to 0.06 Sv $°C^{-1}$. They find significant differences in the evolution of the overturning strength and thereby illustrate the key role of the uncertainty regarding h_2^{tot} in the predictions. Consequently, we also allow for alternative values being $h_2^{tot} = 0.04$ and $h_2^{tot} = 0.06$.

The question of how to calibrate the parameters in the Epstein-Zin utility specification in the context of a climate policy decision remains unanswered. To our knowledge, there is no study that convincingly attempts to evaluate these values for this specific decision. It is

[9] These simulations show that the result with respect to the effect of risk aversion is robust to alternative choices for m_{crit}.

neither clear how to obtain corresponding data nor which market is subject to a similar multitude of risks and could thus serve to provide helpful evidence for a reasonable calibration. One approach, which is also followed by Ackerman et al. [3], is to take the parametrisation from the studies of Bansal and Yaron [4] and Vissing-Jrgensen and Attanasio [79], which estimate the intertemporal elasticity of substitution (IES) at 1.5 and the coefficient of relative risk aversion at 9.5 to 10 for financial markets. We borrow these values for our study as well. Later on, the sensitivity with respect to the IES parameter is examined by implementing the value of 2.

To evaluate the effects of risk aversion on near-term policy, we compare the results for two specifications of the risk aversion parameter α. The first, with α being 2, describes a mildly risk-averse policy maker. The alternative specification of $\alpha = 10$ is – as already mentioned – taken from the above-mentioned studies. The comparison of the resulting policy scenarios gives evidence of the sensitivity of the results with respect to the degree of risk aversion.

All figures in what follows provide this comparison by contrasting the results for the optimal emission control path and the implied dynamics of the THC. The simulations shown at the top of each figure rest on the underlying assumption of α being 2, while those at the bottom result from α being 10. The general idea behind the graphs on the left (i.e. all graphs (a) and (c)) displaying the optimal reduction policy is as follows. As described in section 3.2, the policy maker decides on one policy path until 2075, the year in which the true climate sensitivity value is revealed. This policy path factors in all possible climate sensitivity values and their associated probabilities. Depending on which value is disclosed, the policy maker chooses one of the five policy paths for the time afterwards. The consequences for the overturning strength, illustrated for all five climate sensitivity values, are presented by the graphs on the right-hand side (i.e. Figures (b) and (d)). The dashed horizontal line in these figures indicates the critical value of the overturning strength, $m_{crit} = 10$ Sv, below which the THC related damage costs are incurred as described by equation (1.17).

The simulations in Figure 1.5 are obtained by employing the baseline calibration. Figure 1.5a shows that it is optimal to start with an emission control rate of 24.00 per cent and gradually to increase efforts up to 40.44 per cent in 2075. If a climate sensitivity value of $S_1 = 2.43$ is disclosed, it is optimal to maintain this control rate for several more decades. For all other values, efforts have to be increased – the more so the higher this value turns out to be. In the case of S_5, this would even imply a sudden jump to the control rate of 94.16 per cent. Yet,

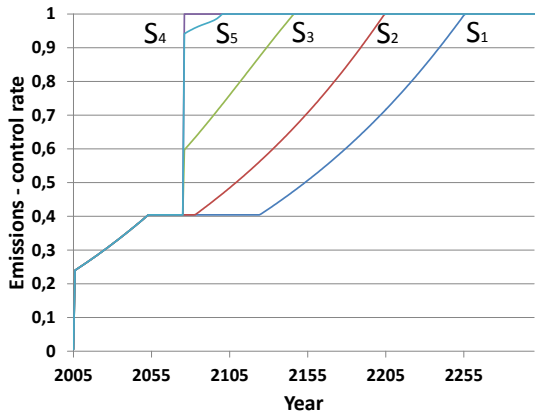

(a) Optimal emission reduction policy

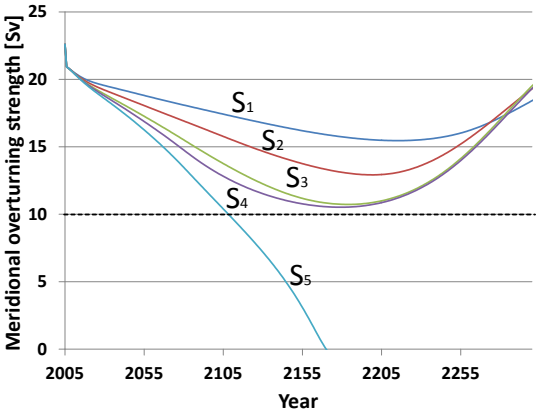

(b) Possible trajectories of the overturning strength

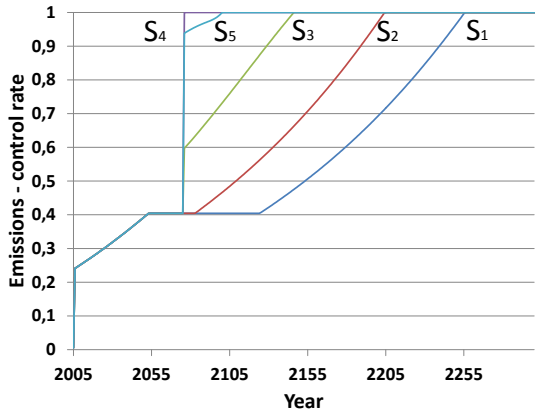

(c) Optimal emission reduction policy

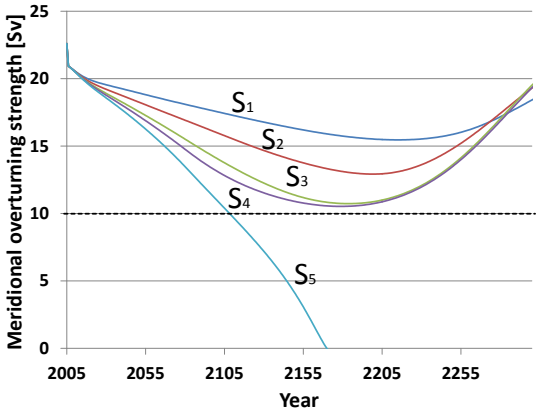

(d) Possible trajectories of the overturning strength

Fig. 1.5 Comparison of the effects of alternative assumptions concerning risk aversion: $\alpha = 2$ (top) and $\alpha = 10$ (bottom)

these massive but late efforts in S_5 cannot prevent critical weakening, which occurs when crossing the dashed line at 10 Sv. Accordingly, we may note the following. Apparently, it is not optimal to increase near-term abatement to avoid a collapse in S_5. A possible explanation may be that the probability of being in state 5 is too small to exert a significant effect on near-term policy. Although in 2075 it is too late to prevent the THC collapse, increased efforts may be justified in view of the non-catastrophic damage costs (i.e. the first term in equation (1.16)). Furthermore, these efforts may help to delay the collapse. In all other states, late policy efforts succeed in safeguarding the THC. Hence, the policy maker has enough time to wait until 2075. Then, the policy maker can adjust policy and can prevent shut-down in the more likely states. Interestingly, the late policy efforts in S_4 are even more intense

than in S_5. To understand this result, we forced the control rate in S_5 to jump to 100 per cent after learning. This simple test revealed that the collapse in S_5 can only be delayed but not prevented by these late efforts. In this situation, optimal policy after 2075 is about weighing the costs against the benefits of postponing the collapse. In contrast, in S_4 emission control is capable of preventing the critical weakening. Consequently, the differences in the benefits of emission control give the reason for a higher control rate in S_4 than in S_5.

The optimal policy for a more risk-averse decision maker is presented in Figure 1.5c. It is striking that this policy path is highly similar to that described before for a mildly risk-averse decision maker. The critical weakening in S_5 occurs almost at the same time. Hence, the assumption of higher risk aversion neither changes the near-term policy in a qualitatively meaningful way nor does it affect the THC dynamics to any great extent. We may draw the conclusion that an even more risk-averse policy does not rate the possible, albeit not very likely, detrimental impacts of S_5 as sufficiently high to make more decisive efforts in the near term. Next, we explore the sensitivity of this result with respect to a change in some key parameters. Table 1.1 summarises the variations in the parameters described above.

Table 1.1 Sensitivity runs

Model Run	h_2^{total}	d_m in %	IES	Year of Learning	Figure
Baseline	0.0525	3.0	1.5	2075	1.5
Lower h_2	0.04	3.0	1.5	2075	1.6
Higher h_2	0.06	3.0	1.5	2075	1.7
Lower d_m	0.0525	1.5	1.5	2075	1.8
Higher d_m	0.0525	4.5	1.5	2075	1.9
Higher IES	0.0525	3.0	2	2075	1.10
Early Learning	0.0525	3.0	1.5	2050	1.11
Late Learning	0.0525	3.0	1.5	2100	1.12

The effects of a lower hydrological sensitivity, h_2^{tot}, are demonstrated in Figure 1.6. A lower h_2^{tot} value means a smaller freshwater input per degree of warming, which translates into a reduced rate of weakening. Accordingly, compared to Figure 1.5a, Figure 1.6a exhibits a lower control rate of 34.02 per cent in 2075. The curves illustrating the policy response after 2075 also indicate less stringent efforts. Only in S_5 does the control jump to a higher

rate, this being 100 per cent. A possible reason is that compared to the baseline case, it proves easier to delay the collapse even further. In total, the shut-down occurs almost 50 years later in Figure 1.6b than in Figure 1.5b. A higher risk aversion again appears to be of subordinate importance for near-term policy. In Figure 1.6c, the control rate in 2075 is only 0.17 percentage points higher than in Figure 1.6a. In addition, this policy does not have a visible effect on the THC dynamics. This result makes sense, as a lower hydrological sensitivity makes the THC dynamics more stable and thus the risk of a possible collapse smaller. This offers even more leeway to postpone decisive action.

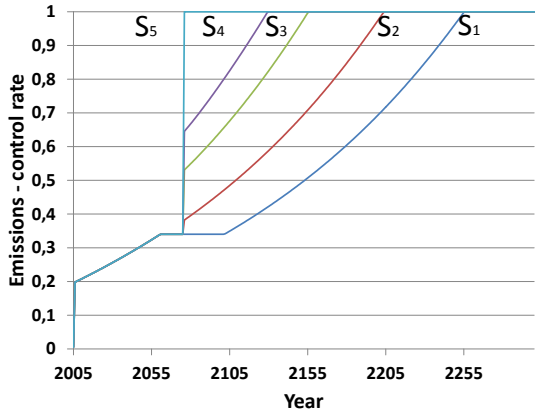

(a) Optimal emission reduction policy

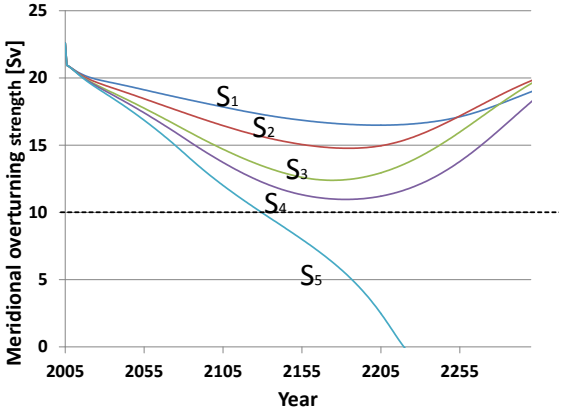

(b) Possible trajectories of the overturning strength

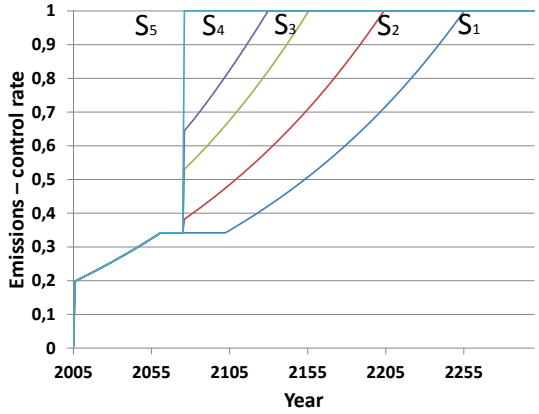

(c) Optimal emission reduction policy

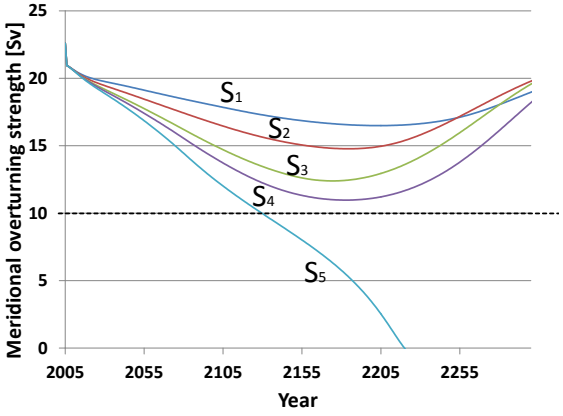

(d) Possible trajectories of the overturning strength

Fig. 1.6 Sensitivity of the results with respect to a lower hydrological sensitivity value i.e. $h_2^{total} = 0.04$

The accelerated weakening of the THC caused by a higher hydrological sensitivity, h_2^{tot}, is counteracted by more abatement in the near term, as demonstrated in Figure 1.7a. In all

considered states S_1–S_5, the risk of a collapse increases and thus requires that more emission reduction to be undertaken. Having implemented this high control rate, the policy maker does not have to adjust the abatement policy for many decades if S_1 turns out to be true. Even in S_2 this rate is maintained for some time. As in Figure 1.5, there are higher efforts in S_4 than in S_5. Although the higher h_2^{tot} leads to a critical weakening in S_4 and S_5, it is reasonable to cut emissions sooner after learning in S_4. The reason is shown in Figure 1.7b. Emission reduction helps the THC to recover after some time in S_4, while in S_5 it will irreversibly collapse. Although the risk of a complete shutdown is more pronounced in this scenario, higher risk aversion does not lead to greater near-term efforts. Consequently, the probability of S_4 or S_5 turning out to be true is too low to affect policy until 2075. For all other states, the policy maker has all means to react in time and to prevent the critical weakening. Hence, risk aversion does not lead to qualitatively different results.
Figure 1.8a illustrates how policy changes if the damages from a critical weakening of a THC are less severe. It is not surprising that policy until 2075 is a little less stringent than illustrated in Figure 1.5a. Although damages are lower, efforts are increased after 2075 and in four of the five cases the irreversible collapse can be prevented. In S_4 the THC weakens critically but soon recovers. As shown in Figure 1.8c, risk aversion has some, albeit small, effect on near-term policy. The increased efforts prevent S_4 from slowing down beyond 10 Sv.

Next we explore the implications of a higher THC-specific damage cost case as depicted in Figure 1.9. Intuitively, the optimal control must be at least as strong as that in the baseline case. In Figure 1.5a, the decision maker successfully reduces the risk of the potential breakdown and prevents the strong weakening in the states of nature S_1–S_4, while taking the risk of the critical weakening in the low probability state S_5. Consequently, the optimal abatement trajectory in the near term is virtually the same as in Figure 1.5a. Yet, in state S_5 higher damage costs imply a more stringent policy after learning of 2.28 percentage points. As a result, 96.64 per cent of emissions are under control by the year 2076. To reduce the long-term risk further is not economically justified and thus higher risk aversion does not have a significant effect.

The effects of an increase in the intertemporal elasticity of substitution are demonstrated in Figure 1.10. As expected, a higher IES leads to stronger abatement efforts in the near term (cf. Figure 1.10a with Figure 1.5a). Under higher risk aversion, the control rate is almost the same. As before, the collapse is only prevented in the more likely states, S_1–S_4. Although a lower discount rate does not alter the implied THC dynamics significantly, it has an effect on the policy path because the future damages are discounted to a lesser extent.

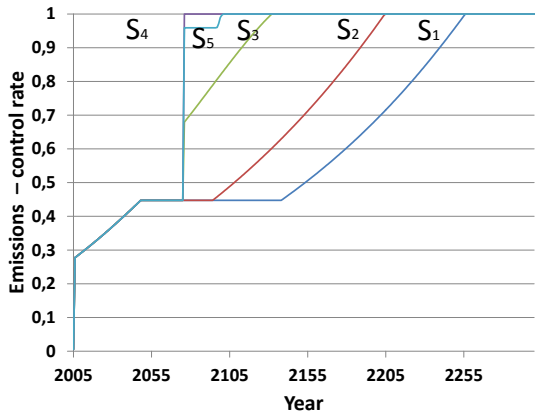

(a) Optimal emission reduction policy

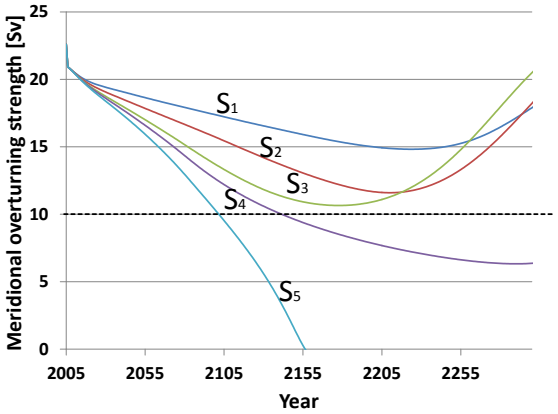

(b) Possible trajectories of the overturning strength

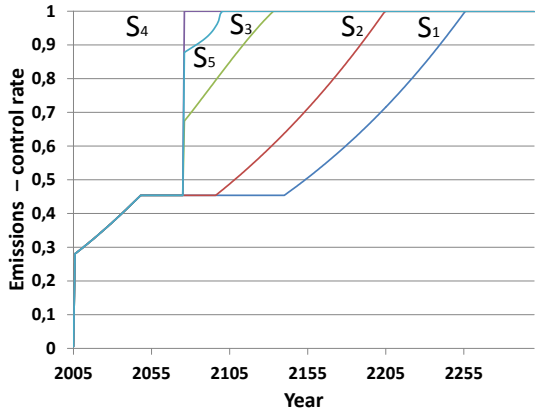

(c) Optimal emission reduction policy

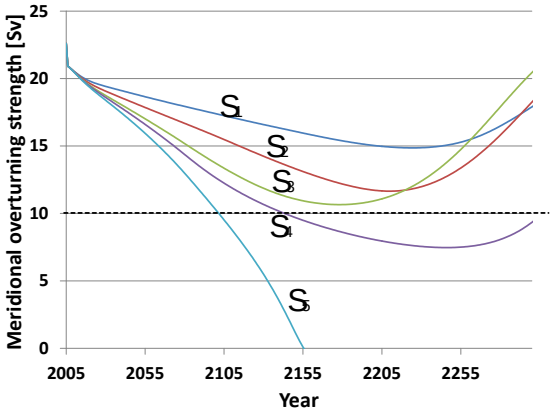

(d) Possible trajectories of the overturning strength

Fig. 1.7 Sensitivity of the results with respect to a higher hydrological sensitivity value, i.e. $h_2^{total} = 0.06$

The next two simulations are devoted to the appraisal of how the assumption on the year of learning influences the results. Urban et al. [76] compare major studies on learning about climate sensitivity and single out Ring and Schlesinger [65], who find, compared to other studies, a relatively quick learning process that resolves uncertainty by 2050. This early learning scenario is depicted in Figure 1.11. It is interesting to see that the opportunity to implement a perfectly tailored solution rather early in time does not significantly alter the outcome for the THC dynamics. Comparing Figure 1.11b with Figure 1.5b shows that the critical weakening in S_5 occurs almost at the same time. The early stringent efforts in S_5 as described by Figure 1.11a only help to delay total collapse by approximately 50 years. Owing to the knowledge of early learning, the level of risk aversion is expected to have even

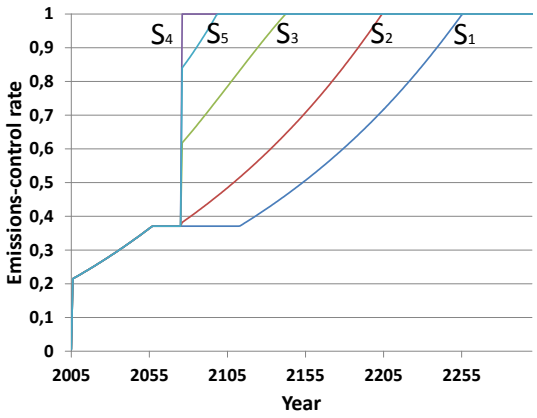

(a) Optimal emission reduction policy

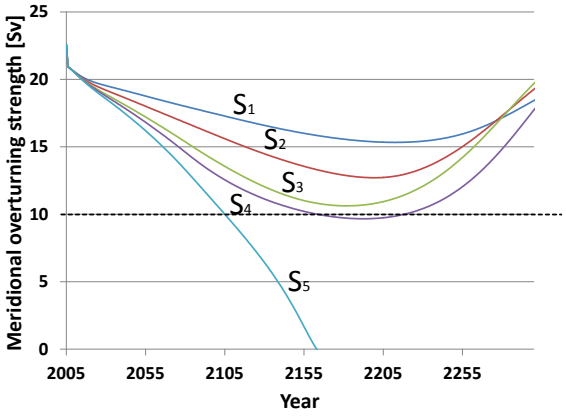

(b) Possible trajectories of the overturning strength

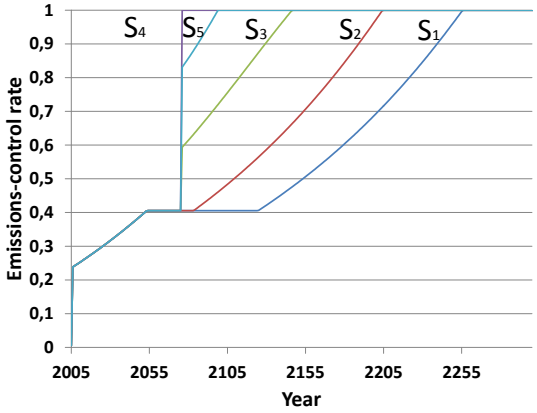

(c) Optimal emission reduction policy

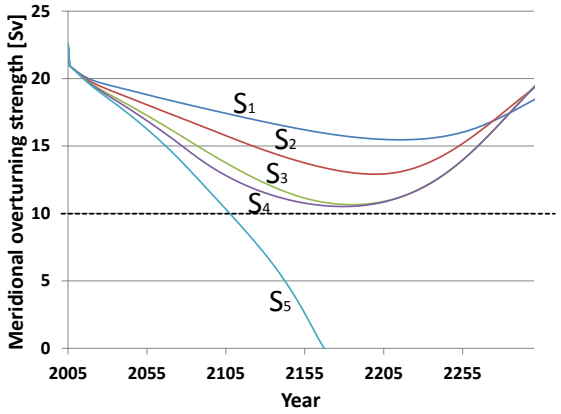

(d) Possible trajectories of the overturning strength

Fig. 1.8 Sensitivity of the results with respect to lower damage costs caused by a critical weakening of a THC, i.e. $d_m = 0.015$

less effect than in the baseline case. As indicated by Figure 1.11c, a higher level of risk aversion increases the abatement efforts until 2050 only negligibly. Risk aversion only has an effect on policy after learning if the worst case, S_5, turns out to be true.

Other studies indicate that perfect learning may take substantially longer. Kelly and Kolstad [35] estimate a learning time of 90–160 years, assuming that learning equals an almost 100 per cent resolution of uncertainty. Urban et al. [76] find that uncertainty can be substantially reduced by 2100 with a (for policy making negligible) 0.1–0.5°C imprecision of the estimates.[10] This year of learning is assumed for the simulation shown in Figure 1.12. Figure

[10]Urban et al. [76] report faster learning rates for lower climate sensitivities than for higher values and explain this by faster ocean response times.

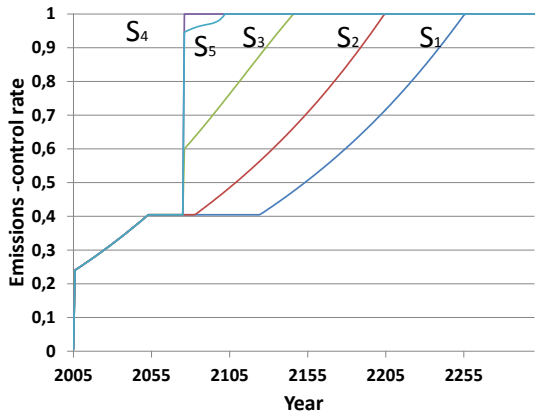

(a) Optimal emission reduction policy

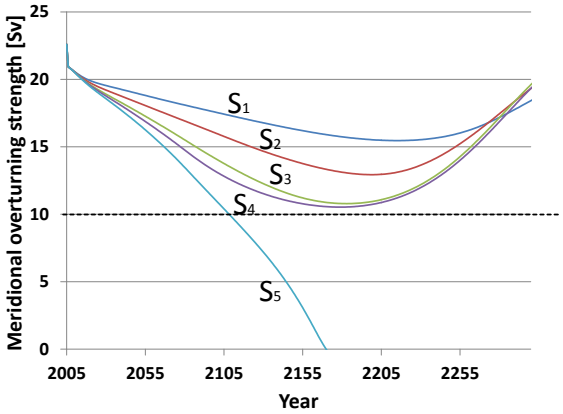

(b) Possible trajectories of the overturning strength

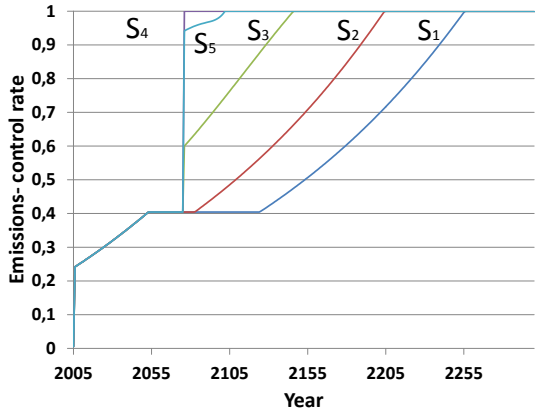

(c) Optimal emission reduction policy

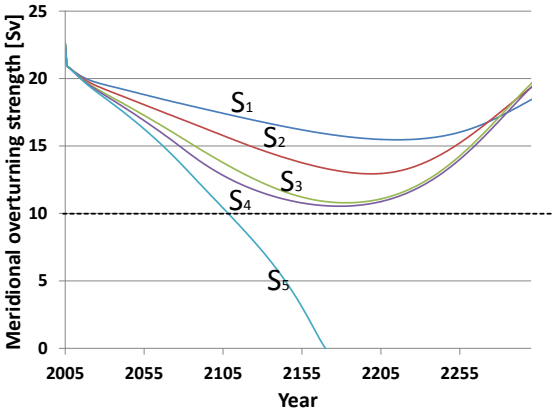

(d) Possible trajectories of the overturning strength

Fig. 1.9 Sensitivity of the results with respect to higher damage costs caused by a critical weakening of a THC, i.e. $d_m = 0.045$

1.12b demonstrates that the THC weakens strongly in state S_4, but does recover after several decades. The implementation of abruptly increased efforts after 2100 is not timely enough as the collapse in S_5 and the extreme weakening in S_4 are already locked in. This is evidence of how limited the strategy to react after learning can be, as it may increase the likelihood of tipping points. It also emphasises the importance of early learning. Interestingly, a more risk-averse policy maker increases the near-term efforts only slightly. The reason for this is that the two states, S_4 and S_5, are only weighted by 5 per cent in the welfare optimisation calculus. The simulation gives evidence that this probability is too small to have a significant impact on decision making towards longer term impacts.

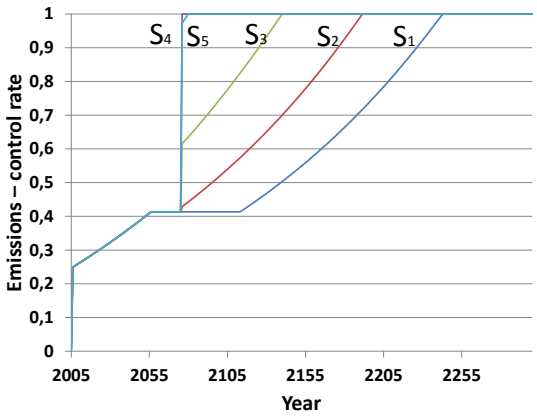

(a) Optimal emission reduction policy

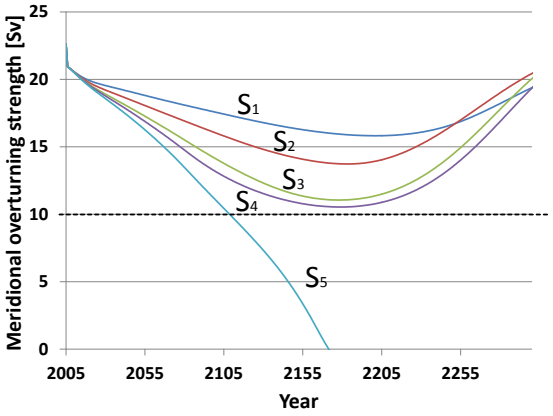

(b) Possible trajectories of the overturning strength

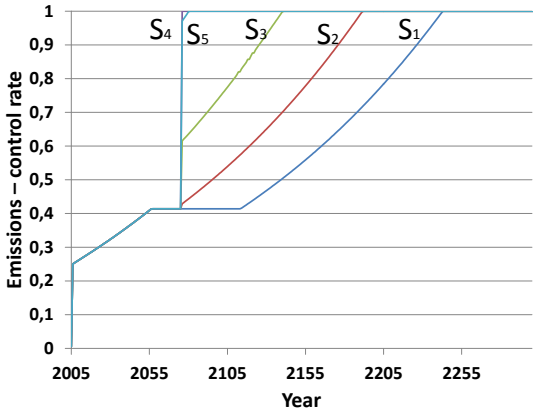

(c) Optimal emission reduction policy

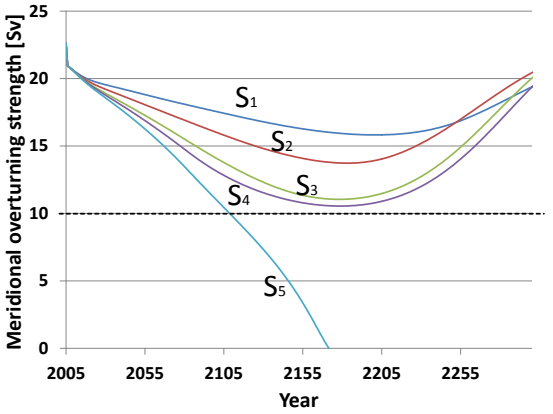

(d) Possible trajectories of the overturning strength

Fig. 1.10 Sensitivity of the results with respect to a higher IES of 2%

Note that in the first set of simulations (Figures 1.5–1.12), no restrictions for the maximum change in the annual emission reduction rate are assumed. The policy maker can instantaneously raise the emission reduction rate up to 100 per cent if needed. However, the assumption that the technology to stop emitting immediately after 2075 will be available may be criticised as a naïve faith in technology. What happens to policy and to the implications in relation to risk aversion if the abatement options are more restrictive than in the original DICE model? In the remainder of this section, we examine how limits on the speed of policy adjustment affect near-term optimal policy. This is expressed by an additional constraint in the model:

$$\mu(t+1) \leq \mu(t) + l, \tag{1.18}$$

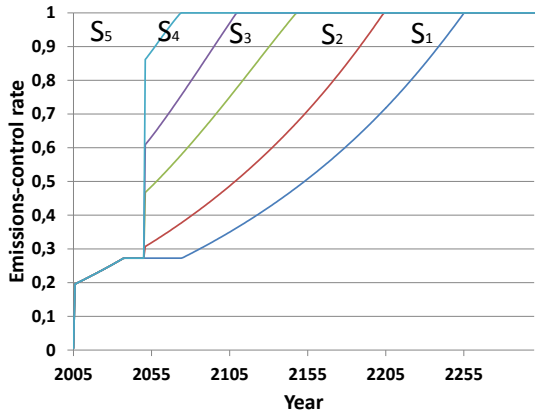

(a) Optimal emission reduction policy

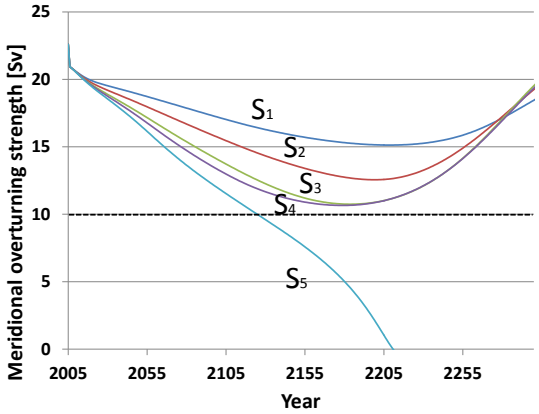

(b) Possible trajectories of the overturning strength

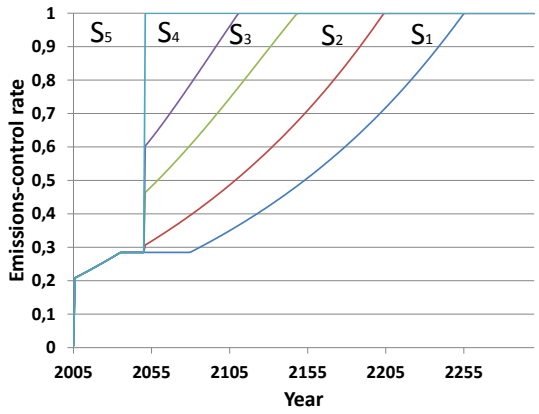

(c) Optimal emission reduction policy

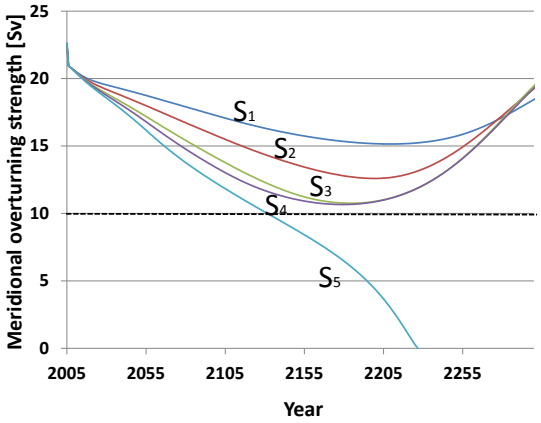

(d) Possible trajectories of the overturning strength

Fig. 1.11 Sensitivity of the results with respect to learning early, i.e. in 2050

where μ is the emissions-reduction rate and l the maximum allowable annual increase in abatement as a fraction of global emissions under control. In the literature, the major constraints are identified as limits in technological progress, policy inertia, or inertia in the economic system (Grübler et al. [21], Ha-Duong et al. [22], Lecocq et al. [41], Waisman et al. [80]). An assessment of mitigation scenarios suggests the maximum plausible annual decarbonisation rate to be around 2.8 per cent (den Elzen et al. [13]). Taking into account technological inertia, but ignoring social inertia, the model IMAGE/TIMER provides an estimate of 3–4 per cent per year and 4–5 per cent per year when bioenergy and carbon storage is additionally accounted for (den Elzen et al. [13]). In the following simulation (Figure 1.13), we assume the most pessimistic estimates of these, i.e. $l = 0.028$. The line $\mu_{max}(t)$ in Figures 1.13a and 1.13c indicates the 'maximum possible abatement effort', which

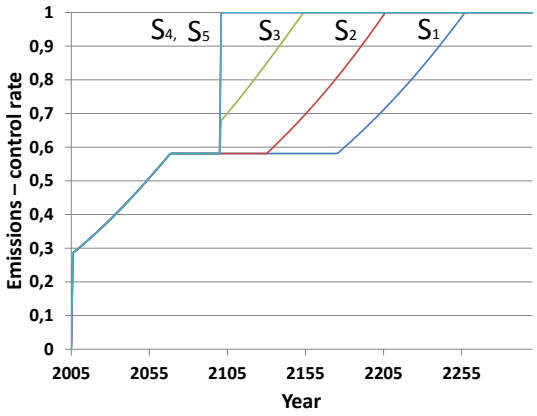

(a) Optimal emission reduction policy

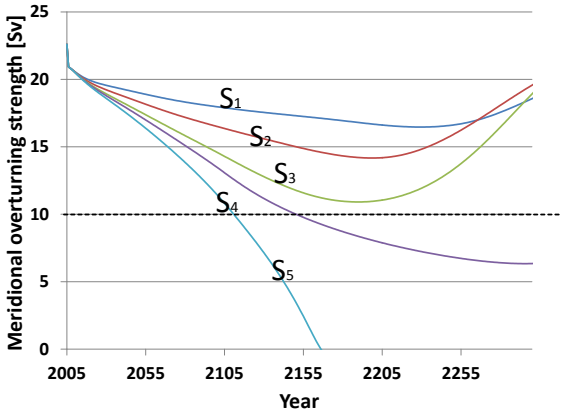

(b) Possible trajectories of the overturning strength

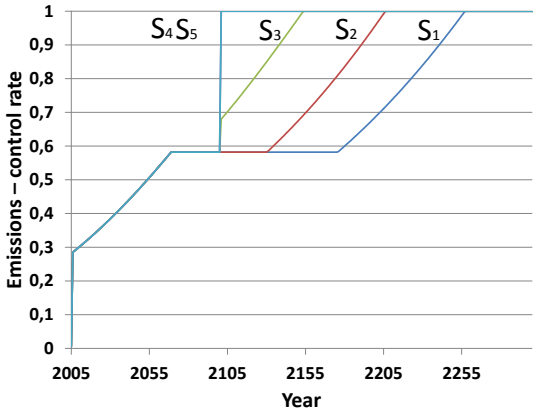

(c) Optimal emission reduction policy

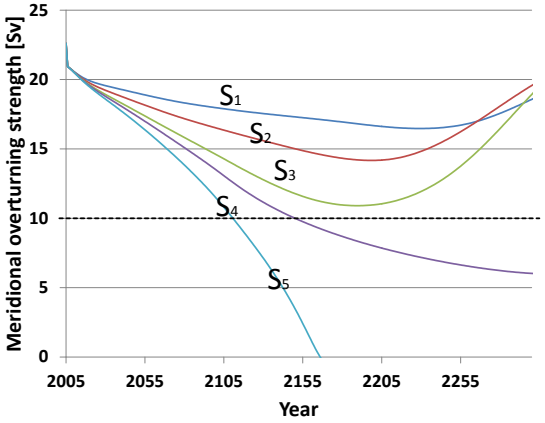

(d) Possible trajectories of the overturning strength

Fig. 1.12 Sensitivity of the results with respect to learning later, i.e. in 2100

corresponds to an annual increase in abatement of l. As expected, the abatement efforts are limited by inertia in the very beginning, which is then compensated for by greater efforts by 2075 compared to the no-inertia case in Figure 1.5. These efforts constitute 45.55 per cent by 2075. These efforts are, however, not sufficient to prevent the THC from collapsing if state S_4 or S_5 turns out to be true. Higher abatement efforts are undertaken by the more risk-averse policy maker as illustrated by Figure 1.13c. More specifically, compared to Figure 1.13a, this level of risk aversion leads to an increase in abatement efforts of almost 7 percentage points by 2075. As a result, the more risk-averse policy maker manages to prevent the THC collapse in S_4.

The next simulation illustrates a thought experiment in which we assume inertia to be

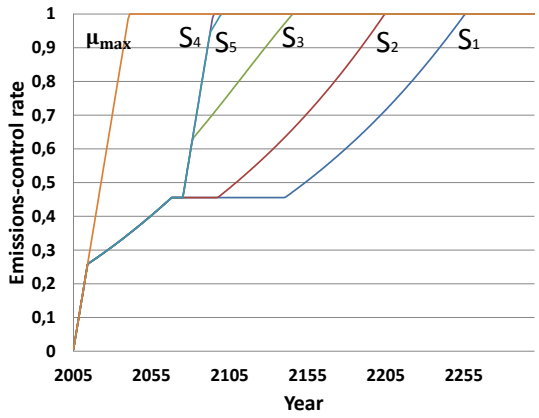

(a) Optimal emission reduction policy

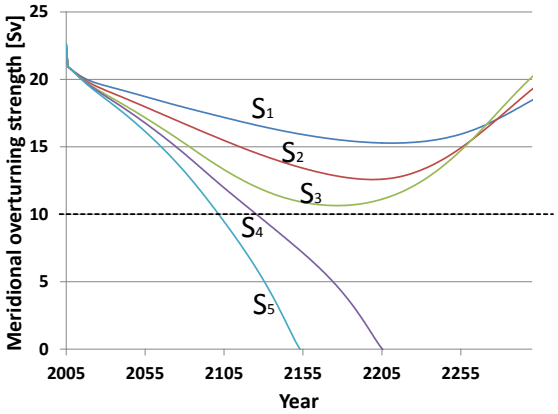

(b) Possible trajectories of the overturning strength

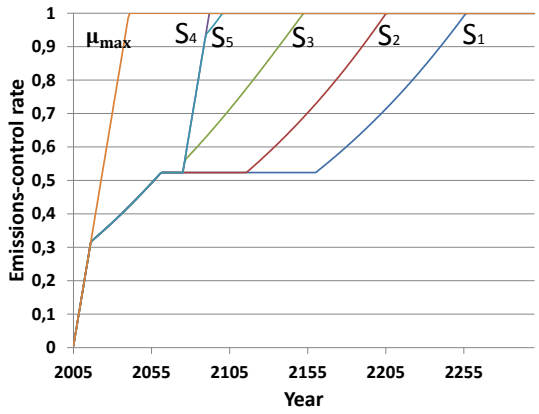

(c) Optimal emission reduction policy

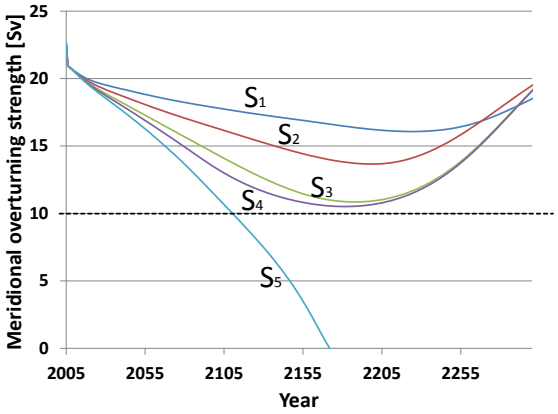

(d) Possible trajectories of the overturning strength

Fig. 1.13 Sensitivity of the results with respect to limited abatement options, i.e. $l = 0.028$

less restrictive. More specifically, we assume the maximum allowable annual increase in abatement l to be 0.25. This number is certainly too high for the very near term, but might be conceivable later on when backstop technologies substitute for our present abatement options. Owing to uncertainty about future abatement options, we present this simulation as an optimistic antipode to Figure 1.13. This may provide us with an impression of how different expectations about future inertia in abatement lead to different policy strategies and thus different effects of risk aversion. Compared to Figure 1.5, Figure 1.14 shows only negligible differences in the optimal control rates and the THC dynamics exhibit the same qualitative behaviour. We may conclude that risk aversion has some effect when inertia is assumed, in particular if inertia implies very restrictive abatement options. However, less restrictive limitations in the future are conceivable, especially if new technologies are

available. For future research, it would thus be worthwhile to improve on the representation of inertia in the model and to account for uncertainty in future abatement options.[11] This would allow investigating how risk aversion is affected by this multi-faceted uncertainty.

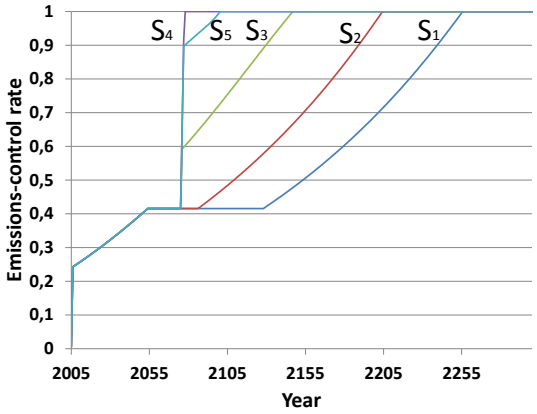

(a) Optimal emission reduction policy

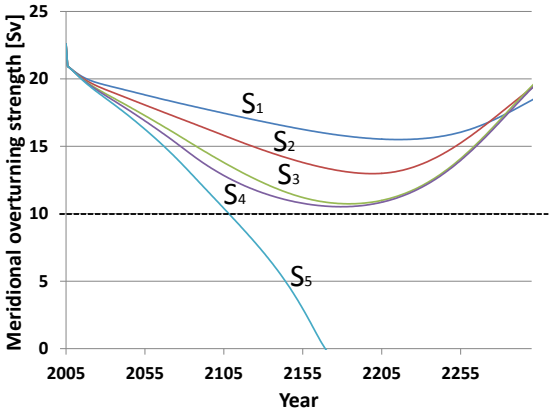

(b) Possible trajectories of the overturning strength

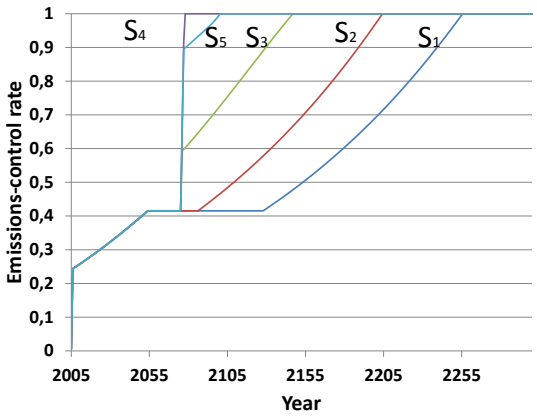

(c) Optimal emission reduction policy

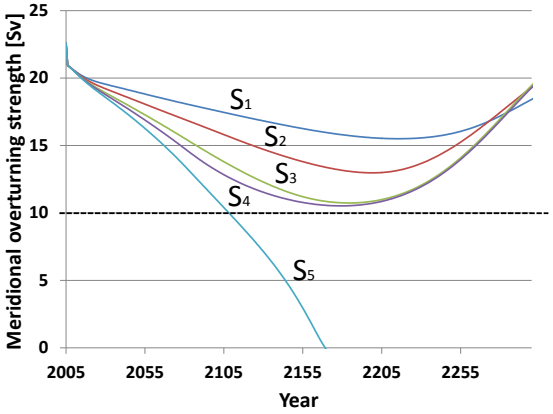

(d) Possible trajectories of the overturning strength

Fig. 1.14 Sensitivity of the results with respect to limited abatement options, i.e. $l = 0.25$

1.4 Conclusion

In the most common IAMs, higher risk aversion does not imply stronger optimal climate policy efforts in the next few decades. This result appears counterintuitive as in particular

[11] A possible approach for a more refined modelling of inertia is to implement quadratic adjustment costs in the costs function. See Ha-Duong et al. [22] for implementation in an IAM and see Dixit and Pindyck [14] for application in real option models tackling general questions of investment under uncertainty.

looming climate catastrophes pose one of the greatest threats of climate change. Accordingly, optimal policy should be susceptible to differing concerns regarding these risks. One cause of this problem is the assumption of the CRRA utility specification, as it leads to an interwoven representation of the decision maker's preferences for time and risk. However, as demonstrated by Ackerman et al. [3], the puzzle is not solved by replacing the CRRA utility with a specification that disentangles these preferences, as shown by the Epstein-Zin utility specification. The reasons that have been conjectured by Ackerman et al. [3], draw upon the model's strong assumptions on abatement and the insufficient representation of catastrophic risk. These assumptions imply that the policy maker has the means at his or her disposal to avoid a meaningful part of the risk after learning, rendering risk aversion irrelevant for near-term climate policies.

To advance the investigation of this puzzle, we fully couple a version similar to the Epstein-Zin-DICE model employed by Ackerman et al. [3] with a dynamic model of the Atlantic thermohaline circulation. The dynamic model of the THC overturning strength promises a more refined representation of climate change risk.

Despite the model extension, the sensitivity of the optimal near-term policy with respect to risk aversion is qualitatively similar to the results obtained by Ackerman et al. [3]. However, in contrast to Ackerman et al. [3], the extended model allows us to monitor the response of a specific climate system at risk. As a result, we can infer how the associated risk of its vulnerability evolves. Hence, we can pinpoint the characteristics of this specific risk element that may lead to the insensitivity result.

Consistent with Ackerman et al. [3], we recognise that risk aversion is of little importance if the policy maker is assumed to have all means at his or her disposal to adjust emission control instantaneously to the desired rate after learning. Late but fine-tuned efforts suffice to prevent the THC from collapsing in the more likely climate sensitivity values. The risk that could influence near-term optimal policy is only caused by a very high and unlikely climate sensitivity value. In this value the near-term optimal policy efforts by a mildly risk-averse decision maker are too late to prevent the THC from shutting down. The simulations, however, prove that even a more risk-averse policy maker does not place much more importance on the risk associated with this value and near-term abatement is only slightly increased.

A thorough sensitivity analysis shows that this result for risk aversion is highly robust to a wide choice of values within reasonable ranges. Even if learning occurs very late, risk

aversion does not increase policy efforts significantly and it does not help prevent the THC from collapsing in a further high climate sensitivity value.

Finally, we direct attention to the reasons for the small effect of risk aversion. For the likely climate sensitivity values, this tipping point is rather distant in the future, which allows late action. Moreover, as indicated by the sensitivity analysis, the ramifications caused by a collapse are great but not great enough to justify taking precautionary measures to reduce the risk in the unlikely states that would put too high a burden on the economy. Additionally, it is assumed that there is no inertia limiting the abatement options. In sum, there are four reasons for the small effect of risk aversion in this fully coupled extended DICE model: the long period until the risk materialises, the relatively low costs incurred by a weakening, the low probability associated with the risk, and the optimistic assumptions with respect to the abatement options.

With respect to the last mentioned point, we also provide simulations in which risk aversion has some effect when inertia restricts abatement options significantly. In this case, a higher concern for risk implies higher abatement efforts that succeed in safeguarding the THC for more climate sensitivity values. However, the extent to which inertia will limit abatement options in the future is highly uncertain. Our simulations also illustrate that more optimistic assumptions would imply little effect of risk aversion. For future research, it would thus be worthwhile to account for uncertainty in future abatement options and to investigate how risk aversion is affected by this multi-faceted uncertainty. Our study can thus be improved by more refined representations of uncertainty. Firstly, uncertainty in many more crucial parameters could be taken into account. Secondly, unlike Urban and Keller [78], but similar to Keller et al. [32], we refrain from modelling the other source of uncertainty in global mean temperature projections, which is the inverse thermal capacity of the atmospheric layer and the upper oceans. The inverse thermal capacity is negatively correlated with climate sensitivity and thus has an antagonistic effect on temperature projections (Yohe et al. [82], Urban and Keller [77], Goes et al. [20]). Our approach might thus be criticised for potentially overestimating the magnitude of transient temperature increase and thus exaggerating the risk involved. Yet, the result that risk aversion has little effect would not change for less severe risk.

Appendices

1 A Robustness Check

As this research clearly relates to the study by Ackerman et al. [3], here we clarify whether our model could reproduce their results. We may demonstrate this for their E_1 model run. We keep the default damage function of the original DICE model, i.e. we set $a_2 = 0.0028388$ and ignore the feedback from the THC module to DICE. Note that there are different assumptions in the two models. Firstly, we apply the updated transient temperature change equation from Cai et al. [6], where, in contrast to Nordhaus [58] and Ackerman et al. [3], the radiative forcing depends only on current carbon concentration in the atmosphere. Secondly, while the EZ-DICE model by Ackerman et al. [3] is designed for decadal time steps, our model incorporates annual time steps as the DICE-CJL model by Cai et al. [6].

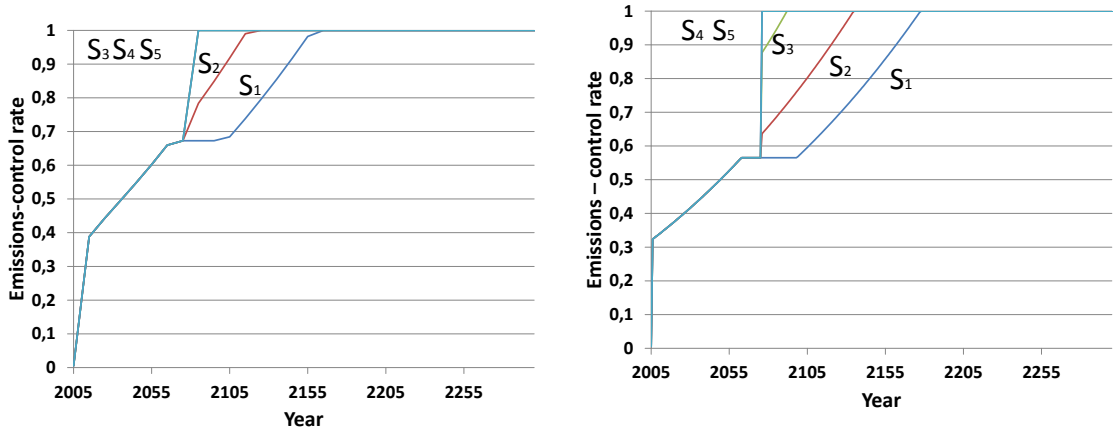

Fig. 1.A.1 Comparison of the optimal emission redution policies generated by the two models, the EZ-DICE model by Ackerman et al. [3] (left) and the IAM in our paper, in which the feedback from the THC to DICE model is ignored (right).

Comparing the results of the two models, we recognise that the assumptions in our model offer a more differentiated view of the optimal policy. While in Ackerman et al. [3] only one policy path is given for three very different climate sensitivity values, $S_3 - S_5$, our model produces two distinct control trajectories. The discrepancy mainly comes from the model recalibration by Cai et al. [6] associated with the refined time scale. This is explained and discussed in more detail by Marten and Newbold [49].

1 B Numerical Solution

Here, we draw attention to the non-convex nature of the optimisation problem. This non-convexity occurs, for instance, when considering tipping elements that switch to another state at some point in time. As finding the computational solution to such a problem is non-trivial, we explain our numerical approach in more detail in the following.

The more refined time step compared to DICE gives rise to a higher dimension of the decision variables space, which amounts to 1200 variables (consumption and abatement paths over 600 years). Furthermore, the existence of the THC stability threshold induces local optima, which creates numerical problems that are commonly tackled by global optimisation methods. Yet, the global solvers available in GAMS are rather restricted with respect to the allowable size of the model. Instead we implement a multi-start heuristic approach to the CONOPT3 solver in the GAMS environment using different initial values.[12] The algorithm in CONOPT3 is based on a generalised reduced gradient (GRG) technique, which relies on the gradient information and has a comparative advantage in handling large models such as ours.[13] The three pillars of successfully applying the solver to a non-linear problem are the initial values, scaling, and bounds. Furthermore, the solver is designed to operate with smooth functions only, which is why throughout the model design process, e.g. developing the damage cost function f_{THC}, we verify this property to ensure convergence.

The approach we implement calls the NLP solver CONOPT3 from 100 random initial vectors within the bounds of the variables. The histogram in Figure 1.B.1 depicts the solutions of the multi-start approach for the default simulation (Figure 5). Out of 100 model runs, 50 converge to a feasible solution with 18 converging to the optimum. As mentioned above, many of the solutions recovered by our algorithm are local. In this respect, a good alternative could be to refer to the differential evolution algorithm, which converges to the same solution for many initial conditions (see Keller et al. [32] and Moles et al. [56]).

To illustrate the non-convexity of the problem, we perturb the near-term optimal emissions-control rate and inspect the associated change in the objective function (first-period Epstein-

[12] The GAMS code is available upon request.

[13] The GRG is a generalisation of the reduced gradient (RG) technique which allows nonlinear constraints. The key idea behind the GRG is to transform the constrained problem to bound constrained and thus reduce the number of independent variables. The further search is performed in the direction of the gradient of the superbasic variables. There are many possible GRG algorithms and CONOPT3 identifies the most appropriate for the particular problem setting. Please refer to Abadie and Carpentier [1] for the concept of GRG and to Drud [16] for its implementation in CONOPT.

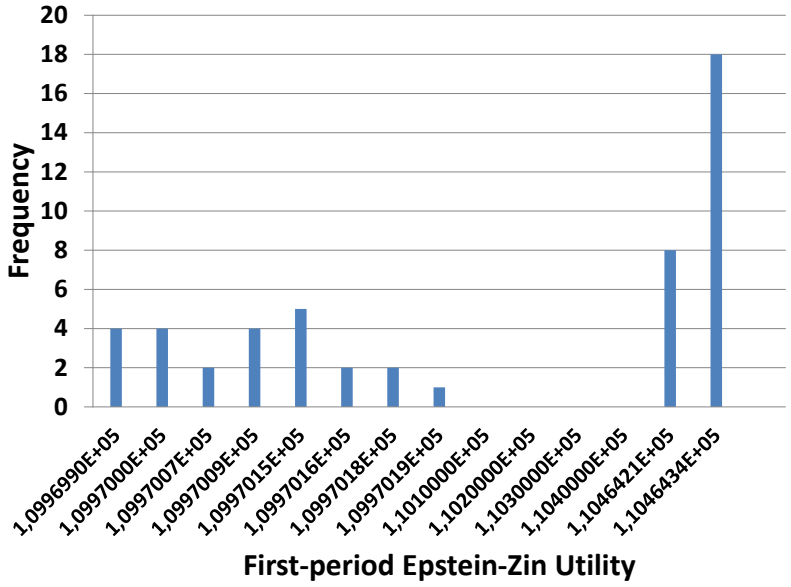

Fig. 1.B.1 Frequency of solutions found by a multi-start approach for different initial values

Zin utility). As the reference we choose the value of the first-period Epstein-Zin utility that corresponds to the optimal emissions-control rate for the scenario in which the THC-related damage costs are neglected. Figure 1.B.2 depicts the relative change of the first-period Epstein-Zin utility value for different abatement rates in the year 2075. The point G is associated with global optimum. An increase in the abatement rate leads to a decrease in utility. The reason is that the benefits associated with delaying the THC collapse do not exceed the near-term costs. Utility is continuously decreasing with the emissions-control rate in the near-term until the abatement efforts are sufficient to prevent the THC collapse in state S_5. As soon as the circulation is safeguarded, the THC-induced damage costs over the long period of time sum up to nearly zero. This is reflected in the sudden increase in the first-period Epstein-Zin utility at about 68.6 per cent of abatement in the year 2075. Nevertheless, the costs of preventing the THC collapse in S_5 exceeds the benefits. Thus, preserving the THC describes only a local optimum, which is depicted by L.

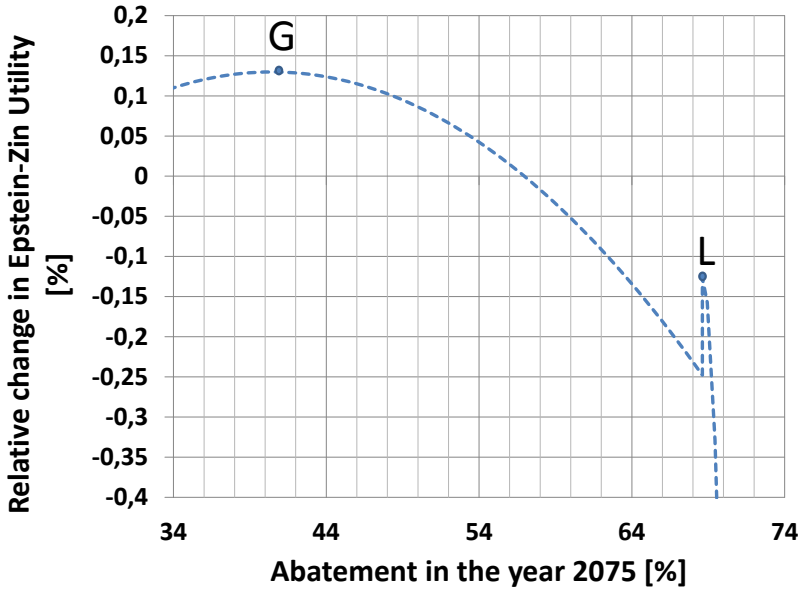

Fig. 1.B.2 Relative percentage change in the first-period Epstein-Zin utility for different values of abatement rates in the year 2075. The percentage change is considered relative to the first-period Epstein-Zin utility for the emissions-control rate that neglects potential THC-related damages. The points *G* and *L* indicate the location of the global and local optimum, respectively

1 C Calibration

For the DICE-CJL model parameters, refer to Cai et al. [6] as well as Cai et al. [7] and the accompanying website.

Table 1.C.1 Parameters crucial to the present study

Parameter	Value
Rate of pure time preference, ρ	0.0113
Intertemporal elasticity of substitution, IES	1.5 per cent
Learning date	year 2075
North Atlantic hydrological sensitivity, h_2^{tot}	0.0525 Sv $^{\circ}C^{-1}$
THC collapse specific damages, d_m	0.03, fraction of global GDP
Initial emissions-control rate, $\mu(1)$ (Kyoto agreement)	0.005

Table 1.C.2 The THC model parameters (Zickfeld [86])

Parameter	Value
Relaxation temperature of the box 1 , T_1^*	$6.6°C$
Relaxation temperature of the box 2, T_2^*	$2.7°C$
Relaxation temperature of the box 3, T_3^*	$11.7°C$
Volume of the box 1, V_1	$1.1 \times 10^{17} m^3$
Volume of the box 2, V_2	$0.4 \times 10^{17} m^3$
Volume of the box 3, V_3	$0.68 \times 10^{17} m^3$
Volume of the box 4, V_4	$0.05 \times 10^{17} m^3$
Thermal coupling constant, box 1	0.059
Thermal coupling constant, box 2	0.059
Thermal coupling constant, box 3	0.1777
Northern Hemisphere temperature conversion constant, p_{NH}	1.07
Southern Hemisphere temperature conversion constant, p_{SH}	0.93
South Atlantic temperature downscaling constant, p_1	0.86
North Atlantic temperature downscaling constant, p_2	1.07
Tropics temperature downscaling constant p_3	0.79
Hydrological sensitivity, h_1	-0.005 Sv $°C^{-1}$
Present day temperature of the box 1, $T_1(1)$	$6.5\ °C$
Present day temperature of the box 2, $T_2(1)$	$4.7\ °C$
Present day temperature of the box 3, $T_3(1)$	$11.4\ °C$
Present day volume transport, $m(1)$	22.6 Sv
Thermal expantion coefficient, ζ	$1.7 \times 10^{-4}\ °C^{-1}$
Haline expantion coefficient, β	$8 \times 10^{-4} psu^{-1}$
Empirical flow constant, k	$25.4 \times 10^{17} m^3 a^{-1}$
Reference salinity, S_0	35 psu

1 D Sensitivity Analysis with Respect to m_{crit}

Here, we discuss briefly an alternative calibration for m_{crit}. For the simulation illustrated in Figure 1.D.1, we adopt the assumption that m_{crit} is zero. In section 1.3 we conjecture that this assumption might render the threat of a THC collapse and the aversion to the risk involved as less important. Figure 1.D.1 confirms this conjecture. Risk aversion has little effect on near–term policy. In both cases of alternative attitudes to risk, the near-term policy efforts are lower than in the baseline case (by 6.58 percentage points), as the THC damage costs are incurred only when circulation stops altogether. These reduced efforts lead to a slowdown in more states of nature than in the baseline case.

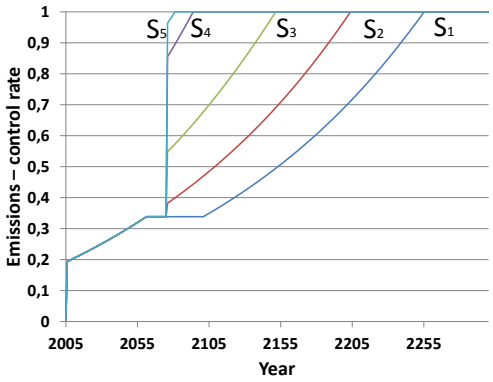

(a) Optimal emission reduction policy

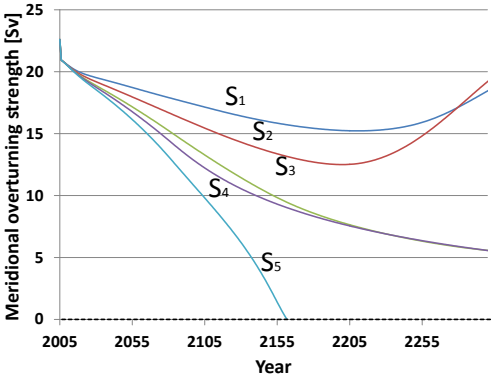

(b) Possible trajectories of the overturning strength

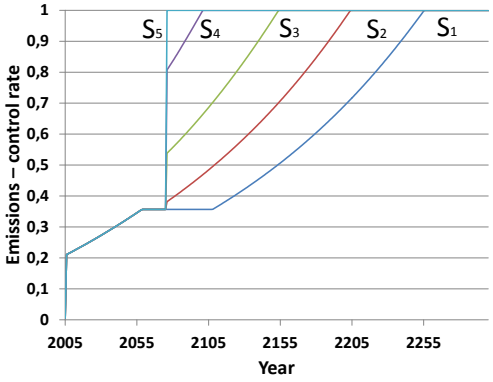

(c) Optimal emission reduction policy

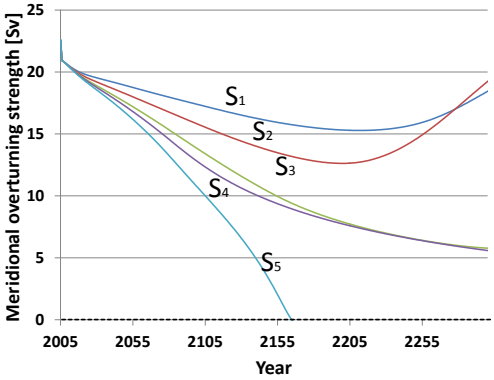

(d) Possible trajectories of the overturning strength

Fig. 1.D.1 Sensitivity of the results with respect to $m_{crit} = 0$ Sv i.e. THC-related damages are associated with the circulation breakdown.

Changing the value of m_{crit} by ± 3 Sv, as in Figure 1.D.2 and Figure 1.D.3, shows that the results on the effects of risk aversion are rather robust with respect to m_{crit}.

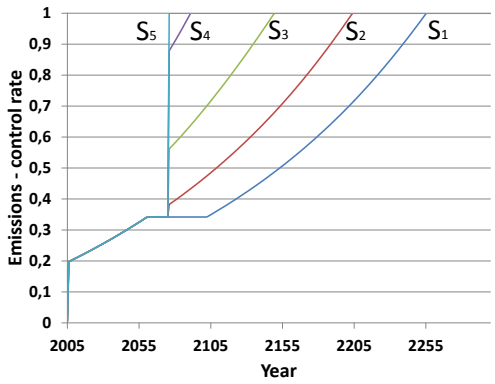

(a) Optimal emission reduction policy

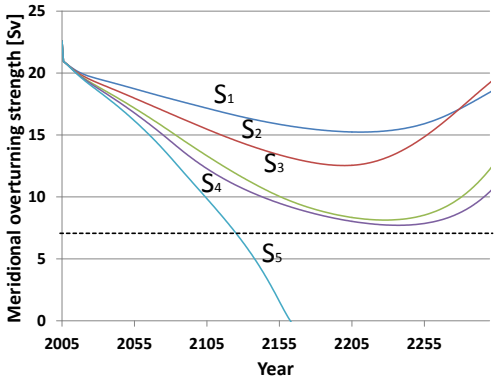

(b) Possible trajectories of the overturning strength

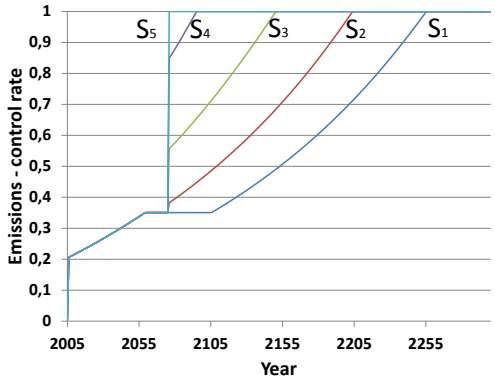

(c) Optimal emission reduction policy

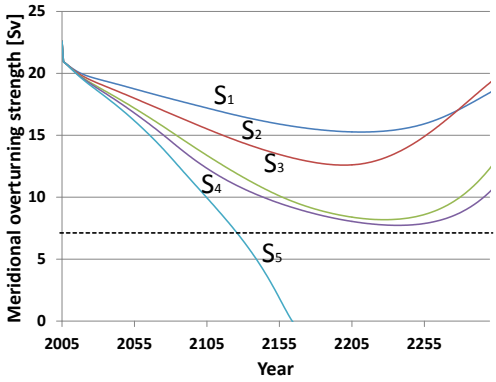

(d) Possible trajectories of the overturning strength

Fig. 1.D.2 Sensitivity of the results with respect to lower value of critical weakening, $m_{crit} = 7$ Sv

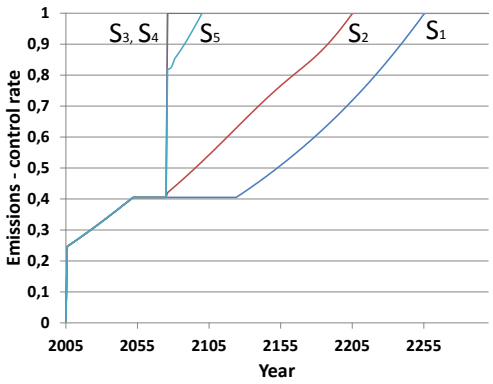

(a) Optimal emission reduction policy

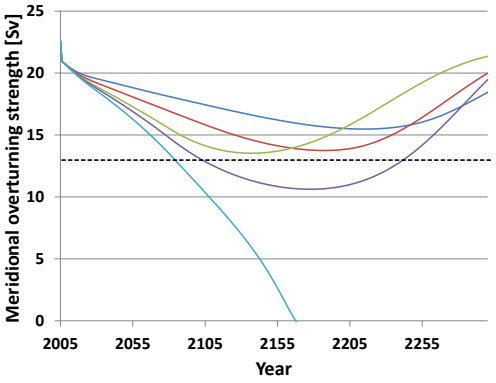

(b) Possible trajectories of the overturning strength

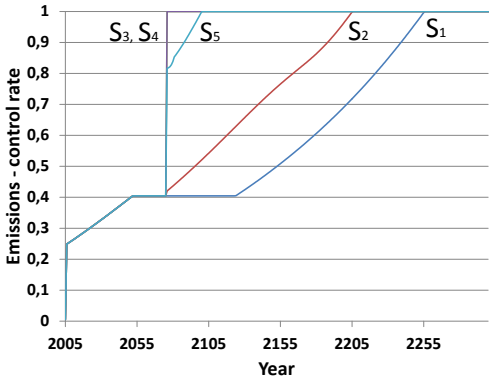

(c) Optimal emission reduction policy

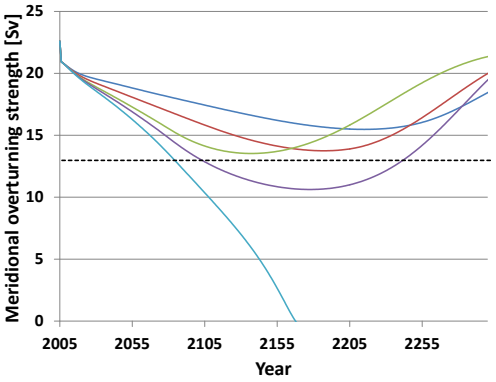

(d) Possible trajectories of the overturning strength

Fig. 1.D.3 Sensitivity of the results with respect to higher value of critical weakening, $m_{crit} = 13$ Sv

References

[1] Abadie, Carpentier, 1969. Optimization. Academic press, Ch. Generalization of the Wolfe Reduced Gradient Method to the case of Nonlinear Constraints, pp. 37–47.

[2] Ackerman, F., DeCanio, S., Howarth, R., Sheeran, K., 2009. Limitations of integrated assessment models of climate change. Climatic Change 95 (3-4), 297–315.

[3] Ackerman, F., Stanton, E. A., Bueno, R., 2013. Epstein-Zin utility in DICE: Is risk aversion irrelevant to climate policy? Environmental and Resource Economics 56 (1), 73–84.

[4] Bansal, R., Yaron, A., 2004. Risks for the long run: A potential resolution of asset pricing puzzles. The Journal of Finance 59 (4), 1481–1509.

[5] Barro, R. J., 2013. Environmental protection, rare disasters, and discount rates.Working Paper 19258, National Bureau of Economic Research.

[6] Cai, Y., Judd, K. L., Lontzek, T. S., 2012. Continuous-time methods for integrated assessment models. Working Paper 18365, National Bureau of Economic Research.

[7] Cai, Y., Judd, K. L., Lontzek, T. S., 2012. Open science is necessary. Nature Climate Change 2, 299–299.

[8] Cai, Y., Judd, K. L., Lontzek, T. S., 2013. The social cost of stochastic and irreversible climate change. Working Paper 18704, National Bureau of Economic Research.

[9] Cass, D., 1965. Optimum growth in an aggregative model of capital accumulation. The Review of Economic Studies 32 (3), 233–240.

[10] Cline, W. R., 1992. The Economics of Global Warming. No. 39 in Peterson Institute Press: All Books. Peterson Institute for International Economics.

[11] Crost, B., Traeger, C. P., 2010. Risk and aversion in the integrated assessment of climate change. CUDARE Working Paper Series 1104R, University of California at Berkeley, Department of Agricultural and Resource Economics and Policy.

[12] DeLong, J. B., Magin, K., 2009. The US equity return premium: Past, present, and future. The Journal of Economic Perspectives 23 (1), pp. 193–208.

[13] den Elzen, M. G., van Vuuren, D., van Vliet, J., 2010. Postponing emission reductions from 2020 to 2030 increases climate risks and long-term costs. Climatic Change 99 (1-2), 313–320. URL http://dx.doi.org/10.1007/s10584-010-9798-5

[14] Dixit, A. K., Pindyck, R. S., 1994. Investment under Uncertainty. Princeton University Press.

[15] Drijfhout, S., Weber, S., Swaluw, E., 2011. The stability of the MOC as diagnosed from model projections for pre-industrial, present and future climates. Climate Dynamics 37 (7-8), 1575–1586.

[16] Drud, A., 1992. Conopt - a large-scale grg code. ORSA journal on computing 6, 207–216.

[17] Epstein, L. G., Zin, S. E., 1989. Substitution, risk aversion, and the temporal behavior of consumption and asset returns: A theoretical framework. Econometrica 57 (4), pp. 937–969.

[18] Epstein, L. G., Zin, S. E., 1991. Substitution, risk aversion, and the temporal behavior of consumption and asset returns: An empirical analysis. Journal of Political Economy 99, 263–286.

[19] Ganachaud, A., Wunsch, C., 2000. Improved estimates of global ocean circulation, heat transport and mixing from hydrographic data. Nature 408, 453–457.

[20] Goes, M., Tuana, N., Keller, K., 2011. The economics (or lack thereof) of aerosol geoengineering. Climatic Change 109 (3-4), 719–744.

[21] Grubler, A., Naki‘cenovi‘c, N., Victor, D. G., 1999. Dynamics of energy technologies and global change. Energy Policy 27 (5), 247 – 280.

[22] Ha-Duong, M., Grubb, M. J., Hourcade, J.-C., 1997. Influence of socioeconomic inertia and uncertainty on optimal CO2-emission abatement. Nature 390, 270–273.

[23] Ha-Duong, M., Treich, N., 2004. Risk aversion, intergenerational equity and climate change. Environmental and Resource Economics 28 (2), 195–207.

[24] Hall, J.W., Lempert, R. J., Keller, K., Hackbarth, A., Mijere, C., McInerney, D. J., 2012. Robust climate policies under uncertainty: A comparison of robust decision making and info-gap methods. Risk Analysis 32 (10), 1657–1672.

[25] Hawkins, E., Smith, R. S., Allison, L. C., Gregory, J. M., Woollings, T. J., Pohlmann, H., de Cuevas, B., 2011. Bistability of the Atlantic overturning circulation in a global climate model and links to ocean freshwater transport. Geophysical Research Letters 38 (10), L10605.

[26] Hofmann, M., Rahmstorf, S., 2009. On the stability of the Atlantic meridional overturning circulation. Proceedings of the National Academy of Sciences 106 (49), 20584–20589.

[27] Hope, C., 2006. The marginal impact of CO2 from PAGE2002: An integrated assessment model incorporating the IPCC's five reasons for concern. Integrated Assessment 6 (1), 19–56.

[28] IPCC, 2007. Summary for policymakers. In: Solomon, S., D., Qin, M., Manning, Z., Chen, M., Marquis, K., Averyt, M., Tignor, Miller, H. (Eds.), Climate Change 2007: The Physical Science Basis. Contribution of Working Group I to the Fourth Assessment Report of the Intergovernmental Panel on Climate Change. Cambridge University Press, Cambridge, United Kingdom and New York, NY, USA.

[29] Iverson, T., Perrings, C., 2012. Precaution and proportionality in the management of global environmental change. Global Environmental Change 22 (1), 161 – 177.

[30] Jensen, S., Traeger, C., 2014. Optimal climate change mitigation under long-term growth uncertainty: Stochastic integrated assessment and analytic findings. European Economic Review forthcoming

[31] Kaufman, N., 2012. The bias of integrated assessment models that ignore climate catastrophes. Climatic Change 110 (3-4), 575–595.

[32] Keller, K., Bolker, B. M., Bradford, D. F., 2004. Uncertain climate thresholds and optimal economic growth. Journal of Environmental Economics and Management 48, 723–741.

[33] Keller, K., McInerney, D., 2008. The dynamics of learning about a climate threshold. Climate Dynamics 30 (2-3), 321–332.

[34] Keller, K., Tan, K., Morel, F. M., Bradford, D. F., Jan. 2000. Preserving the ocean circulation: Implications for climate policy. NBER Working Papers 7476, National Bureau of Economic Research, Inc.

[35] Kelly, D. L., Kolstad, C. D., 1999. Bayesian learning, growth, and pollution. Journal of Economic Dynamics and Control 23, 491–518.

[36] Koopmans, T. C., 1963. On the concept of optimal economic growth. Cowles Foundation Discussion Papers 163, Cowles Foundation for Research in Economics, Yale University.

[37] Kopp, R. E., Hsiang, S. M., Oppenheimer, M., 2013. Empirically calibrating damage functions and considering stochasticity when integrated assessment models are used as decision tools. In: Impacts World 2013 Conference Proceedings.

[38] Kreps, D. M., Porteus, E. L., 1978. Temporal resolution of uncertainty and dynamic choice theory. Econometrica 46 (1), pp. 185–200.

[39] Kriegler, E., Hall, J. W., Held, H., Dawson, R., Schellnhuber, H. J., 2009. Imprecise probability assessment of tipping points in the climate system.

[40] Kuhlbrodt, T., Rahmstorf, S., Zickfeld, K., Vikebo, F., Sundby, S., Hofmann, M., Link, P. M., Bondeau, A., Cramer, W., Jaeger, C., 2009. An integrated assessment of changes in the thermohaline circulation. Climatic Change 96 (4), 489–537.

[41] Lecocq, F., Hourcade, J. C., Ha-Duong, M., 1998. Decision making under uncertainty and inertia constraints: sectoral implications of the when flexibility. Energy Economics 20 (4/5), 539–555.

[42] Lemoine, D., Traeger, C., 2014. Watch your step: Optimal policy in a tipping climate. American Economic Journal: Economic Policy 6 (1), 137–66.

[43] Lempert, R. J., Sanstad, A. H., Schlesinger, M. E., 2006. Multiple equilibria in a stochastic implementation of DICE with abrupt climate change. Energy Economics 28 (5-6), 677–689.

[44] Lenton, T., Ciscar, J.-C., 2013. Integrating tipping points into climate impact assessments. Climatic Change 117 (3), 585–597.

[45] Lenton, T. M., Held, H., Kriegler, E., Hall, J.W., Lucht,W., Rahmstorf, S., Schellnhuber, H. J., 2008. Tipping elements in the Earth's climate system. Proceedings of the National Academy of Sciences of the United States of America 105, 1786–1793.

[46] Link, P., Tol, R., 2011. Estimation of the economic impact of temperature changes induced by a shutdown of the thermohaline circulation: an application of FUND. Climatic Change 104 (2), 287–304.

[47] Lontzek, T. S., Cai, Y., Judd, K. L., 2012. Tipping points in a dynamic stochastic IAM. RDCEP Working Paper 12-03, RDCEP.

[48] Manabe, S., Stouffer, R. J., 1994. Multiple-century response of a coupled oceanatmosphere model to an increase of atmospheric carbon dioxide. Journal of Climate 7, 5–23.

[49] Marten, A. L., Newbold, S. C., Jun. 2013. Temporal resolution and DICE. Nature Clim. Change 3 (6), 526–527. URL http://dx.doi.org/10.1038/nclimate1893

[50] Mastrandrea, M. D., Schneider, S. H., 2001. Integrated assessment of abrupt climatic changes. Climate Policy 1 (4), 433–449.

[51] Matei, D., Baehr, J., Jungclaus, J. H., Haak, H., Mller, W. A., Marotzke, J., 2012. Multiyear prediction of monthly mean Atlantic meridional overturning circulation at 26.5° n. Science 335 (6064), 76–79.

[52] McCarl, B., 2013. McCarl Expanded GAMS User Guide. GAMS Development Corporation.

[53] McInerney, D., Keller, K., 2008. Economically optimal risk reduction strategies in the face of uncertain climate thresholds. Climatic Change 91, 29–41.

[54] McInerney, D., Lempert, R., Keller, K., 2012. What are robust strategies in the face of uncertain climate threshold responses? Climatic Change 112 (3-4), 547–568.

[55] Mehra, R., Prescott, E. C., 1985. The equity premium: A puzzle. Journal of Monetary Economics 15 (2), 145 – 161.

[56] Moles, C. G., Banga, J. R., Keller, K., 2004. Solving nonconvex climate control problems: pitfalls and algorithm performances. Appl. Soft Comput. 5 (1), 35–44. URL http://dx.doi.org/10.1016/j.asoc.2004.03.011

[57] Neubersch, D., Held, H., Otto, A., 2014. Operationalizing climate targets under learning: An application of cost-risk analysis. Climatic Change 126 (3), 305–318.

[58] Nordhaus, W., 2008. A Question of Balance: Weighing the Options on Global Warming Policies. Yale University Press.

[59] Nordhaus, W., 2013. The Climate Casino. Yale University Press. URL http://www.jstor.org/stable/j.ctt5vkrpp

[60] Nal, E., Oppenheimer, M., 2007. The economics of the thermohaline circulation – a problem with multiple thresholds of unknown locations. Resource and Energy Economics 29 (4), 262 – 283.

[61] O'Neill, B. C., Crutzen, P., Grubler, A., Duong, M. H., Keller, K., Kolstad, C., Koomey, J., Lange, A., Obersteiner, M., Oppenheimer, M., Pepper, W., Sanderson, W., Schlesinger, M., Treich, N., Ulph, A., Webster, M., Wilson, C., 2006. Learning and climate change. Climate Policy 6 (5), 585–589.

[62] Pindyck, R. S., 2013. Climate change policy: What do the models tell us? Working Paper 19244, National Bureau of Economic Research.

[63] Rahmstorf, S., Ganopolski, A., 1999. Long-term global warming scenarios computed with an efficient coupled climate model. Climatic Change 43 (2), 353–367.

[64] Ramsey, F. P., 1928. A mathematical theory of saving. The Economic Journal 38 (152), 543–559.

[65] Ring, M., Schlesinger, M., 2012. Bayesian learning of climate sensitivity i: Synthetic observations. Atmospheric and Climate Sciences 2 (4), 464–473.

[66] Roe, G. H., Baker, M. B., 2007. Why is climate sensitivity so unpredictable? Science 318 (5850), 629–632.

[67] Schleussner, C.-F., Levermann, A., Meinshausen, M., 2014. Probabilistic projections of the Atlantic overturning. Climatic Change 127 (3-4), 579–586.

[68] Schneider, S. H., Thompson, L., 2000. Simple climate model used in economic studies of global change. In: DeCanio, S. J., Howarth, R. B., Sanstad, A. H., Schneider, S. H., Thompson, S. L. (Eds.), New Directions in the Economics and Integrated Assessment of Global Climate Change. Pew Center on Global Climate Change, Ch. 5, pp. 59–80.

[69] Stern, N., 2013. The structure of economic modeling of the potential impacts of climate change: Grafting gross underestimation of risk onto already narrow science models. Journal of Economic Literature 51 (3), 838–59.

[70] Stocker, T. F., Schmittner, A., 1997. Influence of co2 emission rates on the stability of the thermohaline circulation. Nature.

[71] Stommel, H., 1961. Thermohaline convection with two stable regimes of flow. Tellus 13 (2), 224–230.

[72] Tallarini, T. D. J., 2000. Risk-sensitive real business cycles. Journal of Monetary Economics 45 (3), 507 – 532.

[73] Tol, R., 1998. Potential slowdown of the thermohaline circulation and climate policy. Discussion paper ds98/06, Institute for Environmental Studies Vrije Universiteit Amsterdam.

[74] Tol, R., 2009. An analysis of mitigation as a response to climate change. Discussion paper, Copenhagen Consensus on Climate.

[75] Trenberth, K. E., Caron, J. M., 2001. Estimates of meridional atmosphere and ocean heat transports. Journal of Climate 14, 3433 – 3443.

[76] Urban, N. M., Holden, P. B., Edwards, N. R., Sriver, R. L., Keller, K., 2014. Historical and future learning about climate sensitivity. Geophysical Research Letters 41 (7), 2543–2552.

[77] Urban, N. M., Keller, K., 2009. Complementary observational constraints on climate sensitivity. Geophysical Research Letters 36 (4), n/a–n/a, l04708. URL http://dx.doi.org/10.1029/2008GL036457

[78] Urban, N. M., Keller, K., 2010. Probabilistic hindcasts and projections of the coupled climate, carbon cycle and Atlantic meridional overturning circulation system: a Bayesian fusion of century-scale observations with a simple model. Tellus A 62 (5), 737–750.

[79] Vissing-Jrgensen, A., Attanasio, O. P., 2003. Stock-market participation, intertemporal substitution, and risk-aversion. The American Economic Review 93 (2), 383–391.

[80] Waisman, H., Guivarch, C., Grazi, F., Hourcade, J., 2012. The Imaclim-R model: infrastructures, technical inertia and the costs of low carbon futures under imperfect foresight. Climatic Change 114 (1), 101–120.

[81] Weitzman, M., 2009. On modeling and interpreting the economics of catastrophic climate change. Review of Economics and Statistics 91, 1–19.

[82] Yohe, G., Andronova, N., Schlesinger, M., 2004. To hedge or not against an uncertain climate future? Science 306 (5695), 416–417. URL http://www.sciencemag.org/content/306/5695/416.short

[83] Zickfeld, K., Bruckner, T., 2003. Reducing the risk of abrupt climate change: Emissions corridors preserving the Atlantic thermohaline circulation. Integrated Assessment 4 (2), 106–115.

[84] Zickfeld, K., Bruckner, T., 2008. Reducing the risk of Atlantic thermohaline circulation collapse: sensitivity analysis of emissions corridors. Climatic Change 91, 291–315.

[85] Zickfeld, K., Levermann, A., Morgan, M., Kuhlbrodt, T., Rahmstorf, S., Keith, D., 2007. Expert judgements on the response of the Atlantic meridional overturning circulation to climate change. Climatic Change 82, 235–265.

[86] Zickfeld, K., Slawig, T., Rahmstorf, S., 2004. A low-order model for the response of the Atlantic thermohaline circulation to climate change. Ocean Dynamics 54, 8–26.

Chapter 2

Can India Prevent Summer Monsoon Extremes? An Integrated Assessment of Climate Change and Environmental Policies

2.1 Introduction

A major concern in the climate change debate is the required stringency of emission reduction efforts to prevent large-scale changes in the Earth system. Accordingly, in the last few years increasingly numerous integrated assessment studies explored optimal emission pathways while explicitly accounting for these changes, also referred to as tipping points (e.g. see Belaia et al. [5] for the Atlantic Thermohaline Circulation, Nicholls et al. [39] for the West Antarctic Ice Sheet and Cai et al. [9] for multiple interacting tipping points).

Other potential tipping elements, such as the Indian Summer Monsoon (ISM) received less attention in integrated assessment studies, despite the fact that: (i) this climate system has the potential to shift rapidly into a radically different monsoon circulation (Wang et al. [58] and Zickfeld et al. [66]); (ii) shifting dynamics have been already observed (Bollasina et al. [7]); and (iii) the lives of more than one billion people are affected by changes in the ISM's precipitation patterns. How the ISM circulation changes partially depends on global warming, to which India as one of many countries, contributes, as well as on local air pollution, which can be controlled by India's own efforts (e.g. Turner and Annamalai [54]). Different combinations of global and local policies can thus lead to different ISM

precipitation patterns in the future. This paper contributes to the literature by providing a framework that allows analysing alternative emission policies and the resultant ISM dynamics in one fully coupled regional integrated assessment model.

The ISM dynamics are complex in nature, featuring interactions with land, the ocean and the atmosphere (e.g. Webster and Yang [60], Liu and Yanai [30], Robock et al. [48], Kucharski et al. [28], Ramisch et al. [47]). Air pollution, for instance caused by sulphur dioxide (SO_2) emissions, can alter these dynamics significantly (e.g. Zickfeld et al. [66]). Sulfur dioxide emissions can lead to a weakening of the ISM rainfall strength, which can ultimately lead to extensive droughts (e.g. Knopf et al. [27], Bollasina et al. [7]). In contrast, increasing temperatures can widen the range possible precipitation strength, which can lead to more unusually heavy rainfall events and destructive floods (e.g. Knopf et al. [27]).

The timely arrival, as well as an even spatial and temporal distribution, of ISM rainfall constitutes an important factor for economic activity in India (Rajagopalan [46]). For some very large regions in India the ISM provides almost the entire rainfall of the whole year (Rajagopalan [46]). Furthermore, half of Indian agriculture is rainfed (Rajagopalan [46]) and approximately 15% of the Indian power generation is hydroelectric from rainfed rivers (Central Electricity Authority India [13]). Rapid transitions in the monsoon circulation may exceed the capabilities to adapt, particularly in poor and rural populations (Zickfeld et al. [66]).

For many years India had been refusing to take on CO_2 emission reduction obligations, arguing that all available resources need to be allocated to reduce poverty and promote economic growth (Atteridge et al. [3]). At the same time, India's CO_2 emissions tripled between 1990 and 2011, making it the world's third largest greenhouse gas emitter (Boden et al. [6], IEA [20]). Its emissions are projected to more than double between 2008 and 2035 on account of the ongoing economic development (IEA [20]). While India has become a major emitting country, it would benefit substantially from limiting global CO_2 emissions, as it is one of the most vulnerable countries to climate change (e.g. Maplecroft [32]).[1] Its concerted efforts to reduce poverty may alleviate some of the vulnerability, but at the same time climate change impacts may exert stress on socio-economic systems and thus impede

[1]The reasons for this significant vulnerability are threefold. Firstly, more than half of its population depends on climate-sensitive sectors, such as agriculture. Secondly, poor infrastructure, weak institutional mechanisms and lack of financial resources limit the capacity to adapt to climate change. Thirdly, it is already exposed to rather high temperatures, so that further warming may have worrying consequences (Ministry of Home Affairs, Government of India [36], Mendelsohn et al. [35]).

economic development (Gupta [19]). Lately the government's discourses on climate change have changed and in October 2016 India ratified the Paris Agreement negotiated at the COP21. India is considered to be on a track to fulfil its pledges, which are framed as emission intensity targets and not as emission targets (Olhoff et al. [43]). However, it is also projected that the rapidly growing energy demands will further the expansion of the carbon-intensive power infrastructure, leading to strong increases in future emissions (CAT [10], PBL [44]). Just as many other countries' pledges, India's commitments are thus criticised as not being ambitious enough, to be far from being a fair contribution and to being inconsistent with limiting global warming to 2°C (CAT[10], Aldy et al. [1]).

Stringent climate policy has the co-benefit of reducing air pollution. Just as CO_2 emissions, emission of SO_2 is a by-product of fossil fuel combustion. Hence, climate policies intended to reduce fossil fuel combustion would thus also curb SO_2 pollution, which has a detrimental effect on ISM dynamics. Another merit of improved air quality is increased public health: exposure to high concentrations of SO_2 can have effects on breathing, cause respiratory illness, alterations in pulmonary defenses, and aggravation of existing cardiovascular disease (e.g. EPA [16]). As SO_2 is a short-lived pollutant and has a limited dispersion radius, these co-benefits of climate policy arise quickly and locally. They thus provide an instantaneous partial compensation for national climate policy costs. However, curbing SO_2 emissions does not only have positive effects. Sulphur is a scattering aerosol, which cloud in the atmosphere and act like a reflecting umbrella that cools the atmospheric temperature. Hence, abating SO_2 emissions unmasks the full warming effects caused by CO_2 emissions.

Climate policy is not essential to reducing air pollution. There are also SO_2 emission reduction technologies available, that do not require cutting back on fossil fuel consumption (Srivastava [52]). A country determined to fight air pollution but reluctant to make climate policy efforts, may opt for implementing these relatively inexpensive technologies.

Irrespective of these solutions to air pollution, India's SO_2 emissions increased rapidly in the last few years, making India the second largest emitter of SO_2 in the world (NASA [38]). A recent study by IEA [21] projects that emissions of SO_2 and other harmful aerosols will keep rising rapidly until 2040. The current air quality standards, which are substantially lower than international standards, appear to be too lax to prevent this spiralling trend (IEA [21]). These standards date back to 1980's and do not account for the technological developments made since then to reduce harmful aerosol emissions (e.g. innovations in coal-fired power plants and in the transport sector, IEA [21]).

There are only a few IAMs incorporating the emissions of CO_2 as well as of SO_2. To assess the consequences for temperature evolution, the IAMs by Bahn and Leach [4] and Yang and Menon [64] model global, as opposed to local temperature effects by aerosol emissions. Recently, Ikefuji et al. [22] developed an IAM based on the RICE model by Nordhaus and Yang [42], which also accounts for local effects involving (i) the cooling property of SO_2; (ii) impairment of health through warming; and (iii) impairment of health caused by air pollution through SO_2. To illustrate the co-benefits of climate policy, the authors also incorporate the possibility to reduce air pollution by adopting climate policy measures. As fossil fuel combustion also leads to the emission of other particles deemed harmful for health, the resulting estimates on the co-benefits appear to be rather conservative.

We fully couple this IAM with a model by Schewe and Levermann [50], which was developed to reflect the multidecadal variability and future changes in the ISM rainfall due to increasing temperatures. It simulates the interplay between two counteracting and self-amplifying feedbacks: the moisture advection feedback, which increases the likelihood of strong rainfall, and the dry-subsidence feedback, which reduces the probability of rainfall in the monsoon regions. The probability for the monsoon onset can be redefined to account for the effects of SO_2 on the ISM. We achieve this by incorporating the findings of Zickfeld et al. [66], which show that the ISM can switch into a different hydrological system if the planetary albedo, which is increased by SO_2 emissions, surpasses some critical threshold. Thus, the modified version of the onset probability explicitly accounts for this threshold effect.

This fully coupled model allows us to assess alternative CO_2 and SO_2 emission policy options for India and the induced changes in the ISM dynamics. In this new framework, India's optimal decisions on CO_2 and SO_2 emissions take into account (i) the damage costs induced by shifted ISM dynamics causing droughts or floods; (ii) the non-health as well as the health-related damage costs incurred by climate change and (iii) the local benefits that accrue for public health if local SO_2 pollution is curbed. While India has full control over the above described SO_2 driven effects on the ISM, it requires global cooperation to prevent the temperature driven effects. The other regions form the decision on cutting CO_2 and SO_2 emissions by accounting for the same kind of damage costs as India, with the only exception of the ISM-related damage costs that only accrue for India. Although the other regions' SO_2 emissions do not have any direct consequences for the ISM, they may have indirectly. When the other regions emit (more) SO_2, the local warming effect by climate change is obscured and they might be tempted to cut back CO_2 emissions less decisively.

As the resulting increased warming affects the ISM dynamics, SO_2 emissions in the other regions thus have an indirect effect on the ISM. Accordingly, the ISM dynamics depend on both, national and international emission decisions.

The remainder of this paper is organised as follows: the subsequent section describes the integrated assessment model and provides background information on the ISM system dynamics; Section 2.3 uses evidence of the past few decades to calibrate the ISM rainfall-related damage function and presents our core results; Section 2.4 concludes and discusses policy implications for India.

2.2 The Model

To explore the coevolution of the climate, the regional economies and ISM, we develop an integrated assessment model (henceforth referred to as RICE-ISM) that is a fully coupled model with three modules: an economic module consists of a Ramsey-type economic growth model, a climate module displaying regional and global warming and an ISM module (Figure 2.1). The economic and climate module is given by an annual time-scale version of the RICE-H model (Ikefuji et al. [22]). RICE-H extends the RICE-96 model (Nordhaus and Yang [42]) by explicitly displaying SO_2 emissions as a representative proxy for SO_4 aerosols in addition to CO_2 emissions.[2] The purpose of RICE-H is to account for the health effects of warming and of air pollution caused by fossil fuel combustion. Although the distinction between health- and non-health impacts are not this study's main research focus, we preserve its modelling in RICE-ISM. A rather detailed description of the different channels through which fossil fuel combustion can affect income may serve useful for future research employing RICE-ISM.

Important for coupling RICE-H with the ISM-module is the information on annual Indian SO_2 emissions and the annual global temperature increase. The ISM module, which builds on the conceptual model by Schewe and Levermann [50], requires this information to derive the ISM rainfall on a daily time-scale within a given year. If the intra-seasonal mean of these values features a precipitation extreme, i.e. relatively poor or relatively strong rainfall, ISM-specific damage costs are caused. In addition to the health-related and general costs computed by RICE-H, these damage costs reduce Indian gross income further.
In the following subsections we explain in detail the model characteristics outlined above.

[2] To be more precise, $SO4$ serves as a proxy for scattering aerosols. We do not account for aerosols that absorb sunlight, rather than reflect it, e.g. such as soot.

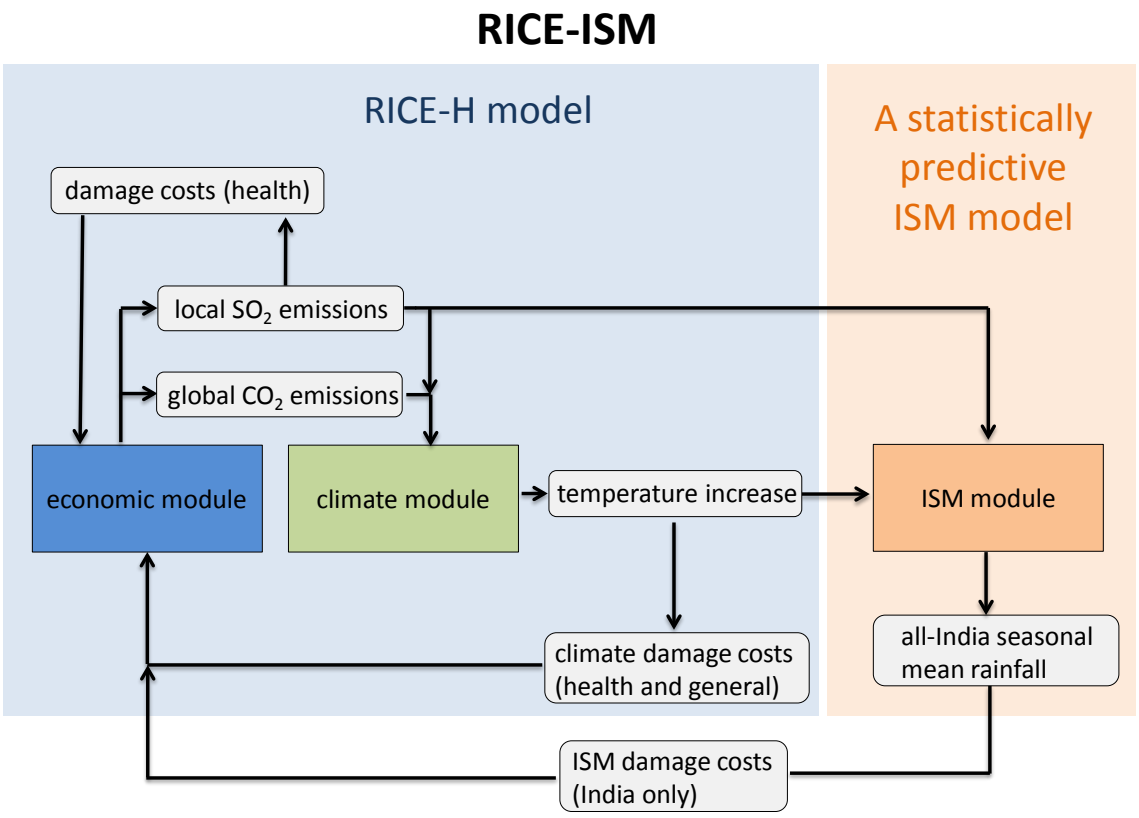

Fig. 2.1 Illustration of RICE-ISM, which unifies the RICE-H model by Ikefuji et al. [22] and an extended version of the ISM rainfall model by Schewe and Levermann [50]. The economic and climate modules give annual information on SO_2 emissions and global temperature increase, which serve as input information for the ISM module. The ISM rainfall is computed on a quasi-daily timescale within each monsoon season, which allows deriving the seasonal mean monsoon rainfall for each year. If the seasonal mean value turns out to be particularly low or particularly high, it induces ISM-specific damage costs decreasing Indian income.

Subsection 2.2.1 shows the modifications to RICE-96 carried out by Ikefuji et al. [22], which are related to the SO_2 emissions and the health effects. At the end of Subsection 2.2.1 we motivate our assumptions that lead to the ISM-specific damage function. In Subsection 2.2.2, the general mechanisms driving the ISM model are explained and formalised. In Subsection 2.2.3, we explicate and model the channels through which anthropogenic interference influences ISM rainfall strength.

2.2.1 The Economic and Climate Module

In RICE-H, the world is divided into 11 regions, $j = 1 \dots 11$, based on geographical position, political proximity and health vulnerability.[3] The time horizon spans 40 periods in total, each lasting five years. As the ISM module generates projections on an annual basis, we recalibrate the RICE-H module at one-year time step (i.e. $t = 1 \dots 200$).[4] The last period is thus given by $t = T$ with $T = 200$.

RICE-H displays the regional policy makers' intertemporal decision of how to optimally allocate the region's net income between investment in productive capital, abatement of SO_2 emissions, reductions of CO_2 emissions and to welfare enhancing consumption. The optimisation thereby depends on the policy scenario considered. The RICE-H model is used to explore three different policy solutions: (i) business-as-usual solution; (ii) the Nash solution; and (iii) the optimal solution, in which all regions cooperate. In the business-as-usual scenario, regions do not actively cut emissions. In the Nash scenario, countries do not cooperate and decide on their own, regional emission policy. In these two scenarios, each regional policy maker's goal is to maximise the domestic welfare, which also depends on other regions' actions. The objective function is thus represented by the regional welfare function W_j, which sums over the discounted logarithmic utility functions over time:

$$W_j = \sum_{t=0}^{T} \frac{L_{j,t}\, log\left(1 + \frac{C_{j,t}}{N_{j,t}}\right)}{(1+\rho)^t}, \tag{2.2.1}$$

where the active labour force is $L_{j,t}$, consumption is $C_{j,t}$, inhabitants are $N_{j,t}$ of a region j and the discount rate ρ. In each period t there are $N_{j,t}$ inhabitants of region j. Some of them are healthy and belong to the active labour force $L_{j,t}$, while others are ill and are unfit to work. The distinction between inhabitants and labour force is used to explicitly model non-market impacts of poor health in the welfare specification in Equation (3.2.1): the worse the health problems in a region the smaller becomes labour force $L_{j,t}$ and the weighting of utility. Another distinguishing characteristic of this welfare function is the addition of 1 to the per capita consumption in the utility function. The multiplication with labour force $L_{j,t}$ thus ensures a preference for low consumption over poor health.

[3] The regions are: USA (USA and Canada), EUR (Western Europe), JPN (Japan), AUS (Australia and Oceania), FSU (Former Soviet Union and Eastern Europe), CHN (China and centrally planned Asia), IND (India and South Asia), SEA (South East Asia), LAM (Latin America and Caribbean), MEN (Middle East and North Africa), AFR (Sub-Sahara Africa).

[4] See Appendix 2 A for details.

In the cooperative scenario, a social planner decides on each region's optimal emission pathway. For this, a weighted average of the regions' welfare is maximised. The weighting follows the Negishi approach. The algorithm used to derive the Negishi weights is described in Nordhaus [40].

While $N_{j,t}$ is exogenously given, active labour force $L_{j,t}$ evolves endogenously:

$$L_{j,t} = (1 - \chi_{j,t}) N_{j,t}, \tag{2.2.2}$$

where $\chi_{j,t}$ quantifies the fraction of the regional population suffering from a climate- and/or pollution-related disease. Only healthy inhabitants can contribute to gross income $Y_{j,t}$, which evolves according to a Cobb-Douglas production function:

$$Y_{j,t} = \psi_{j,t} K_{j,t}^{\varepsilon} L_{j,t}^{1-\varepsilon}, \quad (0 < \varepsilon < 1), \tag{2.2.3}$$

where $\psi_{j,t}$ is region-specific and time-varying technological efficiency and ε is output elasticity.[5] The capital stock $K_{j,t}$ evolves according to the usual capital accumulation function $K_{j,t+1} = (1 - \delta^k) K_{j,t} + I_{j,k}$, where $I_{j,k}$ is investment and δ^k, $0 < \delta^k < 1$ is the depreciation rate.

Climate change does not only affect the economy through a reduction of the active labour force (Equation (2.2.2)), but also by causing general, unspecific damage costs $D_{j,t}$. These climate damage costs reduce the income to $Y_{j,t} - D_{j,t}$, which represents the available resources for the regional policy makers to spend in each time step to maximise regional welfare. Thereby, the policy makers decide on the optimal path of consumption $C_{j,t}$, investment $I_{j,k}$, and abatement $A_{j,t}$ of CO_2 and SO_2 emissions:

$$Y_{j,t} - D_{j,t} = C_{j,t} + I_{j,t} + A_{j,t} \tag{2.2.4}$$

Equations (3.2.1)–(2.2.4) illustrate the channels by which the emissions affect welfare. Health damages reduce the active labour force, $L_{j,t}$, leading to market impacts and non-market impacts. The market impacts materialise as a reduction of gross income (Equation (2.2.3)), rendering the resource constraint tighter (Equation (2.2.4)). The non-market effects reflect that good health also is a factor relevant for welfare assessment (Equation (3.2.1)).

Poor health is assumed to be caused by adverse climate conditions and/or by air pollu-

[5] The existence of low labour force participation rates are usually abstracted from in IAMs.

tion. The share of the regional population that is unfit to work, $\chi_{j,t}$, can be also perceived as a relative frequency or probability of becoming unfit to work. Assuming that the probability of suffering from climate-related diseases $\chi^c_{j,t}$ and the probability to suffer from air-pollution-related diseases $\chi^a_{j,t}$ are stochastically independent, the probability of staying healthy thus becomes:

$$(1-\chi_{j,t}) = (1-\chi^a_{j,t})(1-\chi^c_{j,t}). \tag{2.2.5}$$

Following WHO [62], $\chi^c_{j,t}$ and $\chi^a_{j,t}$ are measured in terms of the disability adjusted life-years lost (DALYs) per capita. Climate-induced illnesses comprise malaria, cardiovascular disease, diarrhoea, and malnutrition in RICE-H. Based on estimations from McMichael et al. [33], Ikefuji et al. [22] assess $\chi^c_{j,t}$ to be of the following form:

$$\chi^c_{j,t} = \beta^c_{1,j} + \beta^c_{2,j}\left(T^{atm}_{j,t}\right)^{\beta^c_{3,j}}, \tag{2.2.6}$$

where the regional temperature increase $T^{atm}_{j,t}$ and parameters $\beta^c_{i,j}$, $i = 1,2,3$. The function giving $\chi^a_{j,t}$ is based on estimations by Spadaro and Rabl [51] that evaluate the damage cost per tonne of SO_2:

$$\chi^a_{j,t} = \beta^a_{j,t} E^a_{j,t}. \tag{2.2.7}$$

where the local SO_2 emissions are $E^a_{j,t}$ and the parameter $\beta^a_{j,t}$ describing the degree of exposure to SO_2 emissions. The degree of exposure incorporates information on the region's population density and (projected) urbanization.

The emissions of SO_2, $E^a_{j,t}$, and of CO_2, $E^c_{j,t}$, are – as mentioned above – a by-product of economic activity:

$$\begin{pmatrix} E^c_{j,t} \\ E^a_{j,t} \end{pmatrix} = \begin{pmatrix} \sigma^{cc}_{j,t} & \sigma^{ca}_{j,t} \\ \sigma^{ac}_{j,t} & \sigma^{aa}_{j,t} \end{pmatrix} \begin{pmatrix} 1-\mu^c_{j,t} \\ 1-\mu^a_{j,t} \end{pmatrix} Y_{j,t}, \tag{2.2.8}$$

where the regional emission control rates are $\mu^c_{j,t}$ and $\mu^a_{j,t}$ for CO_2 and SO_2, respectively, carbon intensity is $\sigma^{cc}_{j,t}$ and sulphur intensity is $\sigma^{aa}_{j,t}$. The interdependencies between CO_2 and SO_2 emissions, which have common sources, such as fossil energy combustion, is captured by the cross-influences $\sigma^{ca}_{j,t}$ and $\sigma^{ac}_{j,t}$. Climate policy that acts to limit combustion of fossil fuels has the positive side effect of curbing SO_2 emissions. Accordingly, $\sigma^{ac}_{j,t}$ assumes a positive value. By contrast, environmental policy targeting SO_2 pollution can, but does not necessarily, lead to mitigation of CO_2 emission. Requiring relatively inexpensive technology, there are also desulphurization solutions that leave CO_2 emissions unaffected. The calibration of $\sigma^{ca}_{j,t}$ being zero thus represents a reasonable assumption.

Reducing emissions of CO_2 and SO_2 cause costs:

$$A_{j,t} = (\alpha^c_{j,t}(\mu^c_{j,t})^{\xi^c} + \alpha^a_{j,t}(\mu^a_{j,t})^{\xi^a})Y_{j,t}, \tag{2.2.9}$$

where the exponents ξ^c and ξ^a are set to be greater than one, making the costs of abatement of CO_2 and SO_2 convex in terms of the respective control rates.

The climate module displays how unabated emissions translate into future climate change. The accumulation of CO_2 in the atmosphere develops according to the same equation as in RICE-96:

$$M_{t+1} = (1-\delta^c)M_t + \sum_{j=1}^{11} E^c_{j,t}, \tag{2.2.10}$$

where δ^c is the depreciation rate of atmospheric CO_2. The specification of the regional temperature increase $T^{atm}_{j,t}$ deviates from the function in RICE. To account for the radiative forcing of regional SO_2 as an endogenously determined effect, the equation from version 5.1 of the MERGE model, originally developed by Manne et al. [31], is adopted:

$$T^{atm}_{j,t+1} = \tau_{0,j} + \tau_1 T^{atm}_{j,t} + \tau_2 T^{atm}_t + \tau^c_j log(M_{t+1}) + \tau^a_{1,j} E^a_{j,t+1} + \tau^a_{2,j} log(1 + \tau^a_{3,j} E^a_{j,t+1}), \tag{2.2.11}$$

where parameters τ_1, τ_2, τ^c_j, $\tau^a_{1,j}$, $\tau^a_{2,j}$, $\tau^a_{3,j}$ being associated with the increases of the regional and global temperature in the last period, the forcing of atmospheric CO_2 and the regional SO_2 emissions, respectively. The parameter τ^c_j is positive and thus describes the warming effect of the greenhouse gas CO_2. By contrast, $\tau^a_{1,j}$ and $\tau^a_{2,j}$ are negative for all regions, reflecting the cooling effect of SO_2 emissions. In fact, these aerosols scatter sunlight back into space, so that less sunlight reaches the Earth's surface (local dimming). The (global) greenhouse effect and the (local) dimming effect thus work in opposite directions. The parameter $\tau_{0,j}$ is introduced to allow the starting value of the regional temperature increase, $T^{atm}_{j,0}$, is set to zero.

The global temperature increase T^{atm}_t evolves as a weighted average of the regional temperature increases:

$$T^{atm}_t = \sum_j \omega_j T^{atm}_{j,t}, \tag{2.2.12}$$

where ω_j denotes the region's share of global landmass.

As in Nordhaus and Boyer [41], region-specific damage costs vary according to:

$$D_{j,t} = \frac{d_{j,t}}{1+d_{j,t}}. \tag{2.2.13}$$

The damage function is given by:

$$d_{j,t} = \gamma_{1,j} T_{j,t}^{atm} + \gamma_{2,j} \left(T_{j,t}^{atm}\right)^2, \tag{2.2.14}$$

where $\gamma_{1,j}$ and $\gamma_{2,j}$ are regional-specific damage parameters.

A novel feature of the present study is the regional damage function of India, $d_{IND,t}$. The new specification accounts for the losses d^{ISM} that are caused, if the months spanning the ISM season are on average extremely dry or rainy.[6] Accordingly, the losses d^{ISM} depend on the value of the seasonal mean rainfall $\bar{P}_t$, which evolves in the ISM module.

To our knowledge, the estimations used to calibrate the Indian damage cost function (Equation (3.2.11)) do not cover ISM-related impacts. We therefore assume that the losses d_t^{ISM} simply add to the temperature-driven damage costs caused in India. Another reason for this assumption is that the seasonal mean rainfall $\bar{P}_t$ depends on complex and stochastic dynamics which are - amongst other factors - influenced by temperature. As the ISM-specific losses do not directly depend on the local temperature increase as postulated in Equation (3.2.11), the ISM-related impacts cannot be captured by Equation (3.2.11) appropriately. Accordingly, we rather claim that the total damage costs incurred in India evolve as:

$$d_{IND,t} = \gamma_{1,j} T_{j,t}^{atm} + \gamma_{2,j} \left(T_{j,t}^{atm}\right)^2 + d^{ISM}(\bar{P}_t). \tag{2.2.15}$$

In view of scarcity of suitable ISM-specific damage estimations, we opt here for postulating two simplifying assumptions that allow us to derive a step function d^{ISM} that bases on the few data available.

$$d^{ISM}(\bar{P}_t) = \begin{cases} D^{drought}, & \bar{P}_t \leq \bar{P}^{drought} \\ 0, & \bar{P}_{drought} < \bar{P}_t < \bar{P}^{flood} \\ D^{flood}, & \bar{P}_t \geq \bar{P}^{flood} \end{cases} \tag{2.2.16}$$

[6] Other notions of extremes that could be of interest for developing a ISM-related damage function are, for instance, the length of dry spells in a year or the maximum rainfall per day.

The first assumption states that only the two the rainfall extremes, i.e. drought or flood, cause damage costs, i.e. all values $\bar{P}_t$ smaller than the threshold $\bar{P}_{drought}$ and all values $\bar{P}_t$ larger than the threshold $\bar{P}_{flood}$. A consequence of designing such an extreme-event-specific damage function is that all values $\bar{P}_t$ outside the extreme value ranges give damage costs of zero.[7] The second simplifying assumption is that within these extreme value ranges, damage costs $D^{drought}$ and D^{flood} are constant. While lacking data limits a more sophisticated development of this damage function at this point of time, future work might extend this function by accounting for the severity of a rainfall extreme, a changing vulnerability over time due to adaptation efforts and economic development and increased costs for the same extreme event occurring in successive time intervals.

For the purpose of numerical solution we refer to the smooth approximation of the step function d^{ISM}, given by:

$$\begin{aligned} \tilde{d}^{ISM}(\bar{P}_t) &= D^{drought}\left(\frac{1}{\pi}\cdot\arctan[\zeta(\bar{P}_{drought}-\bar{P}_t)]+\frac{1}{2}\right) \\ &+ D^{flood}\left(\frac{1}{\pi}\arctan[\zeta(\bar{P}_t-\bar{P}_{flood})]+\frac{1}{2}\right), \end{aligned} \tag{2.2.17}$$

where ζ is a steepness parameter and π is a mathematical constant equal to $3.141593\ldots$. Figure 2.2 illustrates the function. A noteworthy feature in the data is the asymmetry between the flood- and drought-related damage costs, which is also reflected by d^{ISM}. The thus derived function allows gaining some intuition of the economic impacts caused by ISM rainfall extremes.
In Subsection 2.3.1 the calibration of the ISM-specific damage costs is explained in detail.

2.2.2 The Indian Summer Monsoon Rainfall

In this subsection, we give a more detailed explanation of the fundamental mechanism driving the ISM and describe how the interplay of two crucial counteracting feedback processes are reflected by Schewe and Levermann [50]. In the next subsection, we explicate how these mechanisms change with global warming and local air pollution.

The fundamental mechanism driving the ISM is caused by a temperature difference between land and ocean (Figure 2.3). In summer the surfaces of both land and ocean are

[7] Alternatively, one could define an intermediate range in which the damage costs slowly converge rather than drop to zero. As this procedure would have required further scarce information, i.e. on the width of these ranges or on the convergence rate, we opt here to adopt the first approach.

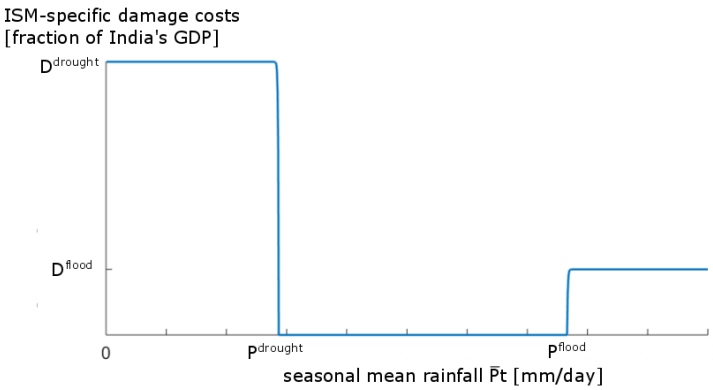

Fig. 2.2 Illustration of the ISM-specific damage cost function d^{ISM}, which describes the economic losses $D^{drought}$ and D^{flood} occurring for extreme deficiency ($\bar{P}_t \leq \bar{P}_{drought}$) or extreme excess ($\bar{P}_t \geq \bar{P}^{flood}$) of summer monsoon rainfall, respectively.

warmed, but land temperatures rise more quickly due to a lower heat capacity.[8] The air above the land warms rapidly, expands, and then rises. It thus forms an area of low pressure in the lower troposphere and an area of high pressure in the upper troposphere. By contrast, the air above the ocean warms less quickly and thereby maintains a relatively high pressure in the lower troposphere and a relatively low pressure in the upper troposphere. This land-ocean pressure gradient in the lower altitudes directs moist sea winds from the ocean to the land. This air rises to a higher altitude over the hot continent and condensates, inducing precipitation over land. In the upper troposphere the pressure gradient forces the winds in the opposite direction, leading to a high-altitude air flow from land to ocean. Above the ocean the air cools and sinks down again, which completes the ocean-land circulation of the monsoon winds. This circulation is sustained as long as the temperatures above the land and ocean differ sufficiently.

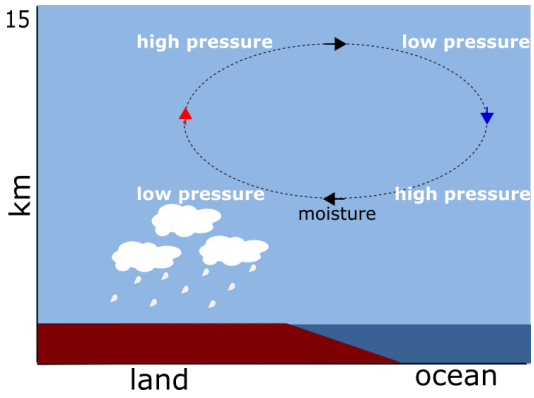

Fig. 2.3 Schematic illustration of the temperature gradient driving the summer monsoon.

[8] Heat capacity quantifies the heat required to raise the temperature of 1g of a substance by 1 Celsius.

Throughout the rainy season the ISM this temperature difference is sustained by a positive feedback effect, the so-called moisture advection feedback (Webster [59]): as precipitation releases heat, referred to as latent heat, the temperature gradient is reinforced and the winds strengthen.

Another feedback process, the dry-subsidence feedback, leads to a qualitatively different circulation pattern in dry years Schewe and Levermann [50]. In these years, the upper-tropospheric air over the Indian subcontinent and the Arabian sea is observed to sink down and to consequently dry out the monsoon winds. The decline in precipitation comes with a decreased release of latent heat, which acts to sustain the dry regime. In addition, the wind in the upper troposphere, which blows westward in normal monsoon seasons, is deflected northward or eastward and thus misses the monsoon regions.

The model by Schewe and Levermann [50] reflects the interplay between the moisture advection feedback and the dry-subsidence feedback throughout the summer monsoon season (May to September). Multi-decadal variability in the ISM rainfall found in simulations with the comprehensive climate model ensemble MPI-M Earth System model (MPI-ESM) (e.g. Jungclaus et al. [24]) can be thus sufficiently reproduced Schewe and Levermann [50]. On a quasi-daily timescale the daily monsoon rainfall $P_{d,t}$, $d = 1 \ldots 135$, in some year t varies between two states: the dry state P^{dry} with minimum precipitation, which is dominated by the dry-subsidence feedback process, and the wet state P_t^{wet} with maximum rainfall, which is maintained by the moisture advection feedback process. The probability $p_{d,t}$ for being in the wet state on day d is determined as

$$p_{d,t} = \frac{\frac{1}{\delta}\sum_{i=d-\delta}^{d-1} P_{i,t} - P^{dry}}{P_t^{wet} - P^{dry}}, \tag{2.2.18}$$

which depends on the average rainfall $\frac{1}{\delta}\sum_{i=d-\delta}^{d-1} P_{i,t}$ in δ days prior to d. The rainier this period is, the more likely day d to be rainy as well. Likewise, if this period is rather dry, then the rainfall probability on day d is relatively small. This memory effect thus reflects the two self-amplifying feedback processes described above. To avoid a lock-in in one of the states, the precipitation probability is constrained by a maximum probability p_m, $0 < p_m < 1$, and a minimum probability $(1 - p_m)$. Equation (3.2.27) applies to the period after the first δ days of the season, i.e. for all $d > \delta$, in which the two self-amplifying feedback mechanism take effect. As described in the next subsection, the first δ days signify the monsoon onset in which the rainfall probability, $p_{d,t} = p_t^{init}$, evolves differently.

The precipitation probability $p_{d,t}$ influences which of the two precipitation states materialize on day d:

$$P_{d,t} = \begin{cases} P_t^{wet}, & Pr_{d,t} < p_{d,t} \\ P^{dry}, & else, \end{cases} \tag{2.2.19}$$

where the random variable $Pr_{d,t}$ is uniformly distributed between zero and one. This variable represents stochastically evolving atmospheric fluctuations inducing variability of the intra-seasonal rainfall. This stochasticity counteracts the memory effect, occasionally causing flips between the two precipitation states on a quasi-daily timescale (Figure 2.4).

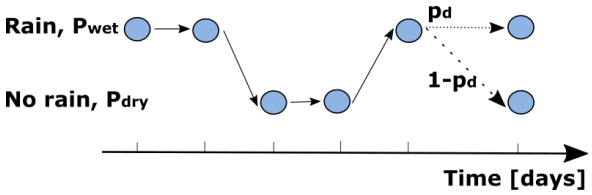

Fig. 2.4 Schematic illustration of the realised precipitation states within some year. On each day, synoptic scale fluctuations and a memory effect determine the probability of whether the precipitation state P_t^{wet} or P^{dry} take effect.

The average of the daily precipitation over the season is the seasonal mean precipitation rate $\overline{P}_t$, $P^{dry} \leq \overline{P}_t \leq P_t^{wet}$:

$$\overline{P}_t = \frac{1}{135} \cdot \sum_{d=1}^{135} P_{d,t}. \tag{2.2.20}$$

2.2.3 Seasonal Mean ISM Rainfall under Global Warming and Local Air Pollution

Here, we explain how the dynamic evolution of the rainfall probability during monsoon onset p_t^{init} and the rainfall intensity P_t^{wet} depends on global warming and on local air pollution (Figure 2.5).
Schewe and Levermann [50] define daily rainfall intensity P_t^{wet} in the wet state as

$$P_t^{wet} = p'' \cdot T_t^{atm} + P_0^{wet}, \tag{2.2.21}$$

with p'' depicting the impact of the global mean temperature increase T_t^{atm} on rainfall. The rainfall intensity in the absence of further global warming is given by P_0^{wet}. Equation (2.2.21) reflects that rainfall intensity increases with rising temperatures, which is due to the ability of warmer air to hold more water vapour (Trenberth [53], Allen and Ingram [2]). As P^{dry} stays constant over time, warming thus extends the range of possible seasonal mean rainfall values $[P^{dry}, P_t^{wet}]$.

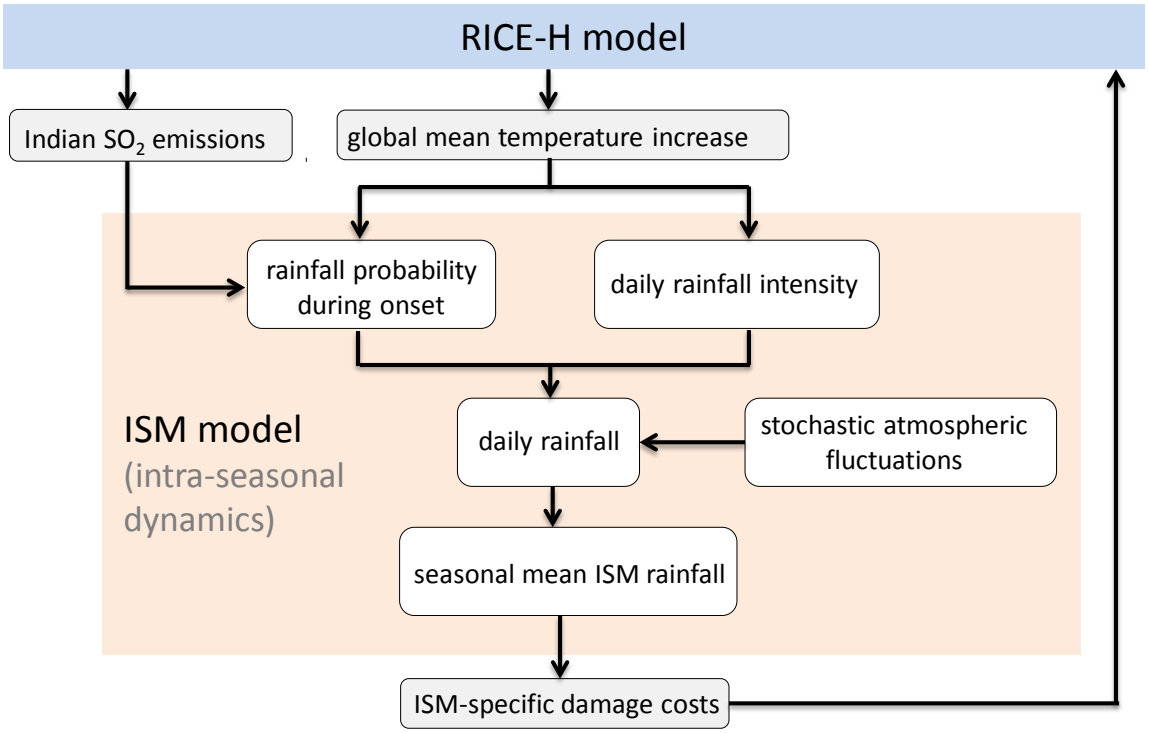

Fig. 2.5 Illustration of the ISM module and its relation to the other model elements.

Dynamic processes that govern the onset period can be captured in the specification of p^{init}. During this period, the El Niño-Southern Oscillation (ENSO) and the associated changes in the Pacific Ocean atmospheric circulation, referred to as the Walker circulation, are found to be of crucial importance for the following monsoon season (Schewe and Levermann [50]). ENSO refers to the interaction between the atmosphere and the ocean in the tropical Pacific that lead to a variation between a warming phase (El Niño) and a cooling phase (La Niña) of different sea surface pressures.[9] The variation between these ENSO phases are associated with changes in the Walker circulation: El Niño comes with a reversing or weakening of this circulation, which can suppress the convection associated with the ISM.[10] Simulations with MPI-ESM reveal that the highest correlation between seasonal mean ISM rainfall and the strength of the Walker circulation is given for the onset period of the monsoon (Schewe and Levermann [50]). Schewe and Levermann [50] derive a linear relationship between the

[9] A nice illustration of the ENSO dynamics and further information can be found on the webpage https://iridl.ldeo.columbia.edu/maproom/ENSO/ENSO_Info.html [17th January 2017].

[10] Historical rainfall data discloses that El Niño does not necessarily lead to poor ISM rainfall. Very severe droughts were accompanied by El Niño years, though (Kumar et al. [29]).

rainfall probability in the onset period $p^{init,1}$ and the state of the Walker circulation strength:

$$p_t^{init,1} = p\prime \cdot (m_t^{NINO3.4} - m_0) + p_0, \tag{2.2.22}$$

where $m_t^{NINO3.4}$ depicts the strength of the Walker circulation in May. It is measured by the decadal-scale anomaly in the mean sea level pressure (MSLP) over an - in this context - crucial Pacific region (NINO3.4., 170-120°W, 5°S - 5°N). The parameters m_0, p_0, and $p\prime$ are calibrated to match the rainfall frequency distributions in the time series generated by the comprehensive MPI-M Earth System model well.[11]

As the Walker circulation is found to weaken under global warming (Vecchi et al. [56]), we extend the model by Schewe and Levermann [50] to incorporate the effects of warming on the value of $m_t^{NINO3.4}$. The frequency distribution shift found in the study by Schewe and Levermann [50] is consistent with a linear trend of the Walker circulation strength in the temperature increase:

$$m_{t+30}^{NINO3.4} = m' \cdot T_t^{atm} + m_0^{NINO3.4}, \tag{2.2.23}$$

where m' and $m_0^{NINO3.4}$ are parameters that we estimate based on the MPI-ESM simulations by Schewe and Levermann [50]. The 30-year delay reflects the inertia in the system, which also involves thermal inertia of the ocean.

Furthermore, we modify Equation (2.2.22) to account for the impact of SO_2 emissions. These emissions convert into sulphate aerosols in the atmosphere, which scatter the incoming solar radiation back to space (direct effect) and serve as 'seeds' for relatively bright clouds (indirect effect). Accordingly, the higher the atmospheric concentration of these aerosols is the higher the ratio of reflected to incoming solar radiation (planetary albedo) and the cooler the atmosphere. As the dispersion radius of these aerosols is limited, cooling mostly takes effect in the area in which SO_2 emissions is emitted, i.e. over land. SO_2 emissions can thus result in a decline of the temperature gradient between land and ocean and thus in a weakening of the ISM. Accordingly, this effect counteracts the warming effect of atmospheric CO_2. These two opposing effects lead to a bifurcation in the ISM system (Zickfeld et al. [66]), which is illustrated in Figure 2.6.

The red dashed lines in Figure 2.6 signify the current values of the planetary albedo (horizontal red dashed line) and of the CO_2 concentration (vertical dashed red lines). The planetary albedo level critical for the ISM strength is depicted by the blue curve. The area underneath

[11] For more information see Schewe and Levermann [50].

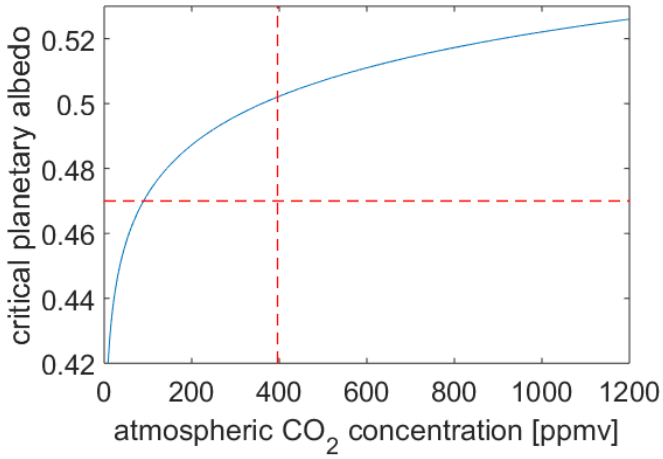

Fig. 2.6 Critical level of planetary albedo in dependence of atmospheric CO_2 concentration (blue curve). If the current values of planetary albedo over India (horizontal red dashed line) and of the atmospheric CO_2 concentration (vertical dashed red lines) alter such that both (i.e the intersection of the red lines) transgress the critical level, then the ISM switches into a weak hydrological cycle.

the blue curve describes all values of planetary albedo and of CO_2 concentration that mean a sufficient land-to-sea temperature contrast. All values above the blue curve destabilize the ISM and render a weak hydrological cycle. Put differently, if planetary albedo A_t^{pl} transgresses its critical value $A_t^{pl,crit}$, the rainfall probability during the first δ days (Equation 2.2.22) is set to its minimum $1-p_m$. Accordingly, Equation (2.2.22) is rephrased as

$$p_t^{init} = \begin{cases} p_t^{init,1}, & A_t^{pl} < A_t^{pl,crit} \\ 1-p_m, & else. \end{cases} \tag{2.2.24}$$

The dependence of the critical albedo value on the atmospheric CO_2 concentration M_t can be expressed by:

$$A_t^{pl,crit} = \alpha_1^{pl} \cdot log(M_t) + \alpha_2^{pl}, \tag{2.2.25}$$

where the parameters α_1^{pl} and α_2^{pl} are derived by a two-point fit to the bifurcation. The change in the actual planetary albedo ΔA_t^{pl} relative to the present value of 0.47 is given by (Charlson et al. [14]):

$$\Delta A_t^{pl} = 2(T^{pl})^2 \cdot (1-A^s)^2 \cdot \beta^{pl} \cdot \alpha_3^{pl} \cdot B_t^{SO4}, \tag{2.2.26}$$

where T^{pl} denotes the fraction of light transmitted by the aerosol layer, A^s is the present value of the surface albedo, α_3^{pl} denotes the mass scattering efficiency and β^{pl} depicts the

backscatter fraction. The regional sulphate burden over the Indian peninsula B_t^{SO4} evolves as

$$B_t^{SO4} = E_{IND,t}^{a} \cdot O \cdot H^{SO2} \cdot V/\Omega \tag{2.2.27}$$

where O is a conversion factor reflecting the chemical reactions in the atmosphere, V is the sulphate lifetime measured in the number of days of the year, H^{SO2} is fractional sulfate yield, and Ω is the size of the land (Venkataraman et al. [57]).

Although we modelled that aerosols affect the ISM directly in its onset phase, the consequence of assuming a weak hydrological cycle are preserved in lowering the rainfall probability throughout the season (Equation (3.2.27)). In a nutshell, CO_2 and SO_2 emissions affect the onset of the ISM, the range of rainfall intensity and thus the rainfall probability throughout the season.

2.3 Simulations

2.3.1 Calibrating the ISM-related Damage Costs

Equation (3.2.14) requires calibration of the threshold values $\bar{P}^{drought}$ and $\bar{P}^{flood}$ marking rainfall extreme events and of the resulting damage costs $D^{drought}$ and D^{flood}.

To calibrate the threshold values $\bar{P}^{drought}$ and $\bar{P}^{flood}$ we use the same frequency distribution, which is given by the MPI-ESM model ensemble, that also served to calibrate the ISM model by Schewe and Levermann [50]. For the baseline calibration we postulate that all seasonal mean rainfall values at the 5th percentile are associated with an especially dry year, and that all values at the 95th percentile represent a year of extremely heavy rainfall. This translates into $\bar{P}^{drought} = 2.8667$ [mm/day] and $\bar{P}^{flood} = 7.6667$ [mm/day].[12]

The calibration of the damage costs $D^{drought}$ and D^{flood} is challenged by the shortage of estimations of past ISM-related damage costs and by uncertainty about the future GDP's vulnerability to extreme monsoon rainfall events. Among the few attempts to assess the impacts of poor ISM rainfall on Indian GDP is the study by Gadgil and Gadgil [17], who base their estimations on time-series from 1951 to 2003. Although the agricultural sector's contribution to GDP is decreasing over time, the impact of severe droughts on GDP remains between 2 and 5 %, which is explained by the indirect impacts amplifying the direct effects:

[12] It is important to note that the seasonal mean rainfall values $\bar{P}_t$ given by MPI-ESM do not necessarily match observational data. Accordingly, the estimation of these threshold values might also differ from observations.

crop failure leads to higher prices of agricultural products, which pushes inflation and reduces the purchasing power, in particular of the rural population (Gadgil and Gadgil [17]). In addition, the damage costs implied by water shortages that cut back energy generation by hydropower plants, thermal and nuclear power plants might also increase in a more developed economy. Following this estimation, we set $D^{drought} \in [2,5]$ % of India's GDP. The average value of 3.5% represents the baseline calibration in this study.

Excess rainfall can lead to major river flooding that can damage important infrastructure and disrupt economic activity. A recent estimate states that the Indian GDP affected by river flooding on average per year is approximately 0.84% (WRI [63]).[13] As the ISM contributes about 80% of the annual precipitation in India (Gadgil and Gadgil [17]), it is reasonable to assume that these flood-related damage costs are mainly caused by excess ISM rainfall. We therefore set $D^{flood} = 0.84$ [% of GDP]. A potential positive impact of excess rainfall on the food grain production is shown to be rather insignificant (Gadgil and Gadgil [17]). As a consequence of lacking data, other damage costs caused in years of excess ISM rainfall are not included in D^{flood}.[14]

The asymmetry in the losses related to droughts and floods is also reflected in a survey of households in Uttar Pradesh, eliciting the household's income and consumption vulnerability to various factors (Gin al. [18]).[15] About 88% of surveyed households consider droughts to be a major risk, while floods represent the biggest concern for only 0.2% of the households.

2.3.2 Results and Discussion

Here, we present the results of the model, where business-as-usual policy corresponds to the A2-ASF scenario from the Special Report on Emission Scenarios (SRES) (IPCC [23]). As this study is concerned with the problem of reconciling global and regional policy, the A2-ASF scenario describing a very heterogeneous world with slow per capita income convergence is of particular interest.[16]

[13] The Aqueduct Global Flood Analyzer is a web-based interactive platform, which allows to estimate current and potential future flood risk for a specific geographic unit, taking into account local flood protection levels.

[14] For example, strong ISM rainfall is often accompanied with extremely strong winds that can prevent economic activity near the coasts.

[15] Among the risks the households were asked to rank the importance of were drought, crop failure, crop disease, loss of livestock, price changes, illness, job loss, fires, flood and loss of land.

[16] For a more detailed description of the A2-ASF scenario see Appendix 2 C.

Given the stochastic nature of the ISM module, we follow Schewe and Levermann [50] in performing 100 model realizations for each simulation. The results are presented in the form of mean value and ± 1 standard deviation range over 100 model realizations.

Results are produced for three different policy scenarios: the business-as-usual scenario in which countries do not reduce emissions actively; the Nash scenario in which countries do not cooperate but adopt their own, national emission policy; and the optimal scenario in which countries pursue a global cooperative mitigation policy. The earliest possible time to cut emissions is the year 2017, i.e. until the year 2016 emissions follow the business-as-usual path.

As expected, India's CO_2 control rate is significantly higher in the optimal scenario than in the Nash solution (Figure 2.7a).[17] The more stringent CO_2 mitigation policy in the optimal scenario lead i) to a lower atmospheric carbon concentration and ii) to instantaneous co-benefits of improved air-quality, which can be achieved with virtually the same sulphur emission policy as in the uncooperative scenario (Figures 2.7b and 2.8b). The u-shaped sulphur control rate curve reflects the initial decrease in the sulphur control rate due to a declining sulphur emission intensity of production and the subsequent increase of the control rate due to decreasing sulphur abatement costs.

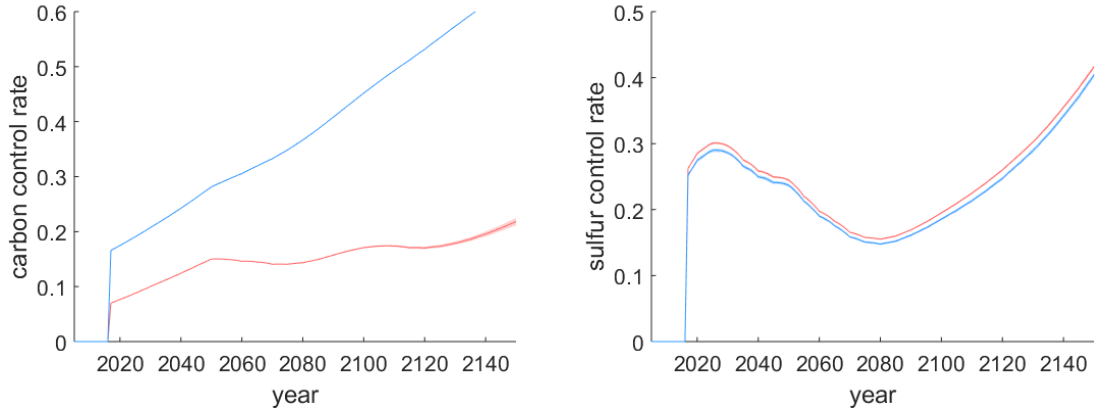

(a) Carbon control rate

(b) Sulphur control rate

Fig. 2.7 India's emissions control rates in the scenario of global cooperation (blue curve) and of no cooperation (red curve).

The effect of the different policies on the ISM rainfall statistics is illustrated by Figure

[17] An overview of all regional CO_2 emissions and CO_2 control rates in the year 2100 is given in Appendix 2 B.

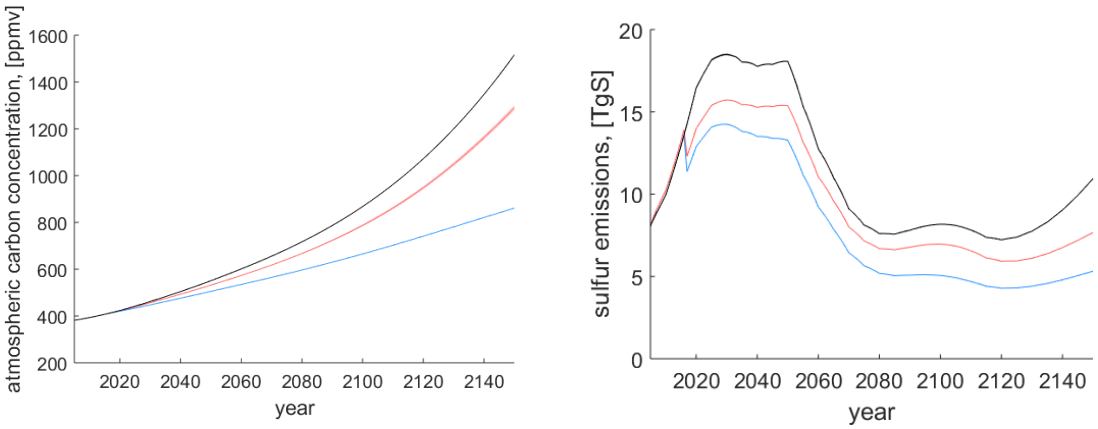

(a) Atmospheric carbon concentration

(b) Sulphur emissions, TgS

Fig. 2.8 Atmospheric carbon concentration and India's sulphur emissions in the scenario of global cooperation (blue curve), of no cooperation (red curve), and the business-as-usual path (black curve).

2.9. To get an impression for the deviations in the statistics caused by anthropogenic interference, we additionally provide a 'historical' seasonal mean ISM rainfall distribution (Figure 2.9a). This means that initial rainfall probability and rainfall intensity on a rainy day are kept constant, i.e $p^{init} = 0.75$ and $P^{wet} = 9$ (Schewe and Levermann [50]). This distribution exhibits two interesting characteristics: ii) it features only few extremely dry and few extremely rainy days (the threshold values $P^{drought}$ and P^{flood} are highlighted by the vertical dashed lines); and ii) the distribution is skewed with many moderately rainy years.

Compared to the 'historical' distribution, the distribution associated with the business-as-usual path is rather flat (Figure 2.9b), featuring fewer years with moderate ISM rainfall and many more years of droughts and torrential rain. Accordingly, anthropogenic interference has a significant impact on the rainfall statistics. Compared to the business-as-usual path, the two scenarios of emission reduction exhibit less many dry years and more years of moderate rain. However, the economically optimal emission reduction efforts in the cooperative and Nash scenario are not stringent enough to maintain the characteristics of the 'historical' distribution' (Figures 2.9c and 2.9d). Accordingly, adaptation to a rather flat rainfall distribution must be key to Indian policy in the future.

We continue examining the role of environmental policy by looking at changes over time. Figure 2.10 depicts an evolution of seasonal mean rainfall under alternative policies. For the illustrative purpose, here we also add the results of a fictional scenario – referred to as "historical" – where climate is characterized by the preindustrial conditions. As we men-

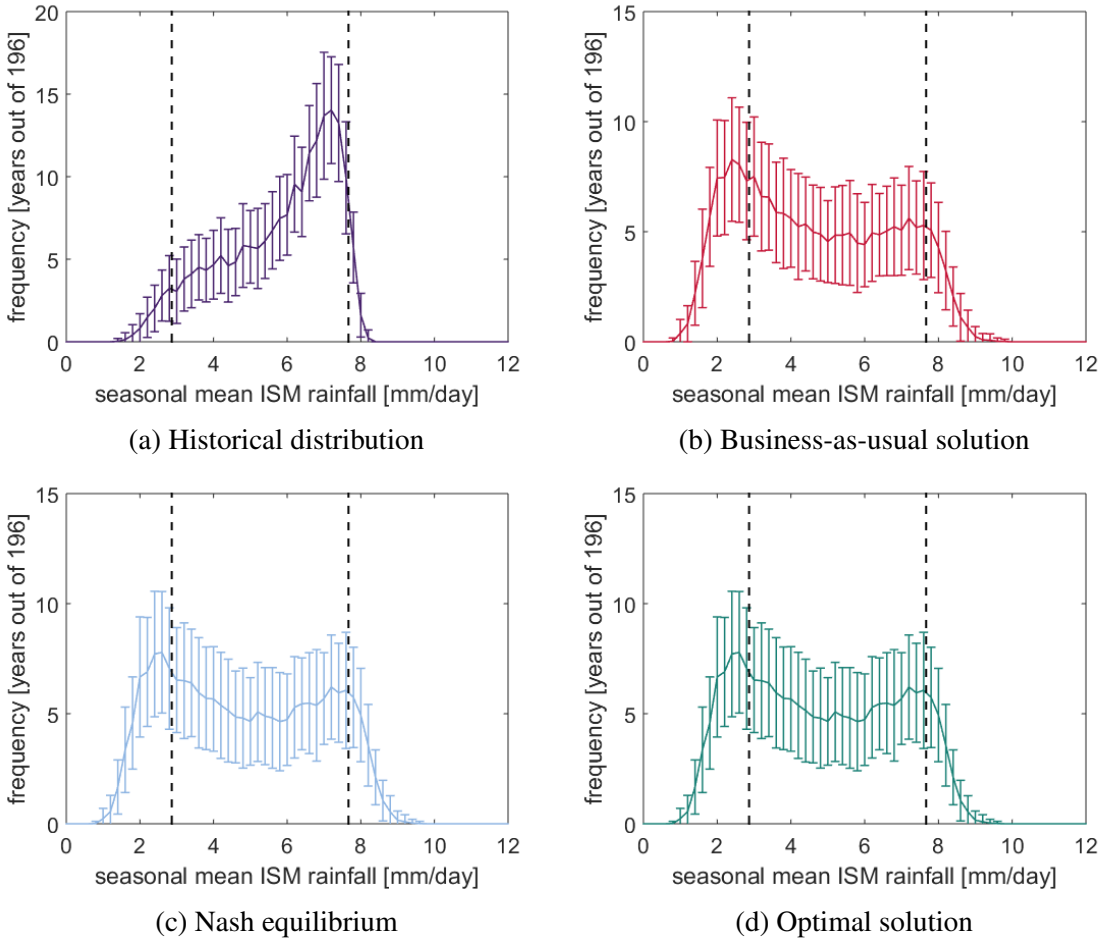

(a) Historical distribution

(b) Business-as-usual solution

(c) Nash equilibrium

(d) Optimal solution

Fig. 2.9 The ISM rainfall statistics. a)-d) Distribution of seasonal mean ISM rainfall. Solid lines show mean value and error bars illustrate $\pm$ 1 standard deviation over 100 realizations of the model. The vertical dashed lines highlight the seasonal mean rainfall values that correspond to the extreme damage-inducing rainfall events.

tioned earlier, under these conditions extreme events – extensive summer flood and drought events – do occur. Business-as-usual solution exhibits stronger variability (Figure 2.10a). It is characterised by "ups and downs" in seasonal mean rainfall values, switching between the periods when rainfall exceeds the no-anthropogenic interference scenario and those when it falls behind. During first simulation years, we observe strengthening of the summer monsoon rainfall as it follows an upward trend. Next, sudden drop occurs with a number of consecutive years of severe rainfall deficiency. Over the course of the following years, rainfall stabilises, reaching and going beyond the long-term mean. Yet, starting from the middle of 21st century, it follows a diminishing trend, which appears as a rather smooth reduction. By the year 2150, years with severe ISM rainfall deficiency are remarkably frequent. In both Nash and optimal

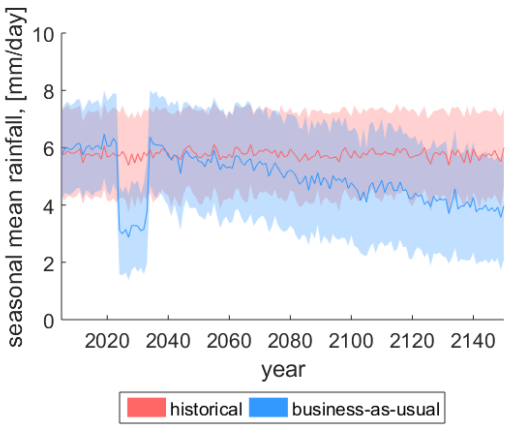

(a) Business-as-usual solution versus historical data

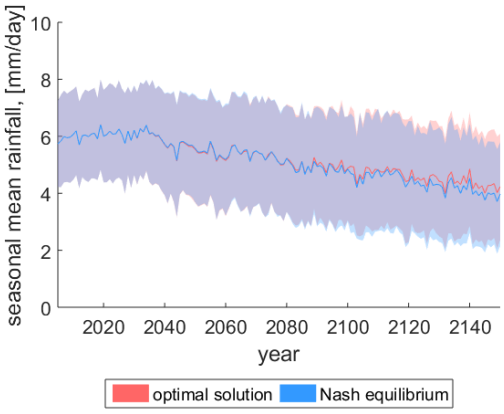

(b) Optimal solution versus Nash equilibrium

Fig. 2.10 Evolution of seasonal mean rainfall over time under alternative emissions control scenarios.

solutions, seasonal mean ISM rainfall follows a diminishing trend, which coincide in the near-term. The difference become more noticeable in a longer term. As evident from Figure 2.10, mean and confidence interval in the optimal solution are slightly above those in Nash equilibrium.

To clarify causality behind the changes in the ISM rainfall over time, we refer to Figure 2.11. Figures 2.11a and 2.11b portray an evolution of daily rainfall intensity and rainfall probability during monsoon onset, which constitute the two channels, through which climate change alter ISM rainfall. As global warming accelerates, water vapour content of the atmosphere increases, which leads to an increased daily precipitation intensity (Figures 2.11a and 2.11b, green curve). In turn, seasonal mean rainfall elevates (Figure 2.10a). The reason behind the sudden drop in rainfall probability during monsoon onset is illustrated in Figure 2.11c. Elevated aerosol burden over India initiates an increase in the planetary albedo, which pushes the ISM system towards the bifurcation point, switching it to a "dry" state during the monsoon onset.[18] However, as atmospheric CO2 concentration rises, the critical planetary

[18]Suppression of the Indian summer monsoon rainfall in response to perturbation of factors, which govern the heat balance of the system, i.e. the planetary albedo, the insolation, and the CO2, is a result of the modelling studies by Zickfeld et al. [66]. Besides, weakening of Indian summer monsoon under sulfate aerosol forcing is found by Meehl et al. [34] in experiments with global coupled ocean-atmosphere GCM. So far, there is no observational evidence in support of this theory. Yet, geological records reveal that such abrupt transitions in monsoon systems occurred in the past. A prominent example is West African Humid period during early to mid-Holocene, when Sahara was much greener that today (e.g. Prentice et al. [45]). It is suggested that an

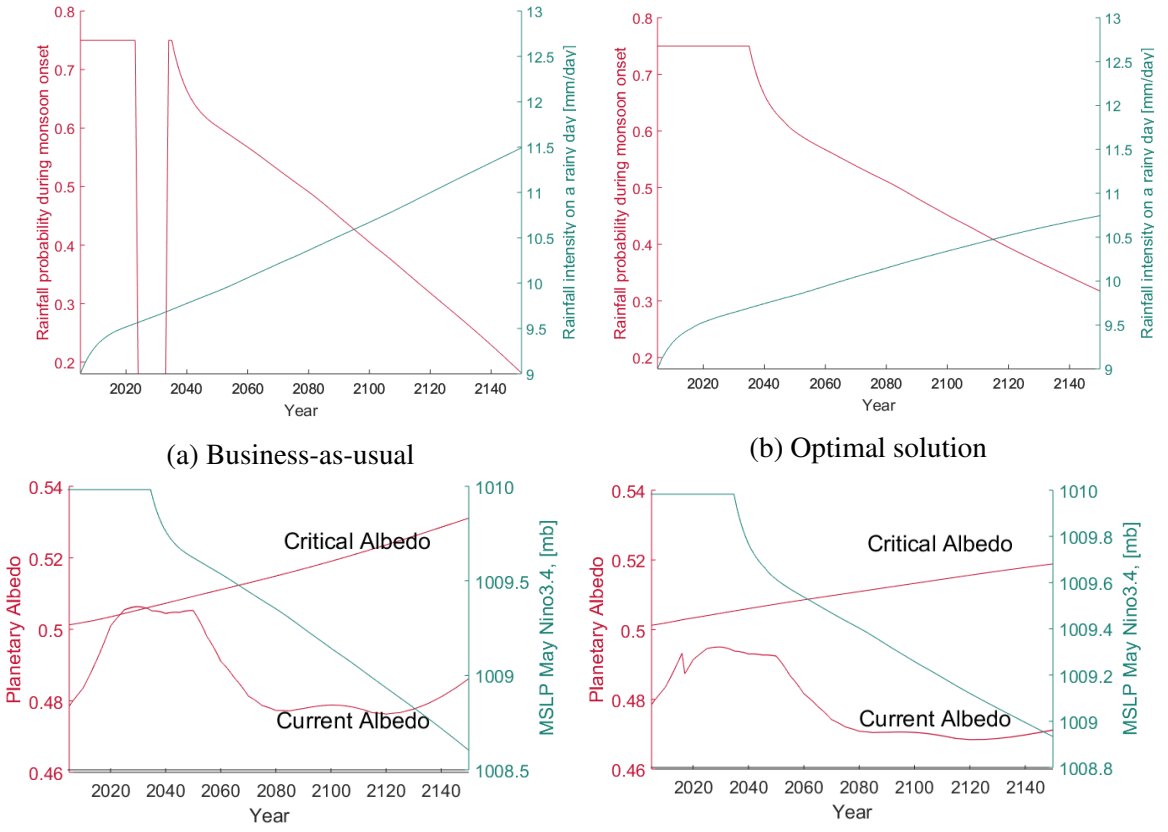

(a) Business-as-usual

(b) Optimal solution

(c) Business-as-usual

(d) Optimal solution

Fig. 2.11 (a,b) Evolution of factors that define seasonal mean ISM rainfall – rainfall probability during the monsoon onset and daily rainfall intensity – in the business-as-usual and the optimal solution; (c,d) Evolution of factors that define rainfall probability during the monsoon onset in the business-as-usual and the optimal solution.

albedo shifts towards higher values thereby keeping the bifurcation point out of reach. Also, aerosol intensity of production is decreasing over time, which widens the gap between the actual planetary albedo and the critical one even further. Albeit, the stringent mitigation efforts in optimal and Nash scenarios suffice to i) keep the albedo below the critical level in every year (Figure 2.11d, red curve) and ii) to limit an increase in daily rainfall intensity (Figure 2.11b, green curve).

important mechanism behind the Sahara greening was lowering effect of expanded North African vegetation cover on surface albedo, which was strong enough to shift a desert into a savannah-type environment for a period of time (Claussen and Gayler [15]). Based on that study, Brovkin et al. [8] developed a simple conceptual model of climate-vegetation interaction, which depicts multiple stable states in the atmosphere-vegetation system – i) low precipitation and absent vegetation and ii) moderate precipitation and permanent vegetation cover. Noteworthy, the model developed by Zickfeld [65] and used in Zickfeld et al. [66] adopts the concept from the box model by Brovkin et al. [8].

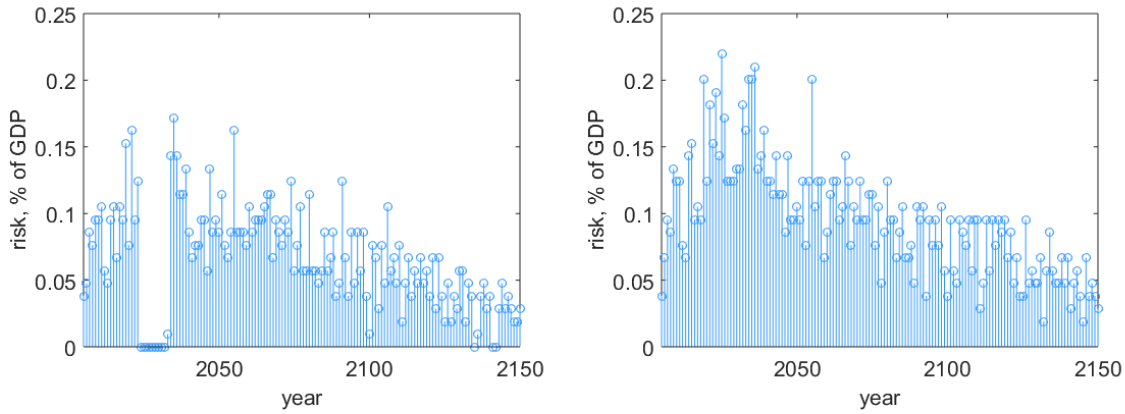

(a) Business-as-usual policy (b) Optimal solution

Fig. 2.12 The economic risk posed by severe excess of the ISM rainfall

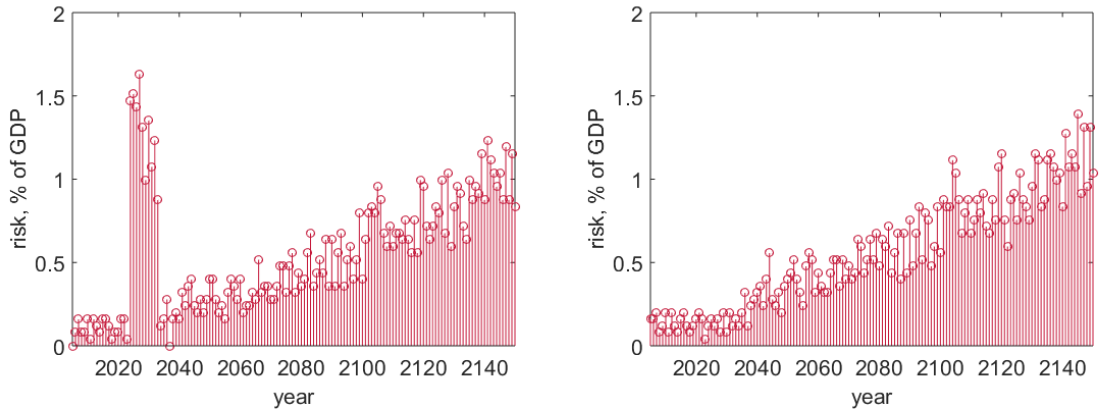

(a) Business-as-usual policy (b) Optimal solution

Fig. 2.13 The economic risk posed by severe deficiency of the ISM rainfall

The implications of the monsoon failure events for India's economy are illustrated in Figures 2.12 and 2.13. Here we calculate the economic risk for both ISM rainfall extremes by multiplying the occurrence of the event by the related damage. The near-term period of prolonged droughts in the business-as-usual solution translates into a period of substantial losses (Figure 2.13a). These costs are reduced in the optimal climate policy (Figure 2.13). However, the efforts in the optimal scenario do now suffice to prevent changes in the climate. First, accelerated global mean temperature increase induces the period of high risk of floods in the near-term (Figure 2.12b). Second, large-scale dynamical changes associated with global warming alter rainfall. In particular, mean sea level pressure over the region NINO3.4 decreases the probability of a moderate rainfall during the ISM season and thus increases the risk of the damage-inducing droughts. We remind that discounting implies less concern for a

longer-term damages. Thereby, present values of the ISM rainfall-related risks, presented in the Figures 2.12 and 2.13, differ over time.

Next, we examine the implications of one-sided environmental policies, which target either air pollution or global warming. Policy μ^{CO2} finds optimal carbon emissions control rate, while making no (direct) effort towards sulphur control, i.e. $\mu^{a}_{j,t} = 0$. Policy μ^{SO2}, in contrast, is committed to curb sulphur emissions while keeping $\mu^{c}_{j,t}$ zero. The resulting seasonal mean monsoon rainfall frequency distributions are depicted in Figure 2.14. We present both against the optimal solution. The policy that targets only air pollution leads to an exposure to an increased future risk of severe rainfall deficiency during summer (Figure 2.15). Even though the sulphur control rate is sufficient to prevent transgressing the bifurcation point, "dry" years become more frequent due to dynamical changes in climate system (here: the MSLP in eastern Pacific). Policy that targets only carbon control is more successfull in reducing the amount of “dry” seasons.[19] That is, in terms of the ISM rainfall extreme events carbon control policy plays bigger role than the sulphur policy. This is because carbon policy has implications for a longer-term and larger scale changes. Importantly, success of carbon policy in preventing the near-term droughts is conditional upon sufficiently strong and early carbon control as these are the requirements for reaping the co-benefit of climate policy. Business-as-usual sulphur emissions peak around the year 2030, thereby this is the time when carbon policy is of particular importance.

Table 2.1 provides a summary of the policies implications for India’s welfare. It is evident that i) global cooperation scenario improves on the no-cooperation scenario; and ii) benefits of only-carbon control significantly exceed those of only-sulphur control.

Table 2.1 Welfare gains of different policies: relative percentage change with respect to the business-as-usual scenario.

Policy	Welfare gains, in %
Optimal solution	0.9867
Nash equilibrium	0.8109
μ^{CO2}	0.8947
μ^{SO2}	0.2357

Coming back to calibration of the ISM-related damage function, we acknowledge uncertainty in future GDP exposure to the ISM rainfall extreme events. As such, apart from agricultural

[19] Although, we remind that sulphur emissions in India peak around the year 2030 and then show diminishing trend as business-a-usual scenario already incorporates sulphur control efforts.

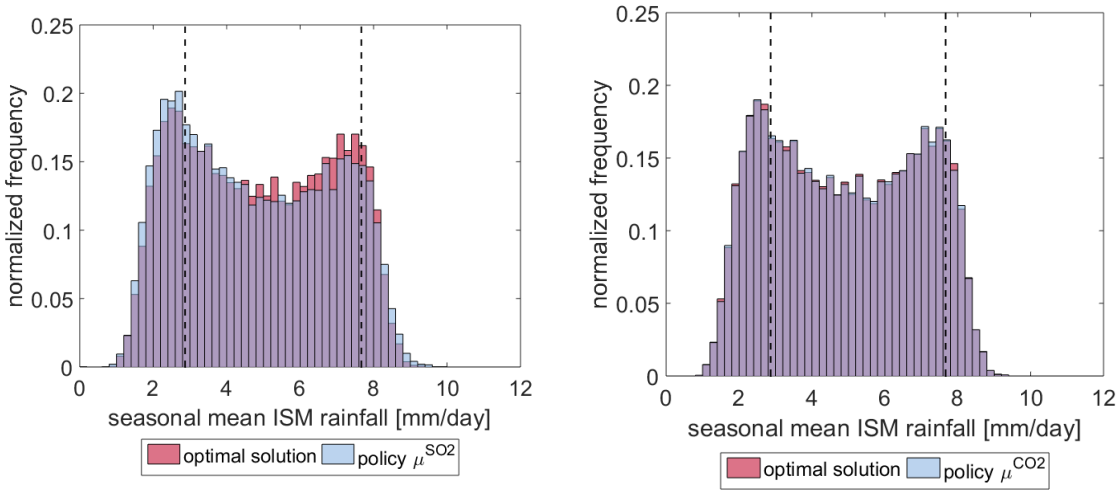

(a) (b)

Fig. 2.14 The ISM rainfall frequency distributions under policy μ^{SO2} (a) and policy μ^{CO2} (b). Both are presented against the optimal solution.

output, water scarcity might also jeopardize energy supply and power generation.[20] Taking this additional impact into account, our parametrisation of D_{dought} might be rather conservative. Accordingly, we consider the case when drought-related damage costs are higher i.e. $D_{drought} = 5\%$ and attempt to answer the question as to what extent the risk of increased droughts defines India's decision on carbon control rate.

Figures 2.16 and 2.17 illustrate the optimal and Nash solutions, respectively, for alternative damage costs specifications. We mention that in both policy scenarios the optimal carbon control rate is identical for alternative damage costs. However, the associated risks differ significantly (Figures 2.16b and 2.17b). Realizing the threat, why would India not initiate substantially stronger control? Limiting atmospheric carbon concentration requires global efforts and cannot be handled by single country. In turn, even assuming international cooperation, countries base their policy decision on regional costs and benefits. Besides, other factors, which are not explicitly modelled in our study, e.g. technological inertia, put a burden on rate of change in the emissions control. Thereby, to some extent future risks

[20]Note that water scarcity does not only affect energy generation of hydropower plant but also of all power plants that are cooled with water such as nuclear power plants and coal-fired power plants. As electricity supply in India strongly depends on coal-fired power plants (IEA [21]), energy supply is threatened by the occurrence of severe droughts. Indeed, there were some incidences in the past, where coal-fired power plants had to be shut down due to water scarcity (see e.g. WEO [61]).

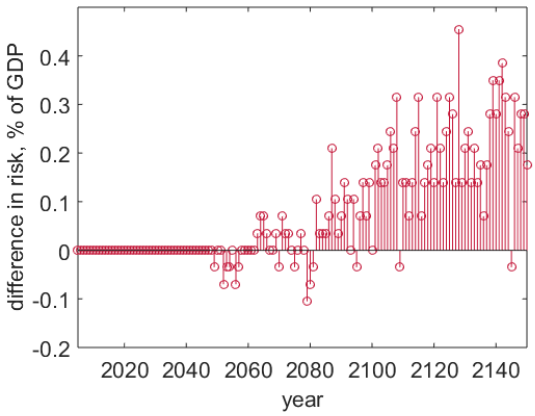

Fig. 2.15 Difference in the risk posed by the deficient ISM rainfall events under policy μ^{SO2} relative to that of the optimal solution.

associated with climate change may already be locked in. In sum, our results highlight yet another important implication for regional strategic planning. Global cooperation on combatting climate change may not be sufficient to ensure avoiding an increase in extreme events. In this view, investments in adaptation to flood- and drought-related events must complement mitigation efforts to secure future regional welfare.

At last, we compare the optimal solutions i) with $D^{drought} = 5\%$ and ii) with $D^{flood} = 5\%$. While optimal carbon controls coincide (not shown here), the associated ISM rainfall risks differ significantly (Figure 2.18). The occurence of severe ISM rainfall excess events is lower in comparison to severe deficiency events. However, floods are mostly near-term risk, while droughts pose bigger threat in the future. This serves as yet another reminder of potential implications of discounting for comparison of the risks that span over the long period of time. In sum, we emphasize the three factors that define the risk of the ISM rainfall extremes in present modelling framework: i) occurrence; ii) implications; and iii) time.
As a final remark, we note that our results are subject to uncertainties, in particular, related to location of bifurcation point in the ISM system. In this respect, the multi-parameter uncertainty analysis of a bifurcation point in surface albedo by Knopf et al. [26] suggests that the occurrence of the bifurcation point in the ISM model by Zickfeld et al. [66] is robust over a wide range of parameter values, but is sensitive to a parameter choice. The identified most influential parameters include integral transmissions function in clear sky atmosphere, parameter that determines outgoing long-wave radiation, constant for the determination of eddy diffusivities, optical thickness of stratus clouds, and parameter of the temperature height dependence. Also, Knopf [25] stresses the potential role of structural uncertainties, such

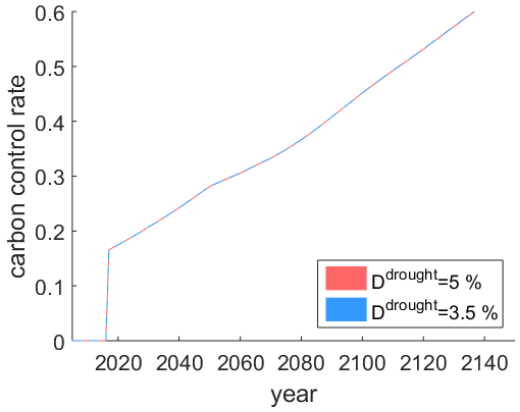

(a) India's carbon control rate

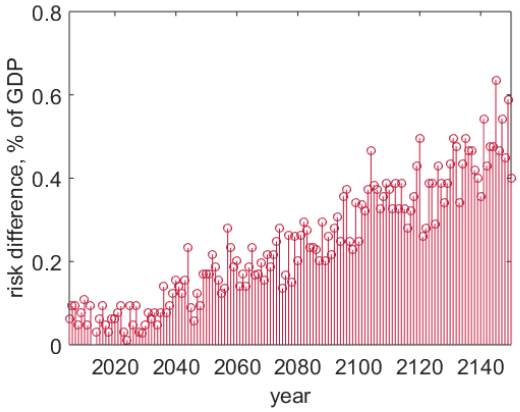

(b) Difference in the risk posed by the deficient ISM rainfall events in case $D^{drought} = 5\%$ relative to $D^{drought} = 3.5\%$.

Fig. 2.16 Optimal solution for alternative drought-related damage costs

as the influence of Tibetan Plateau, which have not been analysed so far. Besides, due to absence of cloud representation in our model, present study is limited to description of the direct effects of aerosols. The indirect effects, i.e. via clouds, may alter current planetary albedo A_t^{pl} towards higher values. All things considered, we stress the qualitative value of our model results. We draw attention to the possibility of abrupt transition of the ISM system towards low-precipitation state, which is characterized by prolonged period of extensive droughts.

2.4 Conclusions

Environmental policy decisions are formed on the basis of the associated costs and benefits occurring for each domestic region. However, a lack of international coordination may have adverse implications for regional economies – for some more profound than for the others. As such, in the present study we explicitly model the ISM system within a regional integrated assessment model. The ISM is one of the tipping elements of Earth's system, but so far it has received unjustifiably little attention in the environmental policy literature.

We show that the ISM system is altered in response to both regional and global policies. However, the geographical position of the South Asian countries predefined their marked vulnerability to deviations in ISM rainfall. Extreme ISM rainfall events – severe floods or severe droughts – hit the economy and compromise the livelihood of its numerous population.

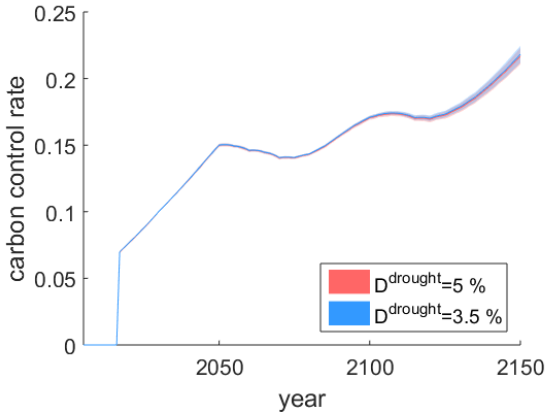

(a) India's carbon control rate

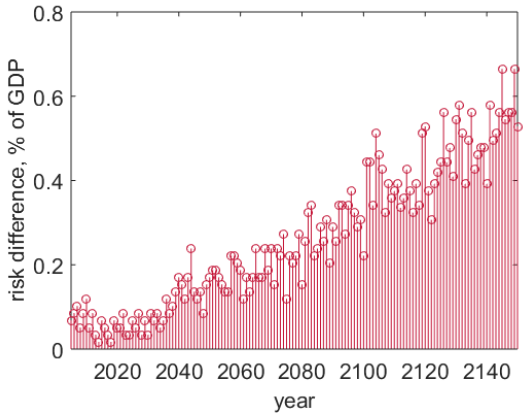

(b) Difference in the risk posed by the deficient ISM rainfall events in case $D^{drought} = 5\%$ relative to $D^{drought} = 3.5\%$.

Fig. 2.17 Nash equilibrium solution for alternative drought-related damage costs

Our results indicate that under a business-as-usual policy there is a potential for an increased frequency of extreme monsoon rainfall events in the following decades. Moreover, we demonstrate that air pollution constitutes costs beyond those of health effects, as high concentration of aerosols may weaken the ISM circulation, leading to prolonged period of droughts. Our results suggest that policy mix in the Nash equilibrium solution suffice to prevent transgressing the bifurcation point in planetary albedo value, although, an increase in future extremes is substantial. The optimal solution improves on the Nash equilibrium solution in terms of India's welfare. Assuming the commitment of all regions to joint action to curb emissions, India, in particular, initiates stronger carbon emissions control and, thereby, reaps the co-benefit of climate policy in terms of better air quality and less frequent years with severe deficiency of the ISM rainfall in the near-term. Nevertheless, we demonstrate that even joint global efforts may not be sufficient to fully eliminate the risk, as discrepancy in costs and benefits among the regions gives rise to a conflict of interests. We also note that inertia in socio-economic system and technological change limit the rate of change in emissions control and thereby the adverse impacts of climate change may already be locked in. Thus, adaptation may be critical to future regional welfare. Research into adaptation strategies for the South Asian region is a fruitful area for future research in the face of more frequent extreme monsoon rainfall events.

To conclude, we answer the question: "Can India prevent summer monsoon extremes?". Our modelling results advocate that it can't; however, India is capable of limiting an occurrence of

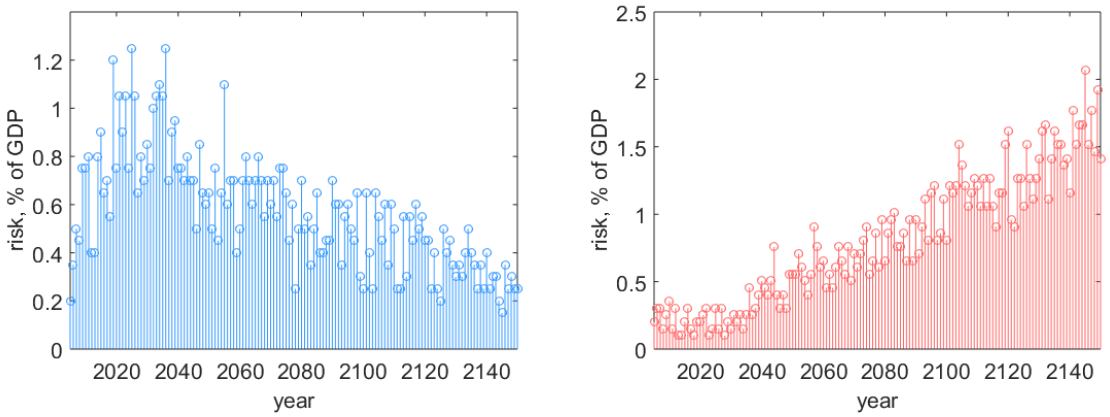

(a) The risk posed by the excess ISM rainfall, where $D^{flood} = 5\%$

(b) The risk posed by the deficient ISM rainfall, where $D^{drought} = 5\%$

Fig. 2.18 Optimal solution for alternative damage costs specifications.

extremes by means of stringent environmental policy. What's more, regional efforts constitute only part of the solution, as global cooperation with sizable contributions is necessary.

Appendices

2 A Temporal Resolution Refinement and Robustness Check

In this section, we provide an overview of changes to the RICE-H model associated with temporal resolution refinement. We denote the RICE-H model with a one-year time step by RICE-H-1. Additionally, to better understand the impact of an alternative time step we present the robustness check. Altering the time step from five-year to annual boils down to interpolation of the time-varying parameters, adjustment of the discount factor, and recalibration of the carbon cycle and capital accumulation equations. Specifically, we perform linear interpolation between the five-year time steps of projections on population growth, urbanization trend, total factor productivity growth, trends of carbon and sulfur emission intensities, and time-dependent coefficients of the abatement cost function.

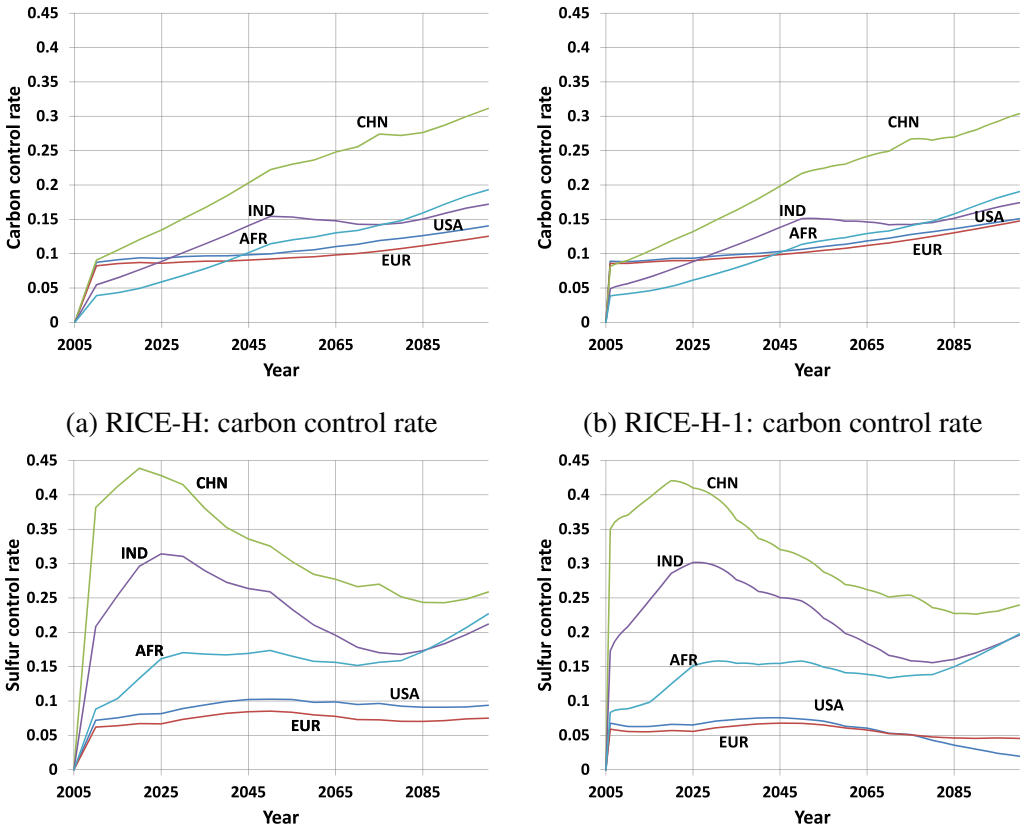

(a) RICE-H: carbon control rate

(b) RICE-H-1: carbon control rate

(c) RICE-H: sulfur control rate

(d) RICE-H-1: sulfur control rate

Fig. 2.A.1 Comparison of RICE-H and RICE-H-1 results: optimal carbon and sulfur control rates in Nash equilibrium.

To demonstrate robustness of the model with a refined temporal resolution we replicate the results shown in Figure 1 in Ikefuji et al. [22]. As evident from the Figure 2.A.1, the key difference between the two models is the possibiliy to alter control rates on an annual basis.

2 B Optimal Carbon Control – Regional Heterogeneity

Figure 2.B.1 illustrates the regional efforts on carbon control rate and associated levels of emissions in the year 2100 in the scenario of global cooperation (optimal) and of no cooperation (Nash).

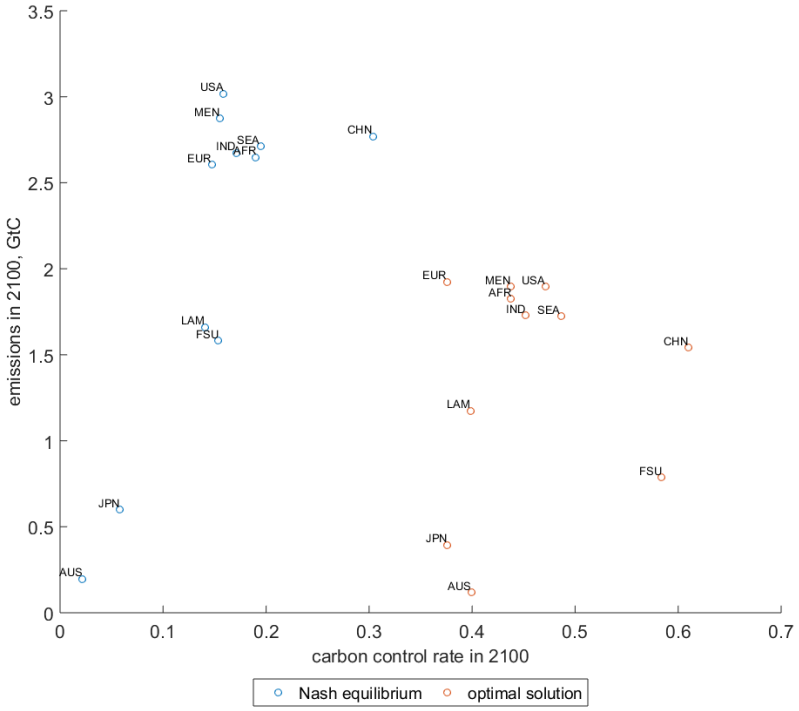

Fig. 2.B.1 Characterization of the regions by carbon emissions and carbon control rate in the year 2100.

2 C Calibration

Here, we direct attention to RICE-ISM parameter values, which correspond to those of RICE-H and are not explained in the main text of the paper. Fixed economic parameters in RICE-H correspond to those from Nordhaus and Boyer [41]. Time-varying parameters are calibrated so that the business-as-usual solution resembles the A2 marker scenario from the Special Report on Emission Scenarios (SRES) that was commissioned by the IPCC (Nakicenovic et al. [37]).[21] The A2 marker scenario is quantified using the Atmospheric Stabilization Framework model (ASF) as described in Sankovski et al. [49] and is thereby denoted by A2-ASF.

Table 2.C.1 Average GNP per capita growth rates in A2-ASF in ASF regions from 1990 until 2100, in % per year (Sankovski et al. [49]).

Africa	Centrally Planned Asia	Eastern Europe and NIS	Latin America	Middle East
2.21	2.77	2.01	1.81	1.41
OECD East	**OECD West**	**Southeast Asia and Oceania**	**USA**	**Global**
1.04	1.13	2.36	1.00	1.32

The A2-ASF is characterized by rapid global population growth, which reaches 11 billion by 2050 and 15 billion by 2100 (Figure 2.C.2a), and relatively slow GNP per capita growth compared to other scenarios. In particular, A2-ASF predefines the regional GNP per capita growth (Table 2.C.1) based on the A2 global GNP growth target in 2100 (trillion USD 1990) of $250 \pm 5\%$. Accordingly, TFP and emissions intensities in RICE-H, illustrated in Figures 2.C.2b - 2.C.3a, are calibrated to fit output and emissions in business-as-usual scenario to those in A2-ASF.

[21] To facilitate model calibration for regions definition different from those in SRES, RICE-H uses the downscaled projected population $N_{j,t}$, population density PD_j, and GDP data from Center for International Earth Science Information Network (Center for International Earth Science Information Network (CIESIN) [11] and Center for International Earth Science Information Network (CIESIN) [12])

Table 2.C.2 The RICE-ISM model parameters.

Parameter	Description	Value	Section
ε	Elasticity of output with respect to capital	0.3	
δ^k	Depreciation rate of capital	0.1	
δ^c	Depreciation rate of CO_2	0.0052	
ρ	Discount rate	3 %/year	2.2.1
$D_{drought}$	Drought-related damage costs	3.5% of GDP	
D_{flood}	Flood-related damage costs	0.84% of GDP	
ζ	Coeff. in the damage function approximation	1e+20	
τ_1	Temperature equation coefficient	0.724	
τ_2	Temperature equation coefficient	0.1	
ξ^c, ξ^a	Abatement cost parameters	2.8	
P^{dry}	Precipitation rate on a dry day	0 mm/day	
P_0^{wet}	Precipitation rate on a wet day (historical)	9 mm/day	2.2.2
p_0^{init}	Initial probability of a wet state	0.75	
p_{max}	Maximum probability of either state	0.82	
δ	Memory period	17 days	
p''	Coefficient in rainfall intensity equation	0.42 mm/day	
p_0	Coeff. in initial rainfall probability equation	0.2	
p'	Coeff. in initial rainfall probability equation	0.41	
m_0	Coeff. in initial rainfall probability equation	1008.649 mb	
m'	Coeff. in the evolution of MSLP under GW	0.29	
$m_0^{NINO3.4}$	Coeff. in the evolution of MSLP under GW	1009.98344547 mb	2.2.3
O	Conversion parameter	1.5	
A_s	Current surface albedo	0.16	
H^{SO2}	Fractional sulfate yield	0.65	
T_{pl}	Fraction of light transmitted by above aerosol layer	0.76	
β_{pl}	Backscatter fraction	0.29	
α_{pl}	Mass scattering efficiency	8.5 m^2/g	
V	Sulfate atmospheric lifetime	2/365	
Ω	South Asian area	$4.12 \cdot 10^{12}$ m^2	
α_1^{pl}	Coefficient in critical albedo relation	0.02	
α_2^{pl}	Coefficient in critical albedo relation	0.37	

Table 2.C.3 Region-specific parameters.

Parameter	USA	EUR	JPN	AUS	FSU	CHN	IND	SEA	LAM	MEN	AFR
$\beta^c_{1,j}$	0.01	0.01	0.004	0.004	0.02	0.054	0.092	0.03	0.01	0.007	0.058
$\beta^c_{2,j} 10^3$	0.0	-0.01	-0.003	-0.003	-0.011	0.239	5.00	0.71	0.0217	0.260	4.000
$\beta^c_{3,j}$	1.00	0.99	1.000	1.000	1.00	0.946	0.601	0.66	0.85	1.051	1.233
$\tau_{0,j}$	-4.3	-6.20	-3.54	-2.971	-6.77	-3.48	-3.896	-3.72	-3.255	-4.422	-4.149
τ^c_j	0.7	0.98	0.56	0.468	1.08	0.572	0.62	0.588	0.52	0.7	0.656
$\tau^a_{1,j}$	-0.03	-0.03	-0.031	-0.01	-0.031	-0.03	-0.031	-0.03	-0.031	-0.031	-0.031
$\tau^a_{2,j}$	-0.10	-0.08	-0.003	-0.01	-0.175	-0.08	-0.020	-0.010	-0.035	-0.022	-0.035
$\tau^a_{3,j}$	1.35	1.7	37.52	21.9	0.786	1.644	6.7	13.5	3.846	6.103	3.925
w_j in %	14.5	3.6	0.3	6.34	17.8	10.31	2.18	3.25	16.7	6.54	18.64
$\gamma_{1,j} \cdot 10^3$	0.01	-0.07	-0.15	-1.199	0.020	0.67	3.3	1.458	-0.56	1.9	2.42
$\gamma_{2,j} \cdot 10^3$	1.41	1.6	1.568	1.418	1.14	1.222	1.520	1.66	1.21	1.455	1.83
$\frac{PD_{j,t}}{80}$	3.6	7.85	13.6	5.510	7.84	21.00	19.63	21.94	8.4	11.99	16.8

Parameters that reflect climate change impacts, urbanization and abatement costs are not represented in A2-ASF and are derived by Ikefuji et al. [22] from various sources. Parameters $\beta^c_{1,j}$, $\beta^c_{2,j}$ and $\beta^c_{3,j}$ in climate-induced health impacts relation reflect regional vulnerability to malaria, cardiovascular disease, diarrhoea and malnutrition. These are quantified by Ikefuji et al. [22] after McMichael et al. [33].

Air-pollution-induced health impacts $\beta^a_{j,t}$ in RICE-H are calibrated after Spadaro and Rabl [51], who trace the passage of the pollutant from the source to the affected receptors and thereby evaluate the damage cost per tonne of sulfur dioxide. In addition, health impacts vary both regionally and over time with urbanization $r_{j,t}$ and population density PD_j. The higher urbanization level and population density, the stronger the impact. Accordingly, $\beta^a_{j,t}$ is defined as:

$$\beta^a_{j,t} = \beta^a_0 \cdot (PD_j/80) \cdot ((1 - r_{j,t}) + 2 \cdot r_{j,t}) \tag{B.0.1}$$

Urbanization is assumed to grow exponentially, converging to 0.95 by the year 2200, and is fitted to match projections by UN [55] until 2050 (Figure 2.C.3c).

Damage function in RICE-H has a functional form that is identical to the one in Nordhaus [40], but coefficients $\gamma_{1,j}$ and $\gamma_{2,j}$ are recalibrated to exclude health impacts.

After Nordhaus [40], carbon abatement cost parameter $\alpha^c_{j,t}$ is chosen so that in every year under 100% carbon control rate marginal cost of abatement matches the backstop price. Calibration of sulfur abatement cost parameter, $\alpha^a_{j,t}$, is based on global estimate by Bahn and Leach [4] (Figure 3.8a).

Temperature equation parameters are chosen to normalize regional temperature changes $Z_{j,0} = 0$. That is, temperature increase is considered relative to the year 2005.

All in all, Table 2.C.2 reports the RICE-ISM model parameters. Region-specific parameters are listed in Table 3.A.1 with values presented in Table 3.A.2. Time-varying parameters are listed in Table 2.C.5 and illustrated in Figures 2.C.2 and 2.C.3.

Table 2.C.4 List of region-specific parameters.

Parameter	Description	Equation
$\beta^c_{1,j}$, $\beta^c_{2,j}$,$\beta^c_{3,j}$	Coefficient in temperature-induced damage function	2.2.6
$\tau_{0,j}$, τ^c_j, $\tau^a_{1,j}$, $\tau^a_{2,j}$, $\tau^a_{3,j}$	Temperature equation coefficients	2.2.11
w_j	Region's share of global landmass	2.2.12
$\gamma_{1,j}$, $\gamma_{2,j}$	Damage function coefficients	3.2.11
PD_j	Population density	B.0.1

Table 2.C.5 List of time-varying parameters.

Parameter	Description	Equation
$N_{j,t}$	Population	3.2.1
$\psi_{j,t}$	Technological efficiency	2.2.3
$\beta^a_{j,t}$	Coefficient in air-pollution-induced damage function	2.2.7
$\sigma^{cc}_{j,t}$, $\sigma^{ac}_{j,t}$, $\sigma^{aa}_{j,t}$	Emissions intensities	2.2.8
$\alpha^c_{j,t}$, α^a_t	Abatement cost coefficients	2.2.9
$r_{j,t}$	Urbanization	B.0.1

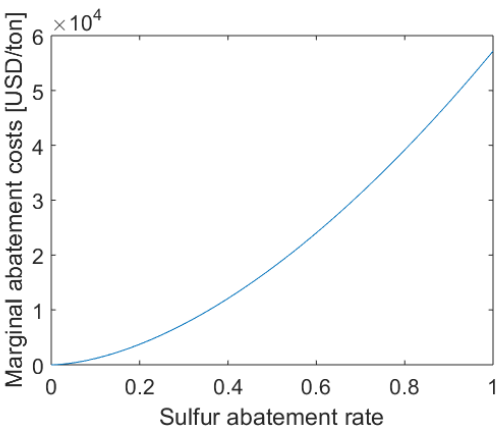

(a) Global MAC (source: Bahn and Leach [4])

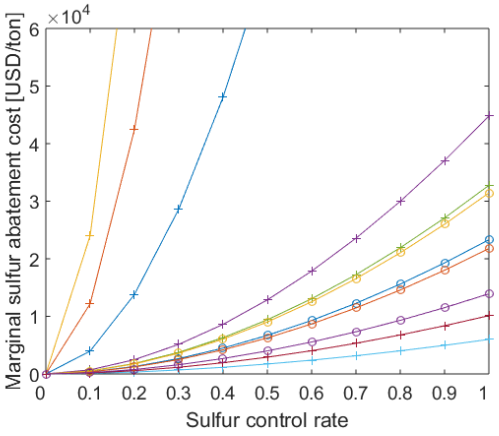

(b) Regional MACs in RICE-ISM: $-\frac{\partial A_{j,t}}{\partial E^a_{j,t}}$

Fig. 2.C.1 Marginal sulfur abatement costs (MAC).

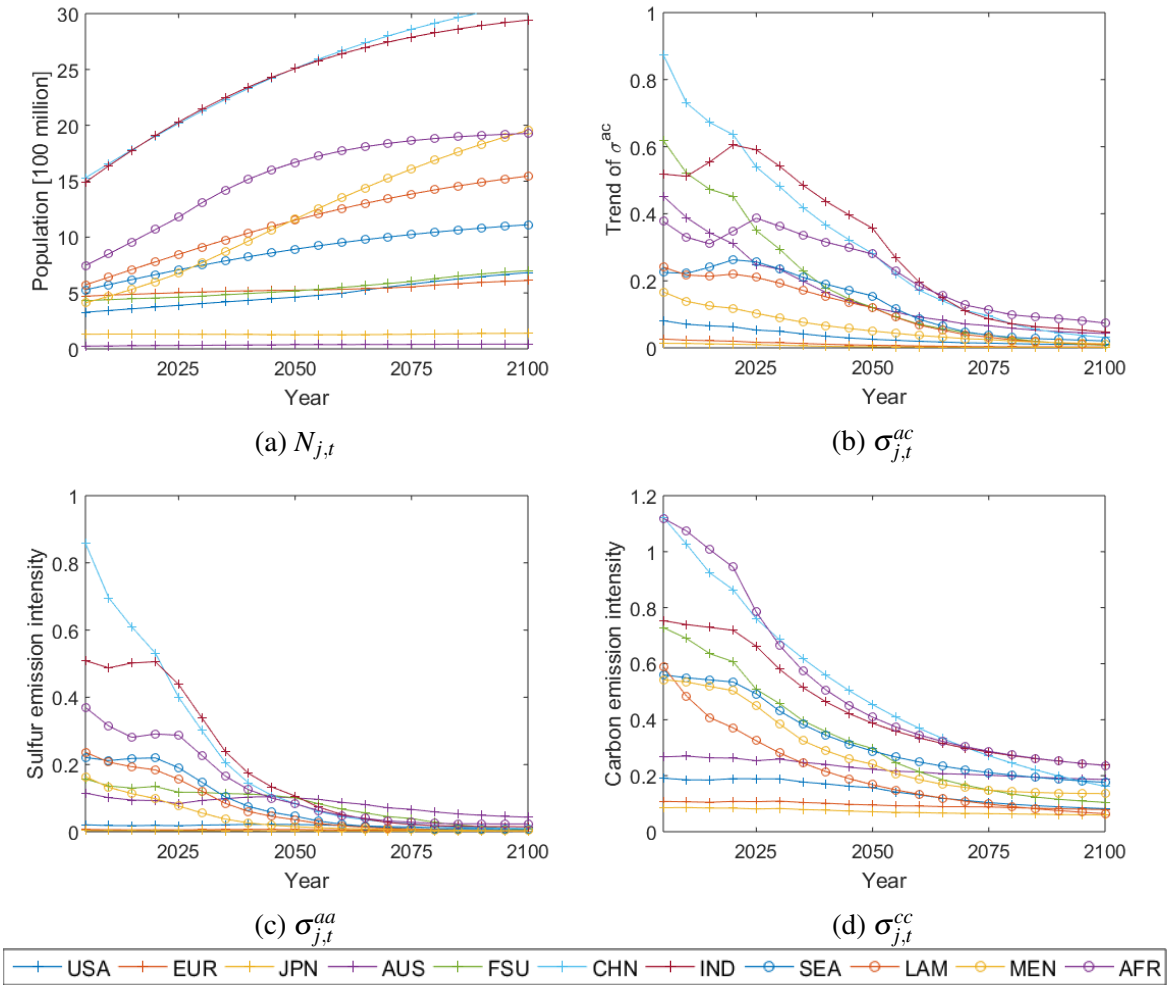

(a) $N_{j,t}$ (b) $\sigma^{ac}_{j,t}$

(c) $\sigma^{aa}_{j,t}$ (d) $\sigma^{cc}_{j,t}$

Fig. 2.C.2 Time-varying model parameters listed in Table 2.C.5

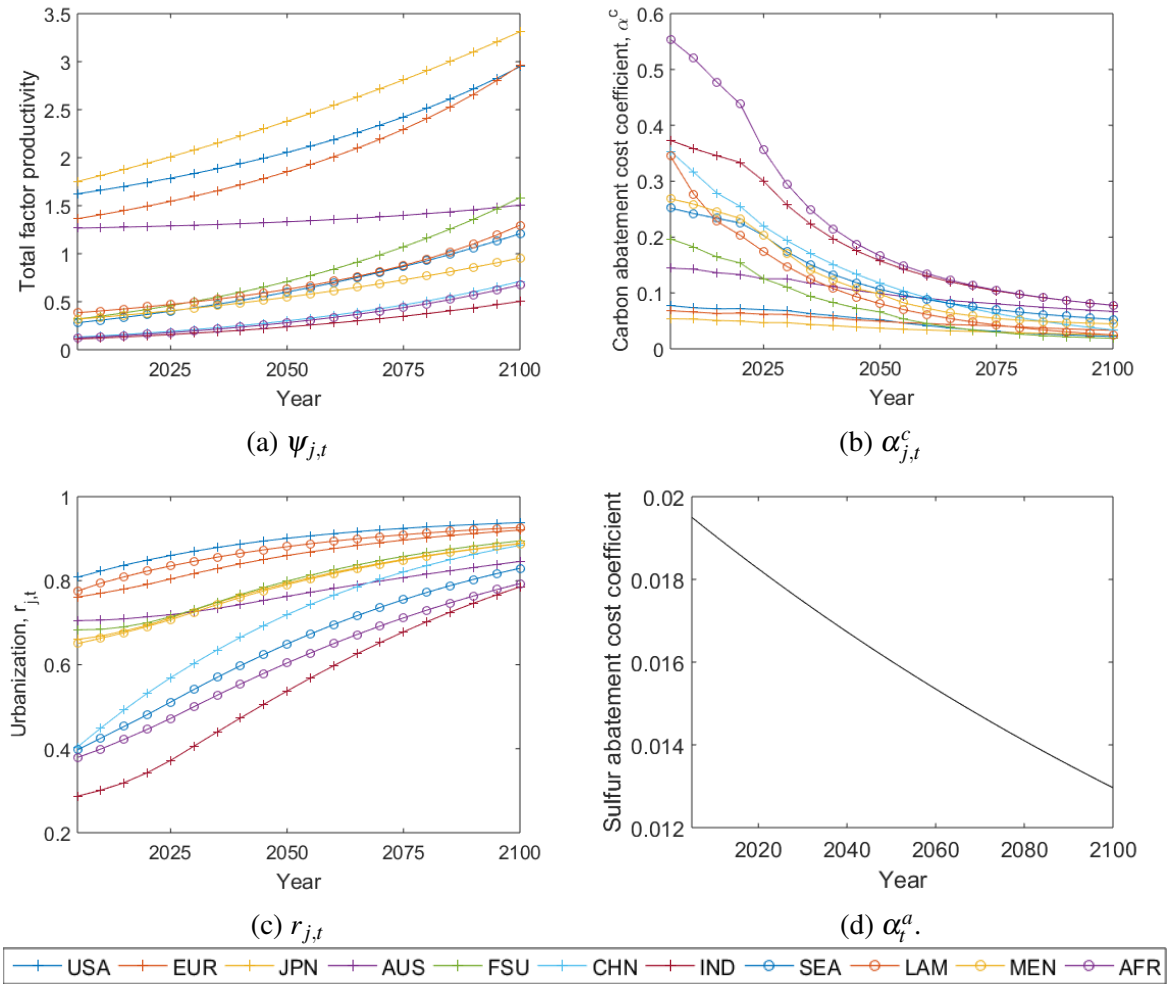

(a) $\psi_{j,t}$ (b) $\alpha^c_{j,t}$

(c) $r_{j,t}$ (d) α^a_t.

Fig. 2.C.3 Time-varying model parameters listed in Table 2.C.5

References

[1] Aldy, J., Pizer, W., Tavoni, M., Reis, L. A., Akimoto, K., Blanford, G., Carraro, C., Clarke, L. E., Edmonds, J., Iyer, G. C., McJeon, H. C., Richels, R., Rose, S., Sano, F., 2016. Economic tools to promote transparency and comparability in the Paris Agreement. Nature Clim. Change.

[2] Allen, M. R., Ingram, W. J., Sep. 2002. Constraints on future changes in climate and the hydrologic cycle. Nature 419 (6903), 224–232. URL http://dx.doi.org/10.1038/nature01092

[3] Atteridge, A., Shrivastava, M., Pahuja, N., Upadhyay, H., 2012. Climate policy in india: What shapes international, national and state policy? AMBIO 41 (1), 68–77.

[4] Bahn, O., Leach, A., 2008. The secondary benefits of climate change mitigation: an overlapping generations approach. Computational Management Science 5 (3), 233–257.

[5] Belaia, M., Funke, M., Glanemann, N., 2015. Global warming and a potential tipping point in the atlantic thermohaline circulation: The role of risk aversion. Environmental and Resource Economics, 1–33. URL http://dx.doi.org/10.1007/s10640-015-9978-x

[6] Boden, T., Marland, G., Andres, R., 2013. Global, regional, and national fossil-fuel CO2 emissions. , Carbon Dioxide Information Analysis Center, Oak Ridge National Laboratory, U.S. Department of Energy, Oak Ridge, Tenn., U.S.A.

[7] Bollasina, M. A., Ming, Y., Ramaswamy, V., 2011. Anthropogenic aerosols and the weakening of the south asian summer monsoon. Science 334 (6055), 502–505.

[8] Brovkin, V., Claussen, M., Petoukhov, V., Ganopolski, A., 1998. On the stability of the atmosphere-vegetation system in the sahara/sahel region. Journal of Geophysical Research: Atmospheres 103 (D24), 31613–31624. URL http://dx.doi.org/10.1029/1998JD200006

[9] Cai, Y., Lenton, T. M., Lontzek, T. S., 2016. Risk of multiple interacting tipping points should encourage rapid CO2 emission reduction. Nature Clim. Change 6 (5). [10] CAT, 2015. Climate action tracker. [Accessed 11 December 2015]. URL http://climateactiontracker.org/countries/india.html

[10] Center for International Earth Science Information Network (CIESIN), 2002. Countrylevel gdp and downscaled projections based on the a1, a2, b1, and b2 marker scenarios , 1990-2100 [digital version]. NY: CIESIN, Columbia University. URL http://www.ciesin.columbia.edu/datasets/downscaled

[11] Center for International Earth Science Information Network (CIESIN), 2005. Gridded population of the world (gpw) version 3. URL http://sedac.ciesin.columbia.edu/data/collection/gpw-v3

[12] Central Electricity Authority India, December 2016. All india installed capacity (in mw) of power stations. Online. URL http://www.cea.nic.in/reports/monthly/installedcapacity/2016/installed_capacity-12.pdf

[13] Charlson, R. J., Langner, J., Rodhe, H., Leovy, C. B., Warren, S. G., 1991. Perturbation of the northern hemisphere radiative balance by backscattering from anthropogenic sulfate aerosols*. Tellus B 43 (4), 152–163. URL http://dx.doi.org/10.1034/j.1600-0889.1991.t01-1-00013.x

[14] Claussen, M., Gayler, V., 1997. The greening of the sahara during the mid-holocene: Results of an interactive atmosphere-biome model. Global Ecology and Biogeography Letters 6 (5), 369–377. URL http://www.jstor.org/stable/2997337

[15] EPA, 2016. Sulfur dioxide basics. [Accessed 7 October 2016]. URL https://www.epa.gov/so2-pollution/sulfur-dioxide-basicseffects

[16] Gadgil, S., Gadgil, S., 2006. The indian monsoon, gdp and agriculture. Economic and political weekly 41 (47).

[17] Gin., Townsend, R. M., Vickery, J. I., 2008. Patterns of rainfall insurance participation in rural india. World Bank Economic Review 22, 539-566.

[18] Gupta, V., 2011. A critical assessment of climate change impacts, vulnerability and policy in india. Present environment and sustainable development 5, 12–22.

[19] IEA, 2013. CO2 emissions from fossil fuel combustion - highlights. Tech. rep., International Energy Agency.

[20] IEA, I. E. A., 2015. India Energy Outlook: World Energy Outlook Special Report.

[21] Ikefuji, M., Magnus, J. R., Sakamoto, H., 2014. The effect of health benefits on climate change mitigation policies. Climatic Change 126 (1-2), 229–243.

[22] IPCC, 2000. IPCC Special Report Emissions Scenarios. Intergovernmental Panel on Climate Change (IPCC), Cambridge University Press: Cambridge, UK.

[23] Jungclaus, J. H., Lorenz, S. J., Timmreck, C., Reick, C. H., Brovkin, V., Six, K., Segschneider, J., Giorgetta, M. A., Crowley, T. J., Pongratz, J., Krivova, N. A., Vieira, L. E., Solanki, S. K., Klocke, D., Botzet, M., Esch, M., Gayler, V., Haak, H., Raddatz, T. J., Roeckner, E., Schnur, R., Widmann, H., Claussen, M., Stevens, B., Marotzke, J., 2010. Climate and carbon-cycle variability over the last millennium. Climate of the Past 6 (5), 723–737.

[24] Knopf, B., 2006. On intrinsic uncertainties in earth system modelling. Ph.D. thesis, University Postdam.

[25] Knopf, B., Flechsig, M., Zickfeld, K., 2006. Multiparameter uncertainty analysis of a bifurcaiton point. Nonlinear Processes in Geophysics 13 (5).

[26] Knopf, B., Zickfeld, K., Flechsig, M., Petoukhov, V., 2008. Sensitivity of the indian monsoon to human activities. Advances in atmospheric sciences 25 (6), 932.

[27] Kucharski, F., Molteni, F., Yoo, J. H., 2006. Sst forcing of decadal indian monsoon rainfall variability. Geophysical Research Letters 33 (3), n/a–n/a, l03709. URL http://dx.doi.org/10.1029/2005GL025371

[28] Kumar, K. K., Rajagopalan, B., Hoerling, M., Bates, G., Cane, M., 2006. Unraveling the mystery of indian monsoon failure during el nino. Science 314 (5796), 115–119. URL http://science.sciencemag.org/content/314/5796/115

[29] Liu, X., Yanai, M., 2002. Influence of eurasian spring snow cover on asian summer rainfall. International Journal of Climatology 22, 10751089.

[30] Manne, A., Mendelsohn, R., Richels, R., 1995. MERGE : A model for evaluating regional and global effects of GHG reduction policies. Energy Policy 23 (1), 17–34

[31] Maplecroft, 2015. Climate change and environmental risk atlas 2015. [Accessed 10 October 2016]. URL https://maplecroft.com/portfolio/new-analysis/2014/10/29/climate-change-and-lack-food-security-multiply-risks-conflict-and-civil-unrest-32-countries-maplecroft/

[32] McMichael, A., Campbell-Lendrum, D., Kovats, S., Edwards, S., Wilkinson, P., Wilson, T., Nicholls, R., Hales, S., Tanser, F., Sueur, D., Schlesinger, M., Andronova, N., 2004. Comparative Quantification of Health Risks: Global and Regional Burden of Disease Due to Selected Major Risk Factors. World Health Organization, Geneva, Ch. Global climate change, pp. 1543–1649.

[33] Meehl, G., Washington, W. M., Erickson, D., Briegleb, B., Jaumann, P. J., 1996. Climate change from increased CO2 and direct and indirect effects of sulfate aerosols. Geophyical Research Letters 23, 3755–3758.

[34] Mendelsohn, R., Dinar, A., Williams, L., 4 2006. The distributional impact of climate change on rich and poor countries. Environment and Development Economics , 159–178.

[35] Ministry of Home Affairs, Government of India, 2011. Indian Census. online. URL http://censusindia.gov.in/Census_And_You/economic_activity.aspx

[36] Nakicenovic, N., Alcamo, J., Davis, G., de Vries, B., Fenhann, J., Gaffin, S., Gregory, K., Grubler, A., Jung, T. Y., Kram, T., Lebre La Rovere, E., Michaelis, L., Mori, S., Morita, T., Pepper, W., Pitcher, H., Price, L., Riahi, K., Roehrl, A., Rogner, H. H., Sankovski, A., Schlesinger, M., Shukla, P., Smith, S., Swart, R., van Rooijen, S., Victor, N., Dadi, Z., 2000. IPCC Special Report on Emissions Scenarios (SRES). Cambridge University Press, UK. URL http://www.ipcc.ch/ipccreports/sres/emission/index.php?idp=0

[37] NASA, 2016. Earth observatory. [Accessed 7 October 2016]. URL http://earthobservatory.nasa.gov/IOTD/view.php?id=87154

[38] Nicholls, R. J., Tol, R. S. J., Vafeidis, A. T., 2008. Global estimates of the impact of a collapse of the west antarctic ice sheet: an application of fund. Climatic Change 91 (1), 171–191. URL http://dx.doi.org/10.1007/s10584-008-9424-y

[39] Nordhaus, W. D., 2010. Economic aspects of global warming in a post-copenhagen environment. Proceedings of the National Academy of Sciences 107 (26), 11721–11726.

[40] Nordhaus, W. D., Boyer, J., 2000. Warming the World: Economic Models of Global Warming. MIT Press, Cambridge Mass.

[41] Nordhaus, W. D., Yang, Z., 1996. A regional dynamic general-equilibrium model of alternative climate-change strategies. The American Economic Review 86 (4), 741–765.

[42] Olhoff, A., Christensen, J. M., Burgon, P., Bakkegaard, R. K., Larsen, C., Schletz, M. C., 2015. The emissions gap report 2015: A UNEP synthesis report. Tech. rep., United Nations Environment Programme, Nairobi.

[43] PBL, 2015. The climate pledge INDC tool. [Accessed December 2015]. URL http://infographics.pbl.nl/indc/

[44] Prentice, I. C., Jolly, D., participants , B. ., 2000. Mid-holocene and glacial-maximum vegetation geography of the northern continents and africa. Journal of Biogeography 27 (3), 507–519. URL http://dx.doi.org/10.1046/j.1365-2699.2000.00425.x

[45] Rajagopalan, B., 2009. Risk assessment and forecasting of indian summer monsoon for agricultural drought impact planning. Completion Report 215, Colorado Water Institute, Colorado State University.

[46] Ramisch, A., Lockot, G., Haberzettl, T., Hartmann, K., Kuhn, G., Lehmkuhl, F., Schimpf, S., Schulte, P., Stauch, G., Wang, R., Wünnemann, B., Yan, D., Zhang, Yongzhan an Diekmann, B., 2016. A persistent northern boundary of indian summer monsoon precipitation over central asia during the holocene. Nature Scientific Reports 5 (13).

[47] Robock, A., Mu, M., Vinnikov, K., Robinson, D., 2003. Land surface conditions over eurasia and indian summer monsoon rainfall. Journal of Geophysical Research: Atmospheres 108 (D4), n/a–n/a, 4131. URL http://dx.doi.org/10.1029/2002JD002286

[48] Sankovski, A., Barbour, W., Pepper, W., 2000. Quantification of the IS99 emission scenario storylines using the atmospheric stabilization framework. Technological Forecasting and Social Change 63 (2–3), 263 – 287. URL http://www.sciencedirect.com/science/article/pii/S0040162599001006

[49] Schewe, J., Levermann, A., 2012. A statistically predictive model for future monsoon failure in india. Environmental Research Letters 7, 1–9.

[50] Spadaro, J. V., Rabl, A., 1999. Estimates of real damage from air pollution: Site dependence and simple impact indices for lca. The International Journal of Life Cycle Assessment 4 (4), 229–243. URL http://dx.doi.org/10.1007/BF02979503

[51] Srivastava, R. K., 2000. Controlling SO2 emissions: a review of technologies. Tech. rep., U.S. Environmental Protection Agency, National Risk Management Research Laboratory.

[52] Trenberth, K., 2005. Uncertainty in hurricanes and global warming. Science 308 (5729), 1753–1754. URL http://science.sciencemag.org/content/308/5729/1753

[53] Turner, A. G., Annamalai, H., 2012. Climate change and the south asian summer monsoon. Nature Clim. Change 2, 587–595.

[54] UN, 2010. World urbanization prospects, the 2009 revision. URL http://esa.un.org/unpd/wup/

[55] Vecchi, G. A., Soden, B. J., Wittenberg, A. T., Held, I. M., Leetmaa, A., Harrison, M. J., May 2006. Weakening of tropical pacific atmospheric circulation due to anthropogenic forcing. Nature 441 (7089), 73–76. URL http://dx.doi.org/10.1038/nature04744

[56] Venkataraman, C., Chandramouli, B., Patwardhan, A., 1999. Anthropogenic sulphate aerosol from india: estimates of burden and direct radiative forcing. Atmospheric Environment 33 (19), 3225 – 3235. URL http://www.sciencedirect.com/science/article/pii/S135223109800140X

[57] Wang, P., Clemens, S., Beaufort, L., Braconnot, P., Ganssen, G., Jian, Z., Kershaw, P., Sarnthein, M., 2005. Evolution and variability of the Asian monsoon system: state of the art and outstanding issues. Quaternary Science Reviews 24 (56), 595 – 629.

[58] Webster, 1987. The elementary monsoon. Monsoons, 399–464.

[59] Webster, P. J., Yang, S., 1992. Monsoon and enso: Selectively interactive systems. Quarterly Journal of the Royal Meteorological Society 118 (507), 877–926. URL http://dx.doi.org/10.1002/qj.49711850705

[60] WEO, 2012.World Energy Outlook 2012: Water for Energy. Organisation for Economic Co-operation and Development.

[61] WHO, 2008. The global burden of disease: 2004 update. URL http://www.who.int/healthinfo/global_burden_disease/estimates_country/en/

[62] WRI, 2015. Aqueduct global flood analyzer. URL http://www.wri.org/floods

[63] Yang, Z., Menon, S., 2013. Tackling negatively correlated global and local externalities – an economic study of multiple gases issue in climate change. Climate Change Economics 04 (03), 1350013.

[64] Zickfeld, K., 2004. Modeling large-scale singular climate events for integrated assessment. Ph.D. thesis, University Postdam.

[65] Zickfeld, K., Knopf, B., Petoukhov, V., Schellnhuber, H. J., 2005. Is the Indian summer monsoon stable against global change? Geophysical Research Letters 32 (15).

Chapter 3

The Indian Summer Monsoon in a Changing Climate: Economic Impacts and Adaptive Strategies

3.1 Introduction

India is currently the fastest growing developing economy. It is projected to remain so in the fiscal year 2017, driven by strong private consumption and domestic reforms (United Nations [39]). Although India's economy is set on a path to growing, it is facing major challenges. As such, (i) gross domestic product (GDP) per capita is still well below the international average; (ii) illiteracy among the population is high; (iii) around 240 million do not have access to electricity, etc. (e.g. The World Bank [36], IEA [14]). Furthermore, India's economy is vulnerable to the inherent climate variability. In particular, it is largely exposed to the inherent variability in the Indian summer monsoon (ISM) rainfall. In fact, ISM-rainfall forecast remains one of the factors cited in the economic development projections. The summer monsoon season spans June and August. During this period, India receives about 80% of its annual precipitation. Years when the summer monsoon arrives late and rainfall is scarce are associated with losses of about $2-5\%$ in India's GDP. Extreme excess rainfall throughout the monsoon season poses a threat to the urban infrastructure, with losses of a little less than 1% in GDP. The inherent inter-annual variability in the ISM rainfall results from its complex interactions with land, ocean and the atmosphere (Zickfeld [44]).

Energy is central to achieving India's development ambitions, which include increasing the contribution of the manufacturing output. So far, three quarters of the energy demand

is met by fossil fuels (IEA [14]) and India is among the top four CO_2 emitting countries, contributing 7% to the total global CO_2 emissions (Olivier et al. [28]). The scale of global emissions creates the risk of significant changes in climate, which pose a particular threat to India; an increase in frequency of the ISM-rainfall extremes being among the projected adverse impacts. For India, this means perpetual future losses. The close links between climate change and sustainable development imply a question of balance between these dual interests: economic development and mitigation efforts.

Recognising the risks that climate change poses, in an attempt to limit the global temperature increase to 2° Celsius, in 2016 world leaders signed a new global climate agreement: the Paris Agreement. The Paris Agreement sets out the architecture for carbon emission reduction after 2020. It safeguards the principle of common but differentiated responsibility, which has remained a non-negotiable aspect of India's climate position. It builds upon the bottom-up approach of voluntary commitments or "intended nationally determined commitments" (INDCs). India's INDCs submission include: i) to reduce the emissions intensity of its GDP by 33–35 per cent by 2030 from the 2005 level; ii) to achieve about 40 per cent cumulative electric power installed capacity from non-fossil fuel based energy resources by 2030, with the help of transfer of technology and low cost international finance; and iii) to create an additional carbon sink of 2.5–3 billion tonnes of CO_2 equivalent through additional forest and tree cover by 2030 (UNFCC [38]).

India's INDCs have attracted international interest because of their fair and ambitious mitigation targets (Center for Science and Environment [5]). However, the feasibility of the targets is still under question. For example, continued growth in coal-fired power generation to meet electricity demand would lead to a lock-in of the carbon-intensive power infrastructure in India. On a global scale, new coal-fired plants in India represent nearly half of the net coal capacity added worldwide (IEA [14]). Also, if India is to meet its substantial development needs, it would be irresponsible for any government to foreclose its development options by declaring a cap on coal or fossil fuels. Much depends on the implementation of India's plans for expanding renewable energy, improvements in technology and the global resources available for a low-carbon transition. The high price to pay for the potential failure of the countries, including India, to meet their mitigation targets makes adaptation an important component of sustainable development ambitions.

The present paper contributes to the literature by providing a long-term context for India's decisions on mitigation and adaptation in a view of region-specific climate risks. For

this, I developed an integrated assessment framework that explicitly captures the ISM system and, in addition to mitigation, allows for adaptation to extreme monsoon rainfall events. To the best of the author's knowledge, there is no existing study that provides such an integrated view on potential rainfall-related future damage costs for India's economy. To this end, existing studies that use regional modelling frameworks to access an interplay between adaptation and mitigation consider highly aggregated damages that increase gradually and smoothly wth temperature increase.

The paper is organised as follows. The following section elaborates on the design of the integrated assessment model RICE-ISM-AD. Section 3.3 presents the model calibration. Simulation results are presented in section 3.4. Section 3.5 summarises the results and draws conclusions.

3.2 The Integrated Assessment Model

In this section, I will elucidate the integrated assessment model (IAM, henceforth referred to as RICE-ISM-AD) that determines India's optimal adaptation strategy in a view of ISM-rainfall extremes. First, I will summarise existing modelling approaches for climate change adaptation, highlighting studies that are of particular relevance to the present research (Section 3.2.1). Sections 3.2.2 and 3.2.3 present the economy and climate modules respectively.

3.2.1 Modelling Regional Adaptation Strategies

The IPCC defines *climate change adaptation* as the process of adjustment to actual or expected climate and its effects (IPCC [16]). The broad spectrum of activities that falls under this definition implies the existence of modelling approaches that differ in purposefulness (e.g. autonomous vs. planned), timing (e.g. anticipatory vs. responsive), temporal scope (short vs. long term), spatial scope (localised vs. widespread), effects (e.g. prevent, protect, tolerate), form (e.g. legal, institutional) and performance (e.g. cost-effective, efficient) (Smit et al. [33]).).

Early integrated assesment modelling studies, with the exception of the PAGE model by Hope (1993), did not explicitly capture adaptation. Instead, they presume the already optimal level of adaptation, which is included in the damage function (Tol and Fankhauser [37]).

Later efforts to access optimal response to climate change start to recognise the impor-

tance of capturing adaptation as a policy variable. Among them, two general approaches to represent the benefits of adaptation can be identified. First, the level of adaptation, which is defined by the adaptive capital stock, enters the welfare function (e.g. Yatsenko et al. [43]). The adaptation stock is accumulated by means of annual investments, thereby improving welfare. Second, adaptation enters the damage costs function (e.g. de Bruin et al. [6]). Furthermore, studies differ in the type of variable that reflects adaptation: stock (Yatsenko et al. [44]), flow (de Bruin et al. [6]) or both (Agrawala et al. [1]).

There are a substantial number of studies based on the central-planner one-region framework examining the optimal adaptation–mitigation mix (e.g. Bretschger and Valente [4]; Millner and Dietz [25]; de Bruin et al. [6]). However, they overlook the dependence of the regional climate policy's success on the policies of the rest of the world. That is, the level of spatial detail required to recognise the costs and benefits of adaptation measures may be more than is possible in globally-oriented models. Local- or regional-level analysis is required (Patt et al. [30]).

Current literature on the synergies and trade-offs between mitigation and adaptation that employ a regional modelling framework is rather sparse. Buob and Stephan study the optimal mix of adaptation and mitigation in a two-stage dynamic game of several identical regions. The IAMs that endogenize an interplay between mitigation and adaptation are spinoffs of existing IAMs e.g. RICE (de Bruin and Dellink) and AD-WITCH (Bosello et. al.). However, it must be pointed out that they adopt damage functions, which neglect the possibility of abrupt changes.

The present study develops a regional framework with explicit modelling of the region-specific risk. In particular, I focused on the risk of more frequent extreme ISM-rainfall events. The only curently available IAM that offers inter-linkages between the economy and inter-annual ISM dynamics is the RICE-ISM model presented in the previous Chapter. I extended RICE-ISM-AD by explicitly modelling adaptation to the ISM extremes. The resulting IAM is elucidated below.

3.2.2 The Economy Module

The world is divided into 11 regions, $j = 1 \ldots 11$, based on geographical position, political proximity and health vulnerability.[1] Each region maximises its own welfare, balancing regional costs and benefits while taking into account actions combatting climate change undertaken by the rest of the world. This is modelled through an open-loop Nash equilibrium. Note, several model parameters are time-varying. The time profile of these parameters is available in Appendix 3 A.

The regional social welfare function is defined by a discounted logarithmic utility of per capita consumption over the period 2005–2200 i.e. $t = 0 \ldots T$ and $T = 195$[2]:

$$W_j = \sum_{t=0}^{T} \frac{L_{j,t} \cdot log(1 + c_{j,t})}{(1+\rho)^t}, \tag{3.2.1}$$

where $c_{j,t} = C_{j,t}/N_{j,t}$ is per capita consumption, $L_{j,t}$ is labour, and $\rho > 0$ is a pure rate of time preference. Labour force $L_{j,t}$ is endogenous[3]:

$$L_{j,t} = (1 - \lambda^a_{j,t})(1 - \lambda^c_{j,t})N_{j,t}, \tag{3.2.2}$$

where $\lambda^a_{j,t}$ and $\lambda^c_{j,t}$ quantify the fraction of the regional population $N_{j,t}$ suffering from a climate- and pollution-related disease, respectively.[4] It is further assumed that loss of health due to disease gives the utility of zero. To reflect the preference for low consumption over dropping out of the labour force due to ill health, the utility function of healthy individuals is

[1] The regions are: USA (USA and Canada), EUR (Western Europe), JPN (Japan), AUS (Australia and Oceania), FSU (Former Soviet Union and Eastern Europe), CHN (China and centrally planned Asia), IND (India and South Asia), SEA (South East Asia), LAM (Latin America and Caribbean), MEN (Middle East and North Africa), AFR (Sub-Sahara Africa). Because India is by far the largest emitter of greenhouse gases among South Asian countries, the present study discusses India's policy while referring to the region IND. For the purpose of clarity in model equation representations, the variables and parameters related to India are quoted in the form $X_{IND,t}$ for variable or parameter $X_{j,t}$.

[2] India's current climate policy fails to distinguish between reducing the risk to existing climate vulnerability and measures that take into account changing risks in the future. In particular, the current strategy for disaster management in India is limited to disaster mitigation and response and long-term planning is absent (lse [18]). However, the long-term focus is especially important in view of the risk of increased intensity and frequency of extreme ISM-rainfall events.

[3] In recent years, an increasing number of studies on air pollution issues has focused on the health feedback based on computable general equilibrium models, see, for example, Matus et al. [22]. The general equilibrium models account for the effects of mortality from chronic exposure that prematurely removes workers from the workforce. This requires not just an accounting of total premature deaths, but also a calculation of how much labour is lost for each of those deaths. This literature provides a useful guide to the analysis of the impacts of air pollution, as well as abatement policies on economic growth and social well-being.

[4] The incidence of climate- and air pollution-related diseases is assumed to be independent.

specified by:

$$\log\left(1+c_{j,t}\right). \tag{3.2.3}$$

Note, $\lambda^a_{j,t}$ and $\lambda^c_{j,t}$ are measured in terms of disability-adjusted life years (DALYs) lost due to disease. Ikefuji et al. [15] defines the following relation between regional temperature change $T^{atm}_{j,t}$ and $\lambda^c_{j,t}$:

$$\lambda^c_{j,t} = \beta^c_{1,j} + \beta^c_{2,j}(T^{atm}_{j,t})^{\beta^c_{3,j}}. \tag{3.2.4}$$

The pollution-related disease burden $\lambda^a_{j,t}$ depends on the level of regional emissions $E^a_{j,t}$ and varies with the region's population density PD_j and urbanisation $r_{j,t}$ (Ikefuji et al. [15]):

$$\lambda^a_{j,t} = \beta^a_0 \frac{PD_j}{80}(1 - r_{j,t} + \zeta r_{j,t})E^a_{j,t}, \tag{3.2.5}$$

where β^a_0 is the marginal impact of sulfur emissions in terms of DALYs per capita.

The regional output $Y_{j,t}$ is produced with a constant-returns-to-scale Cobb-Douglas production function in capital $K_{j,t}$ and labour $L_{j,t}$ given the state of technology $\psi_{j,t}$:

$$Y_{j,t} = \psi_{j,t} K^{\varepsilon}_{j,t} L^{1-\varepsilon}_{j,t}, \tag{3.2.6}$$

where elasticity of output with respect to physical capital is $0 < \varepsilon < 1$. The evolution of the physical capital stock is given by:

$$K_{j,t+1} = (1-\delta^k)K_{j,t} + I^c_{j,t}, \tag{3.2.7}$$

where $I^c_{j,t}$ are investments in physical capital and $0 < \delta^k < 1$ is the associated depreciation rate. Markets are competitive and factors of production are paid the value of their marginal product.

The model exposition below utilises both a diagrammatic and a mathematical representation of the underlying model framework. For convenient access to the model structure, a diagrammatic layout of the model is presented in Figure 3.1.

On a demand side, in all the regions except for India, output net of damage costs is distributed

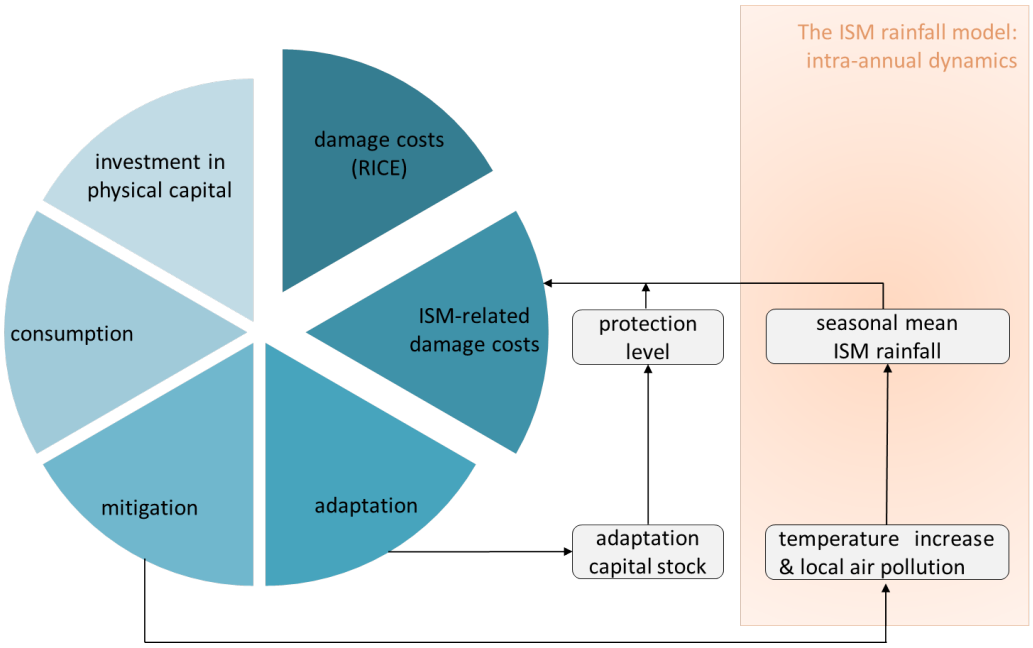

Fig. 3.1 Schematic representation of India's decision space and associated implications for the ISM rainfall.

between consumption, investment in physical capital, and abatement[5]:

$$Y_{j,t} - D_{j,t} = C_{j,t} + I^c_{j,t} + A_{j,t}, \tag{3.2.8}$$

where $D_{j,t}$ denotes the economic impacts of climate change and $A_{j,t}$ - abatement costs.

The abatement costs are proportional to carbon and sulfur control rates:

$$A_{j,t} = \alpha^c_{j,t}(\mu^c_{j,t})^{\xi^c} Y_{j,t} + \alpha^a_{j,t}(\mu^a_{j,t})^{\xi^a} Y_{j,t}, \tag{3.2.9}$$

where $0 < \mu^c_{j,t} < 1$ and $0 < \mu^a_{j,t} < 1$ are carbon and sulfur control rates respectively.

In India's case, output net of regional damage costs $D_{IND,t}$ is distributed between consump-

[5] Adaptation as a policy variable is considered only for India due to an otherwise increased computational cost associated with a wider control variables space. Should all regions choose between investments in adaptation and mitigation, the underlying ISM-related risk may alter towards either increased or decreased frequency of extremes. Nevertheless, the present model setup serves the qualitative nature of the question raised well – India's optimal mitigation–adaptation mix in view of region-specific risk and constrained by mitigation efforts of the rest of the world.

tion, investment in capital stock, abatement, and investments in ISM-related adaptation[6]:

$$Y_{IND,t} - D_{IND,t} = C_{IND,t} + I^{c}_{IND,t} + A_{j,t} + I^{flood,adapt}_{t} + I^{drought,adapt}_{t}, \tag{3.2.10}$$

where $I^{flood,adapt}_{t}$ and $I^{drought,adapt}_{t}$ are annual investments in adaptive capital stocks, $K^{flood,adapt}_{t}$ and $K^{drought,adapt}_{t}$, respectively.

The adverse effects of climate change are driven by regional temperature change. Accordingly, in line with Nordhaus and Boyer [26], damage costs $D_{j,t}$ are given by:

$$D_{j,t} = \frac{d_{j,t}}{1 + d_{j,t}} \cdot Y_{j,t}, \qquad j = 1 \dots 11 \tag{3.2.11}$$

where $d_{j,t}$ is a fraction of output net of damage costs. In all the regions, except for India, $d_{j,t}$ is defined by:

$$d_{j,t} = \gamma_{1,j} T^{atm}_{j,t} + \gamma_{2,j} \left(T^{atm}_{j,t}\right)^2 \tag{3.2.12}$$

where $T^{atm}_{j,t}$ is a regional temperature change relative to the year 2005 and $\gamma_{1,j}$ and $\gamma_{2,j}$ are recalibrated by Ikefuji et al. [15] to exclude health impacts, which are endogenous. The damage function $d_{j,t}$ for India is different and comprises regional-specific climate risks. More precisely, $d_{IND,t}$ is defined as:

$$d_{IND,t} = \gamma_{1,IND} T^{atm}_{IND,t} + \gamma_{2,IND} \left(T^{atm}_{IND,t}\right)^2 + d^{ISM}_{t}, \tag{3.2.13}$$

where d^{ISM}_{t} is a fraction of output net of damage costs lost as a result of extreme ISM rainfall events.

Figure 3.2 illustrates India's damage function, $d_{IND,t}$. Adverse impacts rise quadratically with regional temperature increases (black line). Additional losses occur in years characterised by an extreme deficiency or extreme excess of ISM rainfall, as shown by the red dotted line and blue dotted line respectively. These losses decrease with an increase in the protection level, which is defined by the respective adaptive capital stock. For example, the system of dykes and polders reduces GDP exposure to extensive floods; while GDP exposure to extensive droughts can be reduced by providing sufficient reservoir storage capacity, water recycling,

[6]For an extremely large country such as India, with a diverse cultural, economic and political dynamic, it appears plausible that climate policy is not solely driven by the federal government. Rather, the sub-national Indian states are influential policy–makers and drivers in multi–level climate policy decision-making and in terms of the implementation of national mitigation and adaptation policies. This multi–stage political process is ignored in the modelling framework.

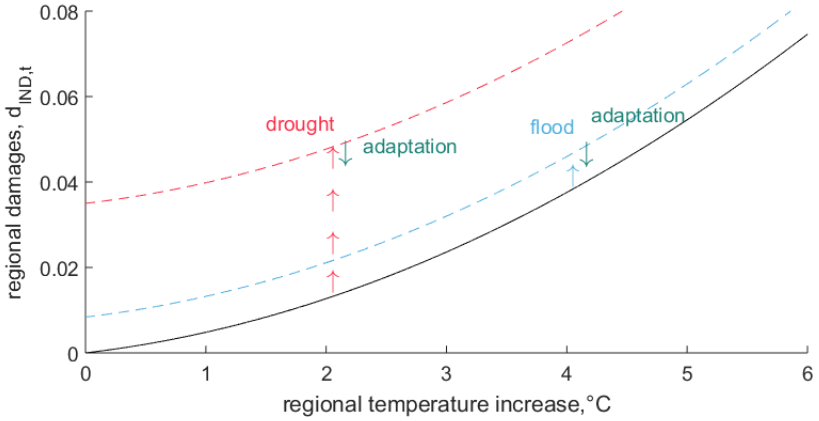

Fig. 3.2 India's damage function, $d_{IND,t}$

rainwater harvesting, and desalination.

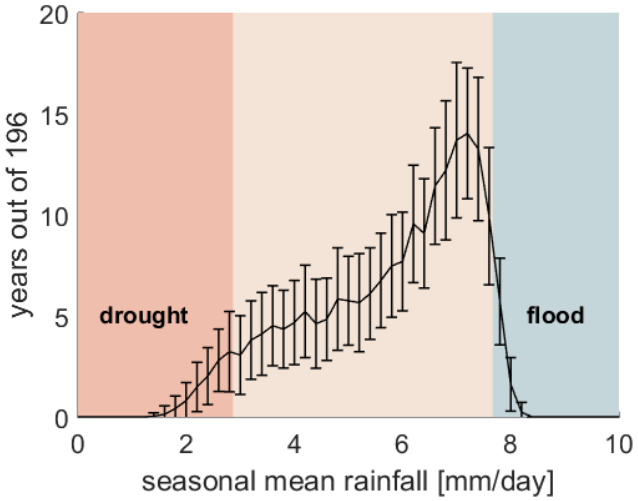

Fig. 3.3 Historical frequency distribution of seasonal (June–August) mean ISM rainfall from 196 runs of a stochastic predictive ISM-rainfall model (the black line depicts mean value, and error bars show ± 1 standard deviation from 100 realisations of the model)

Extreme ISM-rainfall events are defined using the percentile-based index (Figure 3.3). In the present study, an all-India seasonal mean rainfall is used as a proxy to characterise rainfall during the monsoon season (June to August). Extensive damage-inducing floods in a year t correspond to the value of the all-India seasonal mean rainfall $\overline{P}_t$ that exceeds the 95^{th} percentile of the historical rainfall frequency distribution. The value of the all-India seasonal mean rainfall below the 5^{th} percentile signifies damage-inducing droughts. Here, the all-India seasonal mean rainfall $\bar{P}_t$ is determined by a global mean temperature increase and aerosol concentration over India. This is calculated by the simple conceptual ISM-rainfall model

as explained in the subsequent section. The values of $\bar{P}_t$ that correspond to the 5^{th} and 95^{th} percentiles are denoted by $\bar{P}^{drought}$ and $\bar{P}^{flood}$ respectively.

To explicitly account for adaptation to ISM-rainfall extremes, I followed an approach by Agrawala et al. [1] of extending the damage function.[7] The resulting ISM rainfall-related losses in terms of fraction of output net of damage costs are defined by the following step function:

$$d_t^{ISM} = \begin{cases} d^{drought} \cdot \frac{1}{1+\nu^{drought} K_t^{drought,adapt}}, & \bar{P}_t \leq \bar{P}^{drought} \\ 0, & \bar{P}^{drought} < \bar{P}_t < \bar{P}^{flood} \\ d^{flood} \cdot \frac{1}{1+\nu^{flood} K_t^{flood,adapt}}, & \bar{P}_t \geq \bar{P}^{flood} \end{cases} \tag{3.2.14}$$

where parameters $d^{drought}$ and d^{flood} denote fraction of output net of damage costs lost in the absence of adaptation to droughts and floods, respectively, and $K_t^{drought,adapt}$ and $K_t^{flood,adapt}$ are associated adaptive capital stocks.[8] The parameters $\nu^{flood} > 0$ and $\nu^{flood} > 0$ reflect the effectiveness of respective capital stock in reducing the damages. The simple functional form in Equation 3.2.14 suffices to represent the defining property of adaptation commonly accepted in current literature: decreasing marginal productivity of adaptation. It also limits the protection level to between 0 and 1 so that infinitely large adaptive capital stock reduces the ISM-related economic losses to 0 at most. The calibration of $\bar{P}^{drought}$ and $\bar{P}^{flood}$ will be explained shortly in Section 3.2.3.

The adaptive capital stock evolves according to:

$$K_{t+1}^{i,adapt} = (1-\delta^{adapt})K_t^{i,adapt} + I_t^{i,adapt}, \qquad i = \{drought, flood\}, \tag{3.2.15}$$

where $I_t^{i,adapt}$ is India's investment in adaptation and δ^{adapt} is the adaptive capital depreciation rate. The suite of possible adaptation investments, inter alia, include crop and livelihood diversification, the reduction of ecological degradation and desertification in per-

[7] However, in contrast to Agrawala et al. [1], I do not distinguish between proactive and reactive adaptation for two reasons: i) there is no clear distinction between the two types; and ii) a perfect-foresight modelling framework implies the ability to anticipate the impact and choose the optimal strategy in advance. In this spirit, using a growth model with perfect information Dumas 2013 show that optimal adaptation strategy favours proactive, not reactive, adaptation. Proactive measures are designed not only for present, but also for anticipated future climatic conditions.

[8] An alternative way to specify adaptation to the ISM extremes is to model the shift in the thresholds $\bar{P}^{drought}$ and $\bar{P}^{drought}$ with increases in the adaptive capital. The interpretation is intuitive: the rainfall that was considered to be risky is now well-adapted to. However, because it would make calibration even more challenging, the present study refrains from using such a modelling approach.

petual drought regions, expansion of irrigation and integrated water management, risk-based construction planning, improving the drainage systems and flood control measures.

Note, for the purpose of a numerical solution, I considered a smooth approximation of the ISM-related damage function d^{ISM} as given by:

$$\begin{aligned} \tilde{d}_t^{ISM}(\bar{P}_t) &= d^{drought} \cdot \frac{1}{1+\nu^{drought} K_t^{drought,adapt}} \left(\frac{1}{\pi} \cdot \arctan[\zeta(\bar{P}^{drought} - \bar{P}_t)] + \frac{1}{2}\right) \\ &+ d^{flood} \cdot \frac{1}{1+\nu^{flood} K_t^{flood,adapt}} \left(\frac{1}{\pi} \arctan[\zeta(\bar{P}_t - \bar{P}^{flood})] + \frac{1}{2}\right). \end{aligned} \tag{3.2.16}$$

Here ζ is a steepness parameter and π is a mathematical constant. In Equation (3.2.16), $\tilde{d}_t^{ISM}$ is differentiable in the vicinity of the thresholds. Thus Equation (3.2.16) nests the original Equation (3.2.14) without affecting the model properties.

3.2.3 The Climate Module

As mentioned earlier, the ISM rainfall plays a crucial role in the IAM. A climate module aimed at creating a sound IAM for India has to take into account both by-products of fossil fuel combustion – greenhouse gases (GHGs) and aerosols.[9] Carbon dioxide and sulfur dioxide emissions, $E_{j,t}^c$ and $E_{j,t}^a$, are released into the atmosphere according to:

$$\begin{pmatrix} E_{j,t}^c \\ E_{j,t}^a \end{pmatrix} = \begin{pmatrix} \sigma_{j,t}^{cc} & \sigma_{j,t}^{ca} \\ \sigma_{j,t}^{ac} & \sigma_{j,t}^{aa} \end{pmatrix} \begin{pmatrix} 1-\mu_{j,t}^c \\ 1-\mu_{j,t}^a \end{pmatrix} Y_{j,t}. \tag{3.2.17}$$

Emissions are dependent upon i) the time-varying emission-intensity of the output, as captured by parameters $\sigma_{j,t}^{cc}$, $\sigma_{j,t}^{ca}$, $\sigma_{j,t}^{ac}$ and $\sigma_{j,t}^{aa}$; and ii) the chosen carbon and sulfur control rates, $0 < \mu_{j,t}^c < 1$ and $\mu_{j,t}^a$ respectively. Note, a climate policy that targets CO_2 emissions acts to reduce the carbon intensity of energy, and in effect simultaneously reduces the sulfur emissions. However, control of SO_2 emissions might be limited to a relatively cheap technology of flue-gas desulphurization, which has no effect on CO_2 emissions. Thereby, parameter $\sigma_{j,t}^{ca}$ is zero and $\sigma_{j,t}^{cc}$, $\sigma_{j,t}^{ac}$ and $\sigma_{j,t}^{aa}$ are positive.

Further, geophysical relationships describe how emissions are translated into climate change. Carbon cycle dynamics are represented by the single-equation linearized model, which

[9] Here sulfate is representative of aerosol. Anthropogenic sulfate aerosol in the atmosphere derives from the oxidation of sulfur dioxide emissions (Feichter et al. [9]).

defines atmospheric carbon concentration according to:

$$M_{t+1} = (1-\delta^m)M_t + \sum_{j=1}^{11} E^c_{j,t}, \tag{3.2.18}$$

with δ^m reflecting the annual depreciation rate of carbon. After Manne et al. [19], regional temperature change is:

$$T^{atm}_{j,t} = \tau_{0,j} + \tau_1 T^{atm}_{j,t} + \tau_2 T^{atm}_t + \tau^c_j log(M_{t+1}) \tag{3.2.19}$$

$$+ \tau^a_{1,j} E^a_{j,t+1} + \tau^a_{2,j} log(1 + \tau^a_{3,j} E^a_{j,t+1}). \tag{3.2.20}$$

Global mean temperature change is a weighted average of regional temperature change $T^{atm}_{j,t}$:

$$T^{atm}_t = \sum_j \omega_j T^{atm}_{j,t}, \tag{3.2.21}$$

where $T^{atm}_{j,t}$ is regional and T^{atm}_t the global mean temperature change relative to the year 2005. A region's share of landmass is given by ω_j.

Since the climate change–monsoon nexus is at the forefront of the paper, we analyse monsoon dynamics in greater depth. The next equations describe the implications of local air pollution, as given by $E^a_{j,t}$, and of global mean temperature change T^{atm}_t for the inter-annual ISM rainfall variability. To this end, Belaia and Glanemann [3] developed and calibrated the extended version of the ISM-rainfall model by Schewe and Levermann [32]. Below I elucidate the mechanisms that control ISM circulation and define precipitation strength and variability. This is followed by a description of the corresponding conceptual modelling.

In the northern hemisphere summer, when the sun moves north of the equator, the land is rapidly warmed as it absorbs solar radiation. As a result, land surface air expands and starts to rise, forming a low pressure area. On the other hand, oceans have a greater heat capacity and store heat within deep surface layers. That is, the air over land gets relatively warmer and the air pressure becomes lower than over the ocean. The resulting land–ocean pressure gradient force pushes moist air landwards. Thereafter the warmed air rises to higher altitudes. In the upper troposphere the pressure gradient force acts in the opposite direction leading to a high-level air flow from land to ocean. Followed by cooling, the air sinks, closing the loop. In this form the summer circulation is sustained as long as the

ocean–land temperature difference is present.[10] While the ocean-land temperature gradient is a necessary condition for the existence of the monsoon circulation, another important driving force that defines the strength of the circulation is internal feedback. In the simple model, the above-mentioned processes are conceptualised as follows. The model operates on a quasi-daily timescale throughout the summer monsoon season, which spans 135 days i.e. $d = 1 \dots 135$. The model's simplification includes an idealized assumption about two possible states of monsoon circulation, namely dry P^{dry} and wet P^{wet}, with weak and strong daily precipitation respectively. Driven by both external forcing and internal variability, the daily monsoon rainfall $P(d)$ varies for $d = 1 \dots 135$ between the two states. During the onset of the rainy season, rainfall probability p_t^{init} is modulated by i) local air pollution; and ii) other systems of Earth through teleconnections:

$$p_t^{init} = \begin{cases} p\prime \cdot (m_t^{NINO3.4} - m_0) + p_0, & A_t^{pl} < A_t^{pl,crit} \\ 1 - p_m, & else, \end{cases} \tag{3.2.22}$$

where $m^{NINO3.4}$ is the mean sea–level pressure over the region NINO3.4 (5S–5N and 170–120W), which is used as a proxy summarising factors that define the ISM rainfall during its onset.[11] The planetary albedo value A_t^{pl} reflects the state of aerosol pollution over India. In case planetary albedo transgresses the critical value $A_t^{pl,crit}$, the rainfall probability is at its minimum, $1 - p_m$. Calibration of the critical level of the planetary albedo $A_t^{pl,crit}$ is explained in the following section.

The change in the planetary albedo A_t^{pl} relative to the value of 0.47 is defined by the regional sulfate aerosol burden B_t^{SO4}:

$$\Delta A_t^{pl} = 2T_{pl}^2 \cdot (1 - A_s)^2 \cdot \beta_{pl} \cdot \alpha_{pl} \cdot B_t^{SO4}. \tag{3.2.23}$$

where T_{pl}^2 is the fraction of light transmitted by the aerosol layer, A_s is the present value of surface albedo, α_{pl} is the mass scattering efficiency, and β_{pl} is the backscatter fraction.

[10] The fundamental principal behind the monsoon circulation was first formulated by Halley [13]. Further, the theory was revised by Hadley in 1735, who accounted for the Coriolis force, arising from the rotation of the earth, which acts to deflect winds in the Northern Hemisphere to the right.

[11] The simple conceptual model is limited to capturing a single external forcing, which constitutes a good predictor in the comprehensive climate model used in the study. Yet, the monsoon circulation development is furthermore linked to, for example, Indian Ocean sea surface temperature, Eurasian snow cover and current phase of Madden-Julian oscillations. These factors could be included by altering the parameter value p_{init} in the model (Schewe and Levermann [32]).

The regional sulfate burden over the Indian peninsula is given by:

$$B_t^{SO4} = E_{IND,t}^a \frac{O \cdot H^{SO2} \cdot V}{\Omega}, \tag{3.2.24}$$

where O is SO_2 into SO_4 conversion factor, H^{SO2} is the fractional sulfate yield, and Ω is the area.

The critical planetary albedo $A_t^{pl,crit}$ is derived by Belaia and Glanemann [3] from the bifurcation analysis of the ISM rainfall model by Zickfeld et al. [45]:

$$A_t^{pl,crit} = \alpha_1^{pl} \cdot log(M_t) + \alpha_2^{pl}, \tag{3.2.25}$$

where M_t is the atmospheric carbon concentration.

The mean sea-level pressure over the region NINO3.4 weakens in response to global warming:

$$m_{t+30}^{NINO3.4} = m' \cdot T_t^{atm} + m_0^{NINO3.4}, \tag{3.2.26}$$

where parameter m' is negative and $m_0^{NINO3.4}$ is MSLP over NINO3.4 in the absense of global warming. By substituting Equation 3.2.26 into Equation 3.2.22, we mention that global warming indirectly decreases rainfall probability during the onset of the monsoon.

After the monsoon circulation is established, it is sustained throughout the rest of the season by moisture-advection feedback. The released latent heat from precipitation over land leads to an increase in the temperature difference between land and ocean. The resulting enhanced pressure gradient reinforces the monsoon circulation, pushing the moist air towards land. In contrast, a lack of latent heat implies weaker precipitation through dry-subsidence feedback (Schewe and Levermann [32]). In sum, the probability of rainfall on a day d, p_d, depends on the latent heat accumulated during the certain period δ prior to that day. In the model by Schewe and Levermann [32]), the precipitation probability $p_{t,d}$ is proportional to the normalised average rainfall $\hat{p}_d$:

$$\hat{p}_{t,d} \equiv \frac{\frac{1}{\delta}\sum_{i=d-\delta}^{d-1} P(d) - P^{dry}}{P_t^{wet} - P^{dry}}. \tag{3.2.27}$$

Here the time interval $[d-\delta; d-1]$ is referred to as a memory period, and the correlation between p_d and $\hat{p}_d$ as a memory effect. In order to avoid a locked-in precipitaiton state, the normalised average rainfall $\hat{p}_d$ is further adjusted according to a predefined maximum

allowed probability p_{max} for either precipitation state.

$$p_{t,d} = \begin{cases} p_{max}, & \hat{p}_{t,d} \geq p_{max} \\ 1 - p_{max}, & \hat{p}_{t,d} \leq 1 - p_{max} \\ \hat{p}_{t,d}, & else. \end{cases} \tag{3.2.28}$$

Besides the aforementioned factors, to a large extent, the intra-seasonal rainfall variability is influenced by synoptic-scale stochastic atmospheric fluctuations, which are parametrized in the model as a random variable $Pr(d)$ with values uniformly distributed between 0 and 1. Synoptic-scale variability confronts the memory effect, occasionally causing flips between the two precipitation states on a quasi-daily timescale.[12] I performed 100 realisations of the model with random variable $Pr(d)$ uniformly distributed between 0 and 1.[13]

Eventually, precipitation probability $p_{t,d}$ defines the state of precipitation rate $P_{t,d}$ according to:

$$P_{t,d} = \begin{cases} P_t^{wet}, & Pr(d) < p_{t,d} \\ P^{dry}, & else. \end{cases} \tag{3.2.29}$$

Averaging the daily precipitation over the season we arrive at a seasonal mean precipitation rate $\overline{P}_t$, $P^{dry} \leq \overline{P}_t \leq P_t^{wet}$:

$$\overline{P}_t = \frac{1}{135} \sum_{d=1}^{135} P_{t,d}. \tag{3.2.30}$$

In a nutshell, global mean temperature increases T_t^{atm} and regional sulfur emissions E^a alter the seasonal mean monsoon rainfall $\overline{P}_t$. Following Schewe and Levermann [32], the historical frequency distribution of the seasonal mean ISM rainfall is developed by setting $p_t^{init} = 0.75$ and $P_t^{wet} = 9$. This is illustrated in Figure 3.3. Further, the 5^{th} and 95^{th} percentiles of the historical frequency distribution determine the location of the thresholds – $\bar{P}^{drought}$ and $\bar{P}^{flood}$ – in the ISM rainfall-related damage function (Equation (3.2.14)).

The presented ISM-IAM framework provides an elegant and powerful tool to think about climate dynamics and adaptive capacity in India. Our immediate goal is to calibrate the model with data from India and use it to explore the relative importance of adaptation vs. mitigation in the course of climate change.

[12] Synoptic-scale stochastic atmospheric fluctuations allude to regional weather variability.

[13] De facto, the values are pseudo-random and are generated in GAMS through a deterministic algorithm (McCarl et al. [23]).

3.3 Calibration

I will now discuss how the model was calibrated. The constant economic parameters adopted from the RICE model by Nordhaus and Boyer [26] are given in Table 3.1.

Table 3.1 The selected RICE model parameters.

Parameter	Description	Value
ε	Elasticity of output with respect to capital	0.3
δ^k	Depreciation rate of capital	0.1
ρ	Discount rate	3 % per year

The A2-ASF marker emissions scenario from the Special Report on Emissions Scenarios (SRES) serves as a business-as-usual scenario in the model.[14] Accordingly, time-varying parameters are calibrated to fit the A2-ASF trends in technological development, population growth, and CO_2 and SO_2 emissions to the model results under no adaptation and no mitigation efforts.[15] The A2-ASF scenario describes the heterogeneous world shaped by aspirations for regional identity and fragmentation. As such, (i) technological change varies among regions depending on local resource availability, education level, and culture; (ii) slow technology diffusion and differences in productivity maintain uneven economic growth; (iii) technology diffusion barriers result in low energy efficiency and high energy intensity of gross national product (GNP); (iv) resource availability in the region defines its fuel mix; and (v) environmental concerns are mainly related to local air pollution. Among the SRES marker scenarios, the A2-ASF presumes the lowest degree of convergence or "catch-up".[16]

Table 3.2 India's GDP per capita gap relative to the United States in the year 2060. Own calculations for RICE-ISM-AD and RICE-99.

Source	Log point difference, %
RICE-ISM-AD (business-as-usual)	-303.4
RICE-99	-294.4
OECD [27]	-129.5

[14]The A2-ASF scenario belongs to the A2 family of scenarios and is quantified by Sankovski et al. [31].

[15]Appendix 3 A lists the time profiles of the time-varying parameters.

[16]Note, conversion of the national currencies into US dollars is based on the market exchange rates (MER). Although the purchasing power parity exchange rate (PPP) is a better approach for the purpose of welfare comparison across countries, as is the real exchange rate (RER), the PPP data is rather scarce (Van Vuuren and Alfsen [40]). What is crucial in the context of the present research is that the MER-based approach overestimates future economic growth in developing countries. In turn, India's slower economic growth in the PPP exchange rate means it is more vulnerable to climate change.

To relate projections on "catch-up" in RICE-ISM-AD to existing studies, I listed alternative projections of the output per capita gap. Due to the specific interest of the present study, I focused on the output per capita gap between India and the US (Table 3.2).

From Table 3.2, it is evident that RICE-ISM-AD presumes the level of India's catch-up relative to the US (in the year 2060) to be similar to that of the RICE-99 model. The difference between the RICE-ISM-AD model results and the study by OECD [27] can partially be explained by the use of distinct exchange rates. While RICE-99 and RICE-ISM-AD use 1990 USD and 2005 USD market exchange rates respectively, OECD [27] employs constant 2005 PPPs.

Next, I decomposed the factors that drive GDP per capita differences between India and the US in RICE-ISM-AD. The time evolution of these factors is given in Figure 3.4. Followed by population and physical capital, total factor productivity (TFP) plays a major role in defining the gap.[17] Furthermore, it is mainly an increase in TFP that diminishes the gap over time.

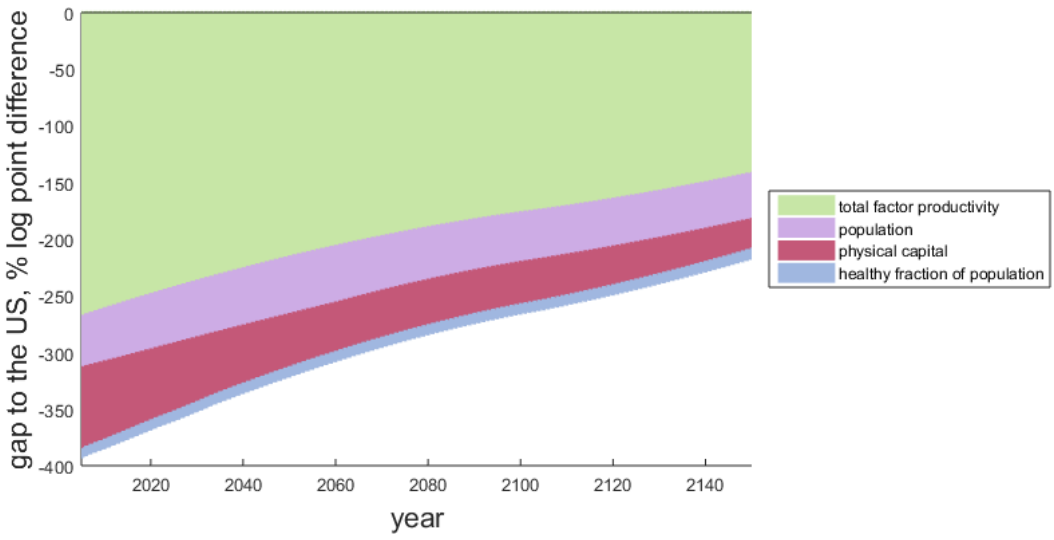

Fig. 3.4 Time-varying contributions of production factors to India's GDP per capita gap relative to the United States at market exchange rates in terms of log point differences: the business-as-usual solution in the RICE-ISM-AD model

To sum up, Figure 3.5 illustrates the heterogeneity between the regions in the business-as-usual scenario in the RICE-ISM-AD model.

[17] Similarly, OECD [27] projects that it is multi-factor productivity that is the most influential factor driving the per capita output difference between India and the US in the year 2060.

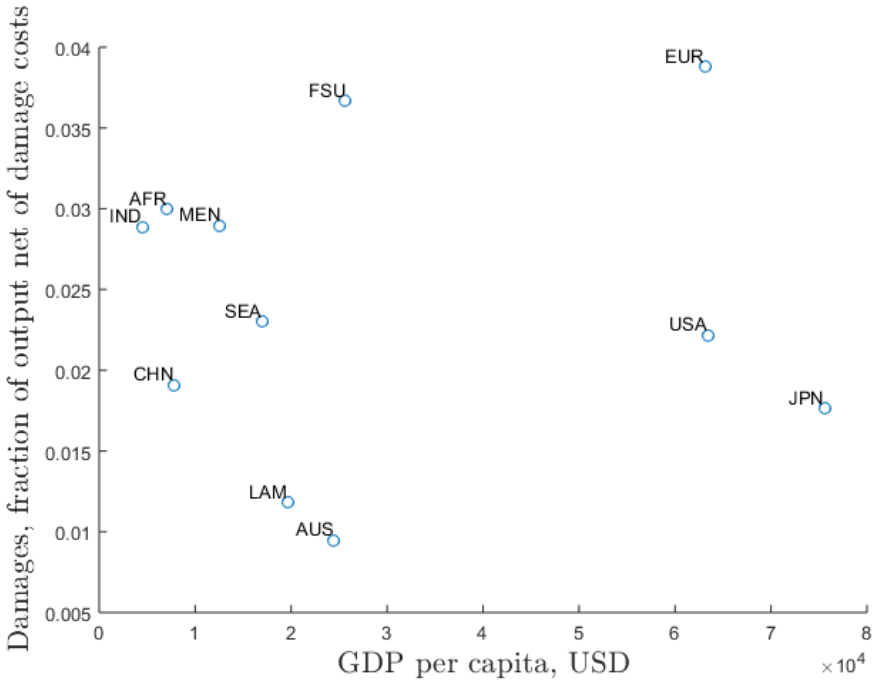

Fig. 3.5 Characterisation of regions in terms of GDP per capita and climate change damage in the year 2100: results of the business-as-usual scenario of the RICE-ISM-AD model

Calibration of the ISM rainfall-related damage function encompasses: (i) definition of extreme events i.e. $\bar{P}^{drought}$ and $\bar{P}^{flood}$; (ii) damage costs in the absence of adaptation i.e. $d^{drought}$ and d^{flood}; and (iii) effectiveness of adaptation i.e. ν^{flood} and $\nu^{drought}$. Extreme events are defined relative to the historical state of seasonal mean ISM rainfall. The seasonal mean ISM-rainfall values corresponding to the 5th and 95th percentiles are $\bar{P}^{drought} = 2.8667$ mm/day and $\bar{P}^{flood} = 7.6667$ mm/day respectively. Damage costs in the absence of adaptation are estimated based on the evidence from the last few decades. In particular, from studies by Gadgil and Gadgil [11] and by WRI [42], Belaia and Glanemann [3] set $d^{drought}$ to 3.5% of India's GDP and d^{flood} to 0.84% of GDP. Severe droughts cause drop in agricultural yield, leading to inflation and diminishing purchasing power among rural communities, which create a snowball effect that sweeps through the entire economy. Note, 57% of India's population is rural (The World Bank [35]) and 51% of total employment is in agriculture (The World Bank [34]), hence, India's GDP exposure to severe drought. Besides agricultural output, water scarcity may also jeopardise energy supply and power generation. The economic impacts of floods include infrastructural damage and disruptions in economic activity. In particular, the value d^{flood} reflects the level of GDP exposed to river flooding. The ISM-rainfall damage function in the absense of adaptation is illustrated in Figure 3.6.

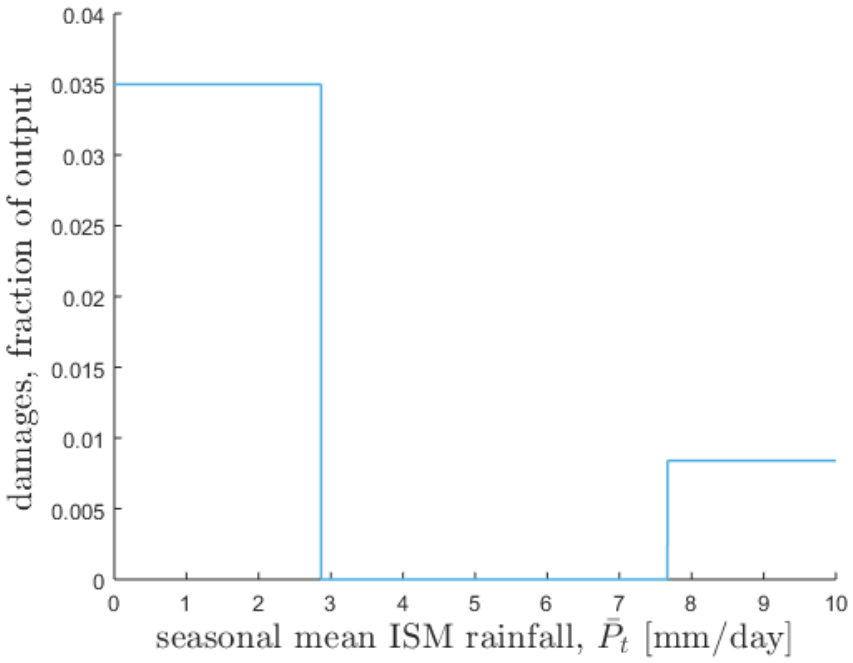

Fig. 3.6 The ISM rainfall-related damage function d_t^{ISM} in the absense of adaptation.

To increase resilience to extremes, India may choose to "climate-proof" the investments by building adaptive capital stocks.[18] The existing estimates on financial flows needed are rather conservative.[19] I calibrated ν^{flood} and $\nu^{drought}$ based on the findings by Margulis and Narain [20]. Margulis and Narain [20] use the results of two climate models for the A2 emissions scenario to evaluate potential risks of floods and water scarcity, which makes it a particularly good fit for the present modelling framework. For the identified risks, they calculate annual investments until the year 2050 in industrial and municipal water supply and the riverine flood protection necessary to reach the level of the baseline condition of no climate change. The flood protection measures include a system of dykes and polders, costing 50 000 USD per square kilometre in urban areas and 8000 USD per square kilometre in agricultural areas. Future industrial and municipal water demand is met by increasing the capacity of surface

[18]Naturally, India's capability to cope with climate change impacts can also be improved via new legislation and institutional frameworks. For example, economic losses due to climate change may be mitigated via well-developed insurance system that can be accessed by all households and companies. The difference in losses between the no-insurance and the full-insurance case arises from two factors. First, with insurance companies and households can restore their assets, allowing for a more rapid recovery of the economic activity. Second, insurance prevents a reduction in the final demand from affected companies and households that have to rebuild their savings or pay back their debt. Such institutional adaptations to cope with climate change are beyond the scope of the present modelling approach.

[19]It is fair to acknowledge that the uncertainties in climate cost estimates are great and the effectiveness of adaptation measures will depend strongly on the quality of implementation.

reservoir storage. When it costs more than 0.30 USD a cubic metre, the other measures are implemented – recycling, rainwater harvesting, and water desalination – at a cost of 0.30 USD a cubic metre. Accordingly, Margulis and Narain [20] estimate that the necessary annual investments in flood protection in South Asia are up to 1.6 billion USD, and annual investments in water supply are up to 2.4 billion USD. Based on this data, I evaluated the capital stocks necessary to fully eliminate the risks by 2050 and calibrate ν^{flood} and $\nu^{drought}$ accordingly. Specifically, I set $\nu^{flood} = \nu^{drought} = 1000$. Note, in line with the physical capital depreciation rate, the depreciation rate of adaptive capital δ^{adapt} is set to 0.1. Figure 3.7 illustrates the residual damages, which are dependent to the size of the adaptive capital stock.

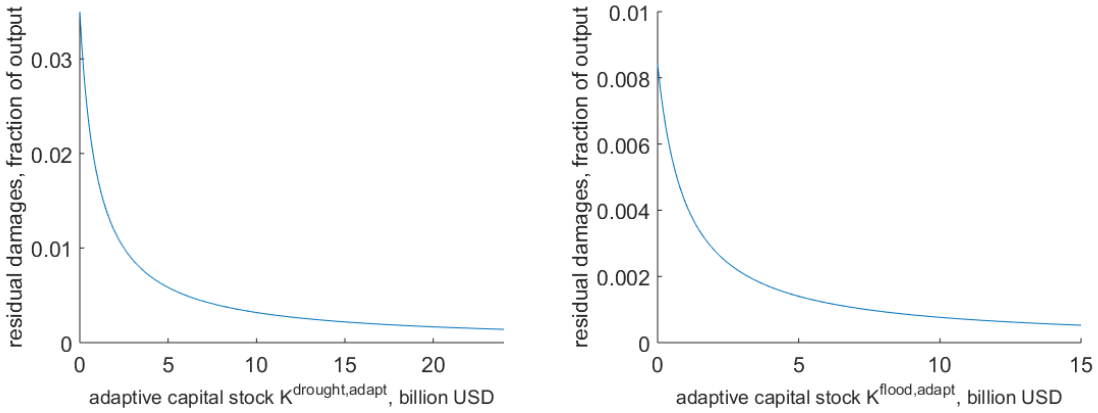

(a) Drought-related damage costs (b) Flood-related damage costs

Fig. 3.7 Residual damage costs as a function of adaptive capital.

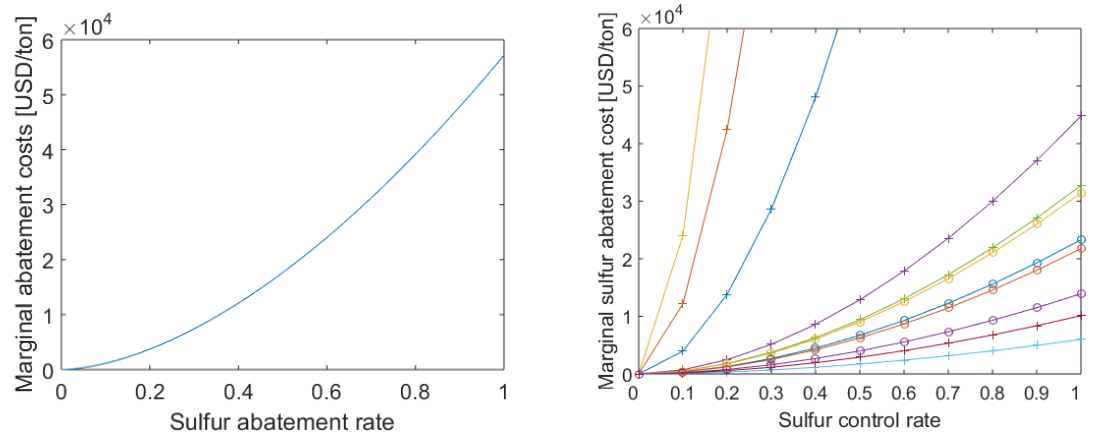

(a) Global MAC (source: Bahn and Leach [2]) (b) Regional MACs in RICE-ISM: $-\frac{\partial A_{j,t}}{\partial E^a_{j,t}}$

Fig. 3.8 Marginal sulfur abatement costs

Table 3.3 The climate module parameters

Parameter	Value	Source
τ_1, Temperature equation coefficient	0.724	Ikefuji et al. [15]
τ_2 , Temperature equation coefficient	0.1	
P^{dry}, Precipitation rate on a dry day	0 mm/day	Schewe and Levermann [32]
P_0^{wet}, Precipitation rate on a wet day (historical)	9 mm/day	
p_0^{init}, Initial probability of a wet state	0.75	
p_{max}, Maximum probability of either state	0.82	
δ, Memory period	17 days	
p'', Coefficient in rainfall intensity equation	0.42 mm/day	Belaia and Glanemann [3]
p_0, Coefficient in initial rainfall probability equation	0.2	
p', Coefficient in initial rainfall probability equation	0.41	
m_0, Coefficient in initial rainfall probability equation	1008.649 mb	
m', Coefficient in the evolution of MSLP	0.29	
$m_0^{NINO3.4}$, Coefficient in the evolution of MSLP	1009.9835 mb	
O, Conversion parameter	1.5	
A_s, Current surface albedo	0.16	
H^{SO2}, Fractional sulfate yield	0.65	
T_{pl}, Fraction of light transmitted by aerosol layer	0.76	
β_{pl}, Backscatter fraction	0.29	
α_{pl}, Mass scattering efficiency	8.5 m^2/g	
V, Sulfate atmospheric lifetime	2/365	
Ω, South Asian area	$4.12 \cdot 10^{12}$ m^2	
α_1^{pl}, Coefficient in critical albedo relation	0.02	
α_2^{pl}, Coefficient in critical albedo relation	0.37	

The health impacts of increased temperatures are calibrated after McMichael et al. [24], who estimates the likely proportional change in the burden of each disease under climate change. Since long-term observational data of health consequences of climate change is missing, McMichael et al. [24] adopt a model-based approach. They link the Hadley Climate Model (Johns et al. [17]) projections of geographical distribution of changes in the principle characteristics of climate to disease-specific models to evaluate changes in relative risk of each disease under climate change.

After Nordhaus and Boyer [26], parameters ξ^c and ξ^a are set to 2.8, indicating that abatement costs increase with emissions control rates. Calibration of $\alpha^c_{j,t}$ and $\alpha^a_{j,t}$ (i) entails an assumption of the diminishing price of backstop technology over time; and (ii) relies on the global marginal sulfur abatement cost curve from Bahn and Leach [2] (Ikefuji et al. [15]). Figure 3.8b illustrates the global marginal abatement cost by Bahn and Leach [2] (a) and downscaled to regions' marginal abatement cost functions by Ikefuji et al. [15].

The fixed climate module parameters are given in the Table 3.3. Putting all these numbers together, what do they imply for the ISM dynamics and welfare maximising policies in India? In the next section I present numerical model simulations.

3.4 Results

I start by analysing the business-as-usual scenario, where neither mitigation nor adaptation efforts are undertaken in the period between year 2005 and 2200. The climate impacts of such policies include temperature increase and local air pollution. In the case of India, anthropogenic interference also alters the variability of the ISM rainfall. To depict the changes in the inter-annual ISM rainfall variability, I contrast the solution of the business-as-usual scenario to the historical ISM-rainfall distribution (Figures 3.9a and 3.9b). The vertical dashed lines in Figure 3.9 show the definition of the extreme rainfall events. Business-as-usual policy is characterised by a shift in the inter-annual ISM-rainfall variability compared to the historical distribution. In particular, years with severe excess and severe rainfall deficiency are more frequent, while moderate rainfall events are less frequent. Next, I turn to the description of the Nash equilibrium solution, where the objective is regionally optimal climate policy.[20]

[20]The risk of increased ISM rainfall extremes is faced by South Asian countries with no direct impact on the rest of the world. Therefore, the present study refrains from consideration of the optimal solution, where the regions balance the global costs and benefits.

The Nash equilibrium is solved using the iterative algorithm.[21]

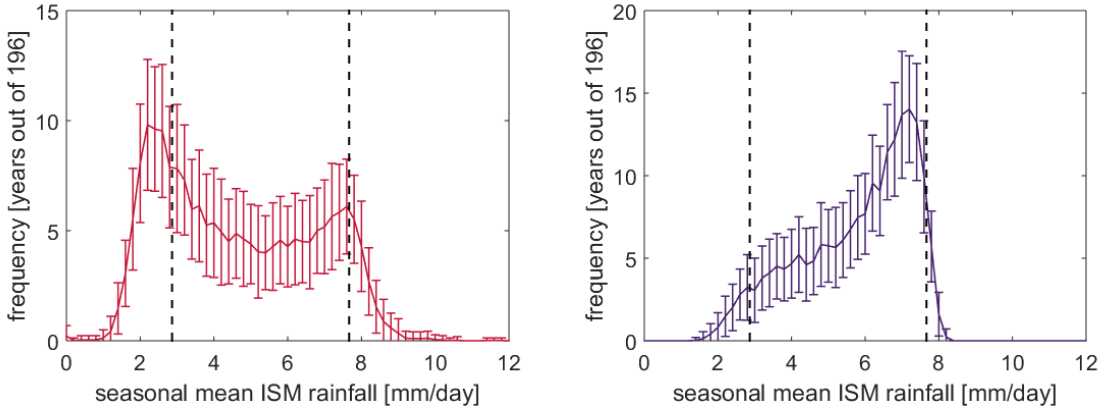

(a) Business-as-usual solution (2005-2200) (b) Historical frequency distribution

Fig. 3.9 Frequency distribution of seasonal mean rainfall

Balancing the regional costs and benefits of climate policy, regions initiate emissions controls. India, in addition, evaluates the costs and benefits of adaptation to the ISM-rainfall events. Resulting sulfur and carbon control rates are illustrated in Figure 3.10. In the absence of adaptation, there is less output available to invest in mitigation. Thereby, optimal emissions control rates under no adaptation are slightly lower. In both cases – with and without adaptation – stringent policy is not sufficient to prevent ISM rainfall extremes (Figure 3.11). The two distributions are visually identical to the business-as-usual solution.

The evolution of economic risks associated with an increased frequency of extremes in the business-as-usual and Nash equilibrium solution are illustrated by Figure 3.12. Both presume the absence of adaptation efforts. Here, the risk is defined by the likelihood of occurence of the extreme (out of 100 realisations of the model) times the impact. Although the two scenarios share similar frequency distribution of the seasonal mean rainfall, the evolution of economic risk over time highlights the difference. The stacked-bars plot in Figure 3.12 also sheds more light on the proportional risk of both scenarios. In particular, in the absence of mitigation efforts, droughts pose greater risks than floods do. First, the the impact is 2.66 percentage points greater. Second, the near-term "dry" years are likely to occur due to enhanced aerosols concentration, which is followed by the weakening of the

[21]The algorithm is based on the application of the backward induction procedure in finite games of perfect information (Mas-Colell et al. [21]). The optimisation problem is solved in the General Algebraic Modeling System (GAMS Development Corporation [12]).

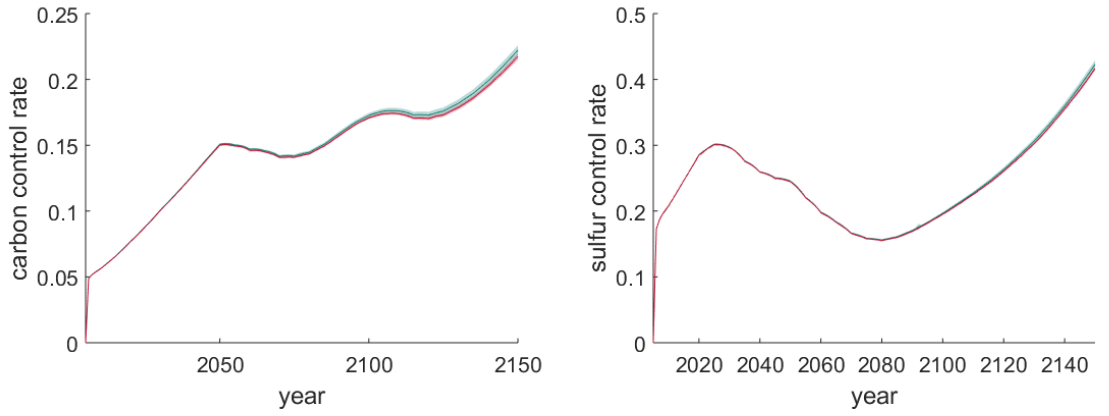

(a) Carbon control rate (b) Sulfur control rate

Fig. 3.10 India's optimal emissions control rates in the Nash equilibrium with adaptation (green line) and in the absense of adaptation (red line) to the ISM-rainfall extreme events

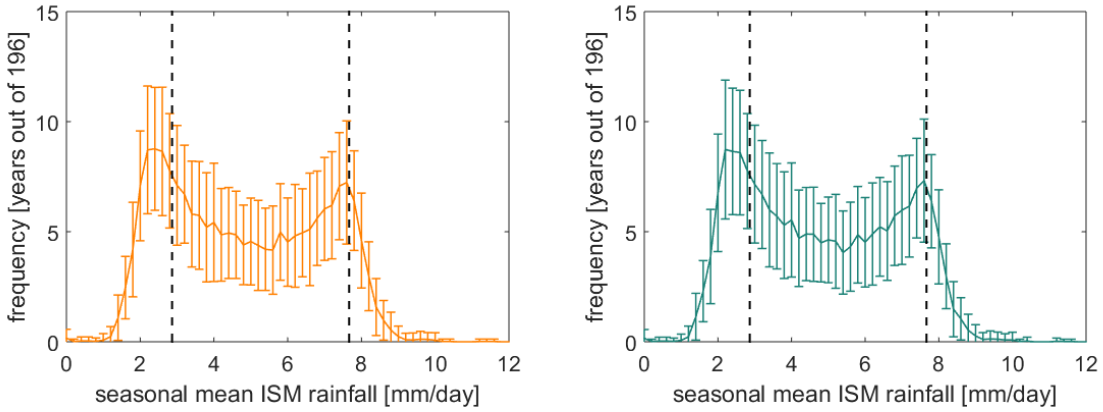

(a) No adaptation (b) Adaptation

Fig. 3.11 Frequency distribution of seasonal mean rainfall over the period 2005-2200 in Nash equilibrium

monsoon circulation.[22] Mitigation efforts do not lower the risk, but do change the major contributing factor to the risk in the near-term. As global warming accelerates, floods become more frequent. Despite the relatively low impact of floods – 0.84% versus 3.5% of GDP, in the near-term, they pose a threat comparable to that of droughts.

Next, we answer the question whether investments in adaptive capital are justified i.e. whether they pay off over time. The evolution of adaptive capital stocks for scenarios with and without mitigation is illustrated in Figure 3.13. The choice between investment into flood- or drought-related adaptation depends on the presence of emissions control. In the absence of

[22] After the IPCC report, the term "likely" is used to indicate a likelihood of more than 66%.

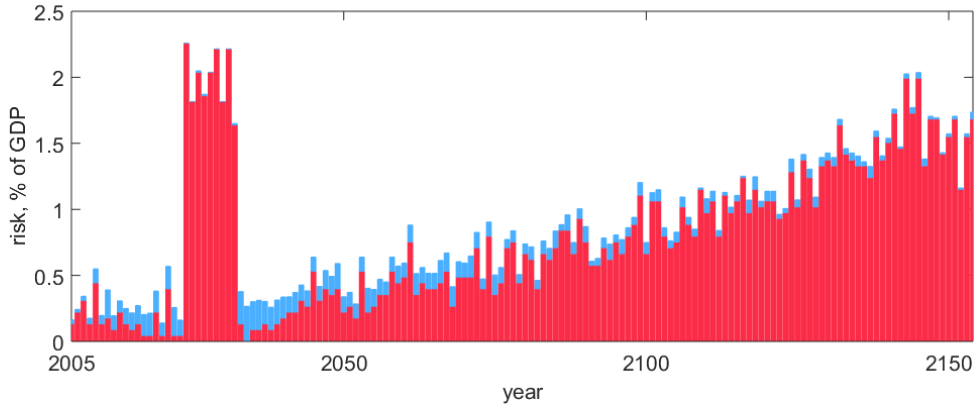

(a) No mitigation

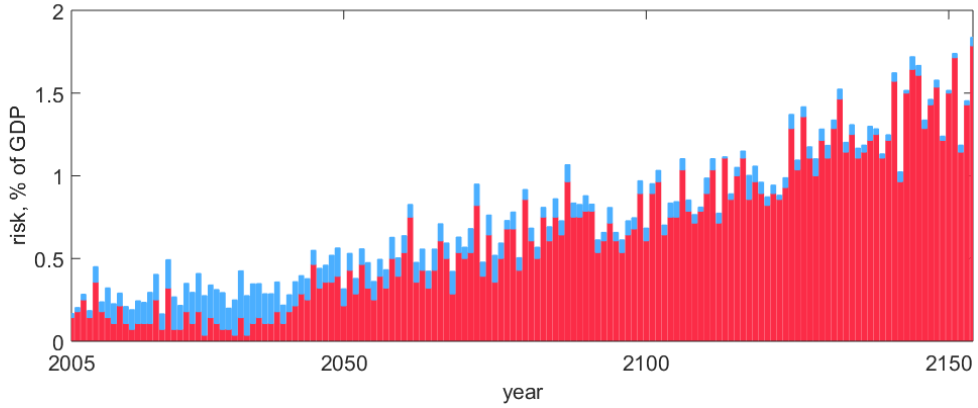

(b) Mitigation

Fig. 3.12 Evolution of the economic risks in the absense of adaptation: flood-related (blue bars) and drought-related (red bars)

mitigation, droughts represent a primary risk and requires stringent adaptation efforts. While initiated mitigation efforts are sufficient to reduce the risk of near-term droughts, global mean temperature increases drive up the risk of floods. Thus, optimal policy is characterised by stronger investments in flood-related adaptation. In both scenarios of emissions control, the benefits of investments in adaptation are apparent (Figure 3.14).

To sum up the above discussion, I calculate the welfare gains relative to business-as-usual policy for three alternative policy mixes: i) mitigation and adaptation; ii) adaptation and no mitigation; and iii) mitigation and no adaptation. The results are given in Figure 3.15, from which I derive two main policy conclusions. First, the policy that simultaneously addresses both a reduction of the risk (mitigation) and a reduction in vulnerability (adaptation) gives greater welfare gains. Second and most important, adaptation appears to be of greater impor-

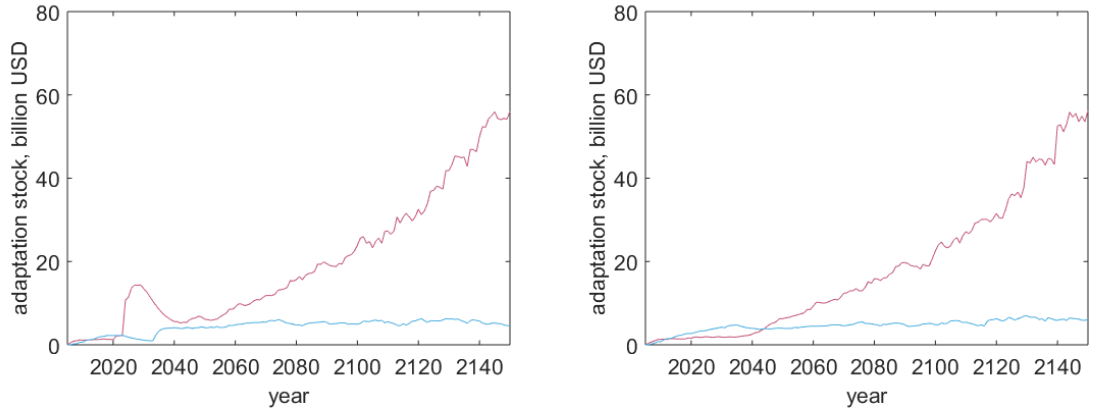

(a) No mitigation (b) Mitigation

Fig. 3.13 Evolution of adaptative capital stocks $K_t^{drought,adapt}$ (red line) and $K_t^{flood,adapt}$ (blue line) under alternative emissions control policies

tance than mitigation. This result is driven by the limited success of mitigation in reducing the risk, which in turn is a consequence of the problem often referred to as "the tragedy of global commons"[23]. The incremental cost of each individual region to increase emissions control exceeds the benefit. The rational decision is then to continue emitting. As a result of inter-regionally uncoordinated emissions, the so-called natural capital is degraded. That is, individual region's rationality leads to collective irrationality. India's ability to reduce the future occurence of ISM-rainfall extremes is constrained by the actions of the rest of the world. Benefits from actions on adaptation, in contrast, are enjoyed locally. Therefore, from the perspective of welfare gains, our results suggest the need to implement adaptation strategies.

Lastly, I finish on a note of caution. I see this paper as a first attempt to balance the benefits and costs of adaptation measures in India. In this regard, inevitably the study would have benefited from a more disaggregated setup including a greater number of adaptation strategies. However, due to the limitation of existing data, this study concentrates on highly aggregated abatement policies. In time such adaptation data may be forthcoming therefore allowing more important analyses of even greater benefit to the Indian policymakers.

[23] See Friedman (1971) for the economics of the common pool.

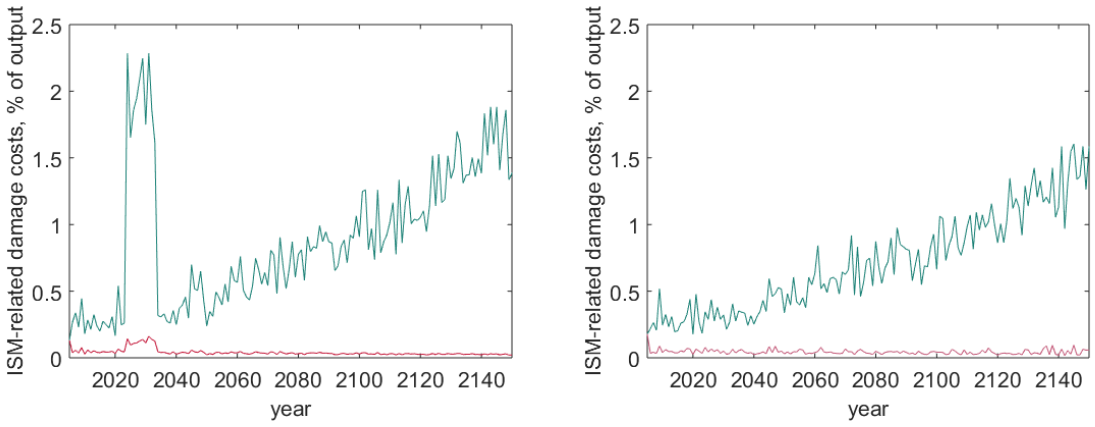

(a) No mitigation (b) Mitigation

Fig. 3.14 ISM rainfall-related damage costs with adaptation (red line) and without adaptation (green line) under alternative emissions control policies

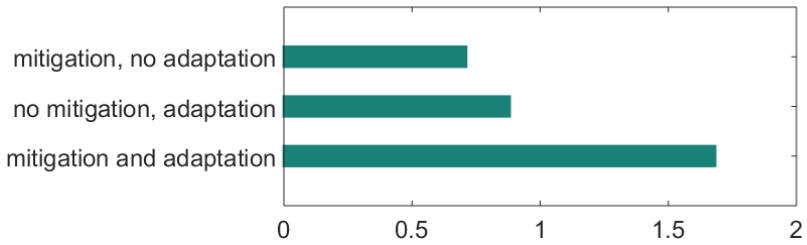

Fig. 3.15 Welfare gains for alternative emissions control and adaptation policies: percentage change relative to the business-as-usual scenario

3.5 Conclusions

It is now widely recognised that developing countries are particularly vulnerable to climate change. Yet, the question remains: what is the optimal response to potential future threats posed by a changing climate. Put differently, what is the relative importance of adaptation efforts? To answer this question one needs to evaluate the associated economic risk. The economic risks vary with region-specific climate conditions and GDP exposure to climate change. Hence, development of adaptation strategies requires a better understanding of the region-specific risks. The present study focuses on India's adaptation strategies in view of a projected risk of increased frequency of the ISM rainfall extremes under anthropogenic interference. Alteration of the Indian summer monsoon (ISM) rainfall variability is considered to be among the most significant potential impacts of climate change on India (e.g. Panda [29]).

The modelling framework in the present research is characterised by the integrated adaptation–

mitigation view, regional detail for impacts and adaptation strategies, intertemporal decision-making, and connection with empirical work on the impacts and adaptation costs. It advances on previous studies which: i) draw upon isolated treatment of adaptation (e.g. Fankhauser et al. [8]), ii) are static; iii) employ a global modelling framework (e.g. Bretschger and Valente [4], Millner and Dietz [25], de Bruin et al. [6]); and iv) employ a highly aggregated damage function (e.g. Bosello et. al.). The integrated adaptation–mitigation view is essential for two reasons. First, the monsoon rainfall–related risk is attributed to both the extent of climate change and India's GDP exposure to floods and droughts and therefore can be moderated through both mitigation and adaptation. Second, the two policy substitutes – mitigation and adaptation – compete for investment.

In line with the literature (e.g. de Bruin et al. [6]), I find that complementing mitigation with adaptation has a positive effect on regional welfare and that benefits of adaptation only, exceed those of mitigation only. In fact, adaptation is already a powerful tool to reduce adverse effects in the short-term. Interestingly, in contrasting scenarios with and without adaptation, results suggest that in the presence of adaptation, India initiates increased (although, slight) mitigation efforts. This increase is attributed to the following reasons. By decreasing the GDP exposure to the ISM rainfall events, adaptation decreases the risks that are locked-in. The locked-in effects occur due to India's limited ability to reduce the occurrence of the extremes, i.e. combat climate change without the stringent mitigation efforts initiated by the rest of the world. Thereby, adaptation acts to increase the output net damage costs available for investment in mitigation.

The potential future extensions to the model include: i) distinction between the three types of adaptation: market adjustments, protective/defensive expenditures and adaptive/coping expenditures; ii) explicit treatment of uncertainty; and iii) representation of induced innovation in adaptation-related technologies. These would advance the model to satisfy five characteristics of the ideal integrated assessment model focusing on climate impacts and adaptation as identified by Fisher-Vanden et al. [10].

Appendices

3 A Time-varying and Region-specific Model Parameters

Table 3.A.1 List of region-specific and/or time-varying parameters.

Parameter	Description	Equation
$N_{j,t}$	Population	3.2.2
$\beta^c_{1,j}$, $\beta^c_{2,j}$,$\beta^c_{3,j}$	Temperature-induced damage function coeff.	3.2.4
$r_{j,t}$	Urbanization	3.2.5
PD_j	Population density	3.2.5
$\psi_{j,t}$	Technological efficiency	3.2.6
$\alpha^c_{j,t}$, α^a_t	Abatement cost coefficients	3.2.9
$\gamma_{1,j}$, $\gamma_{2,j}$	Damage function coefficients	3.2.11 and 3.2.12
$\tau_{0,j}$, τ^c_j, $\tau^a_{1,j}$, $\tau^a_{2,j}$, $\tau^a_{3,j}$	Temperature equation coeff.	3.2.19
$\sigma^{cc}_{j,t}$, $\sigma^{ac}_{j,t}$, $\sigma^{aa}_{j,t}$	Emissions intensities	3.2.17
w_j	Region's share of global landmass	3.B.1a

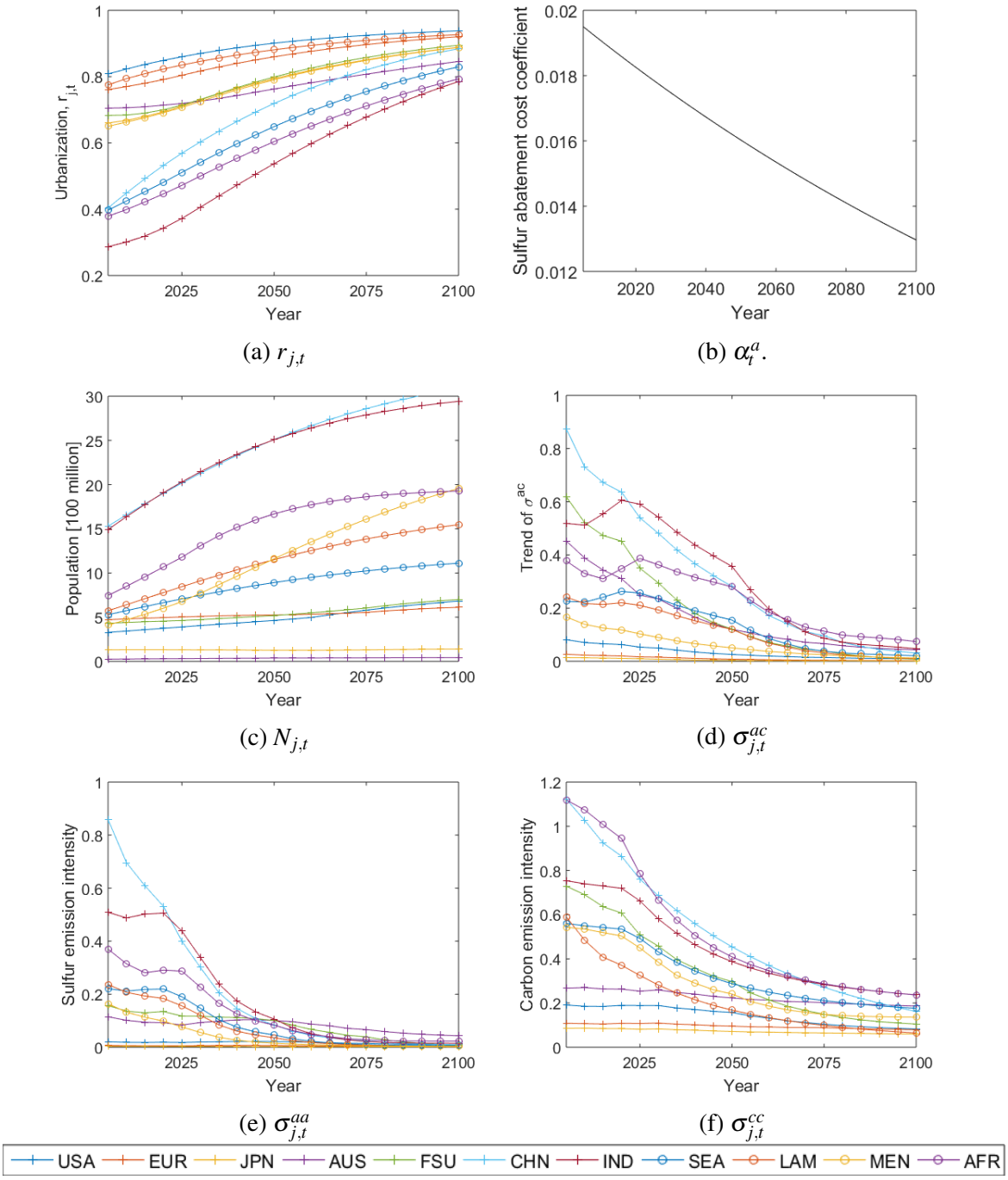

(a) $r_{j,t}$ (b) α_t^a.

(c) $N_{j,t}$ (d) $\sigma_{j,t}^{ac}$

(e) $\sigma_{j,t}^{aa}$ (f) $\sigma_{j,t}^{cc}$

Fig. 3.A.1 Time-varying parameters I

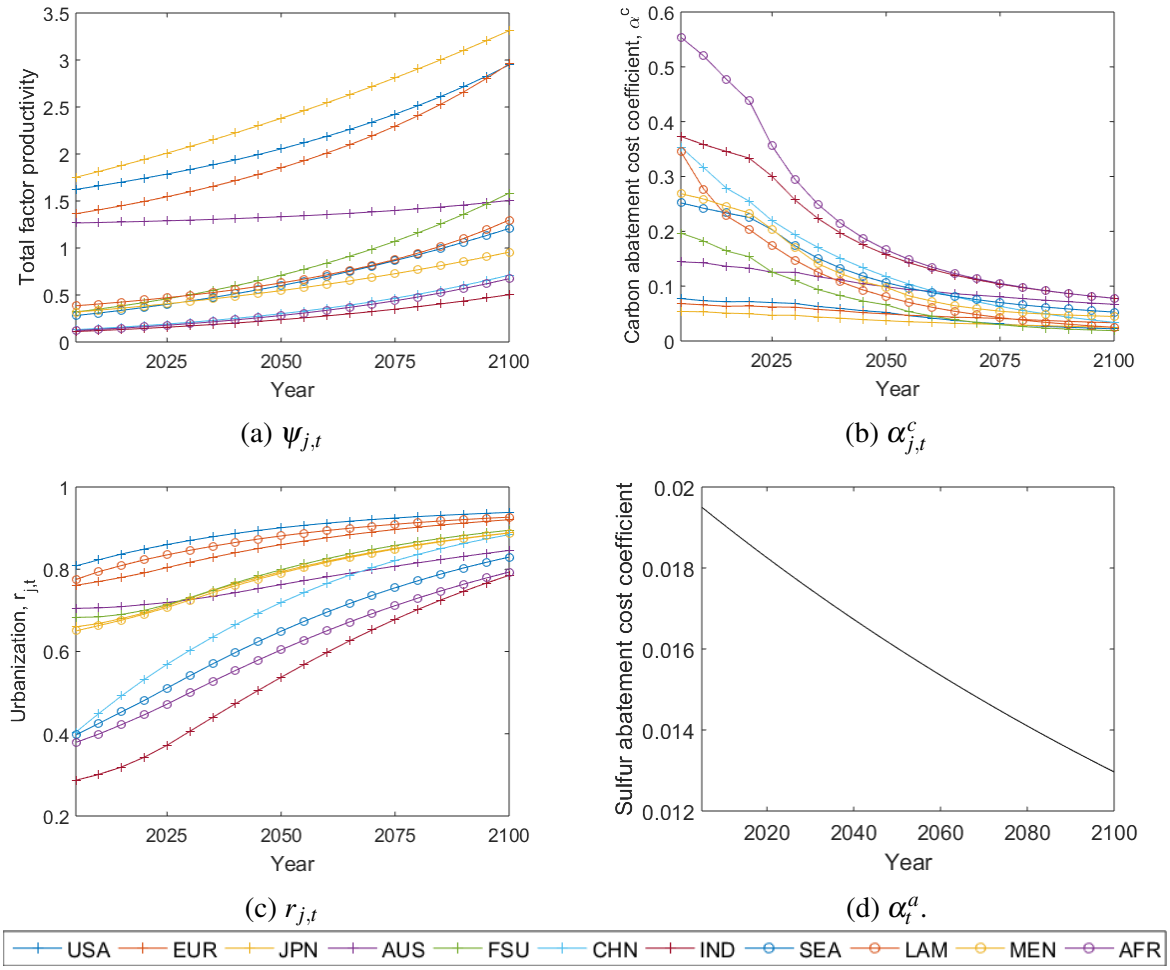

(a) $\psi_{j,t}$ (b) $\alpha^c_{j,t}$

(c) $r_{j,t}$ (d) α^a_t.

Fig. 3.A.2 Time-varying parameters II

Table 3.A.2 Region-specific parameters.

Parameter	USA	EUR	JPN	AUS	FSU	CHN	IND	SEA	LAM	MEN	AFR
$\beta^c_{1,j}$	0.009	0.012	0.004	0.004	0.020	0.054	0.092	0.033	0.013	0.007	0.058
$\beta^c_{2,j}10^3$	0.000	-0.007	-0.003	-0.003	-0.011	0.239	5.000	0.709	0.022	0.260	4.000
$\beta^c_{3,j}$	1.000	0.998	1.000	1.000	1.000	0.946	0.601	0.664	0.846	1.051	1.233
$\tau_{0,j}$	-4.34	-6.20	-3.538	-2.971	-6.767	-3.480	-3.9	-3.723	-3.255	-4.42	-4.15
τ^c_j	0.696	0.978	0.555	0.468	1.077	0.572	0.619	0.588	0.522	0.698	0.656
$\tau^a_{1,j}$	-0.03	-0.031	-0.031	-0.031	-0.031	-0.031	-0.031	-0.031	-0.031	-0.03	-0.031
$\tau^a_{2,j}$	-0.10	-0.083	-0.003	-0.006	-0.175	-0.08	-0.020	-0.010	-0.035	-0.02	-0.035
$\tau^a_{3,j}$	1.352	1.651	37.52	21.89	0.786	1.644	6.668	13.498	3.846	6.103	3.925
w_j in %	14.46	3.57	0.28	6.34	17.75	10.31	2.18	3.25	16.66	6.54	18.64
$\gamma_{1,j}10^3$	0.005	-0.07	-0.154	-1.199	0.020	0.671	3.311	1.458	-0.557	1.900	2.415
$\gamma_{2,j}10^3$	1.409	1.558	1.568	1.418	1.139	1.222	1.520	1.663	1.205	1.455	1.828
$\frac{PD_{j,t}}{80}$	3.624	7.853	13.56	5.510	7.837	21.00	19.63	21.94	8.412	11.99	16.8

3 B The Inter-annual ISM-rainfall Variability

Here, I shed more light on the processes that drive changes in the ISM rainfall under anthropogenic interference, and define the economic risk illustrated in Figure 3.12. To do so, I present the evolution of selected climate variables over time for two alternative policies: mitigation (Nash equilibrium solution) and no mitigation efforts (business-as-usual). Both policies are characterised by the absence of adaptation.

Global mitigation efforts in Nash equilibrium lead to lower global mean temperature increase relative to the business-as-usual policy (Figure 3.B.1a). Sulfur emissions reduction is a result of India's climate policy and application of flue-gas desulphurization techniques i.e. μ_t^c and μ_t^a (Figure 3.B.1b). Note, certain level of sulfur emissions control is already assumed in the A2-ASF scenario. Specifically, India's sulfur emissions peak around the year 2030 in the business-as-usual policy. Global warming is accompained by i) an increase in daily rainfall intensity (Figure 3.B.1c, dashed lines); ii) weakening of sea level pressure gradient over the region NINO3.4 (Figure 3.B.1c, solid lines); and iii) shift of the critical albedo towards higher values (Figure 3.B.1d, dashed lines). Sulfur emissions form aerosols in the atmosphere. In case of the business-as-usual policy, elevated aerosols concentration over the land increases albedo to the level above its critical value (Figure 3.B.1d). Hence, abrupt decrease in rainfall probability during monsoon onset followed by severe deficiency of seasonal mean ISM rainfall (Figure 3.B.1e and 3.B.1f). Over time, sulfur intensity of production decreases and thus albedo decreases accordingly. In addition, critical albedo shifts with CO_2 towards higher values, widening the gap between actual and critical albedo. Emissions control in Nash equilibrium suffice to prevent transgressing the critical albedo value and thereby limit the risk of near-term droughts. However, in both scenarios the mitigation is not sufficient to limit the temperature increase. The associated changes in the external forcing – weakening of mean sea level pressure gradient – influence rainfall probability during onset period (Figures 3.B.1c and 3.B.1e). Low probability of rainfall during the monsoon onset, robust with respect to alternative weather conditions, translates in decreasing values of seasonal mean rainfall (Figure 3.B.1f).

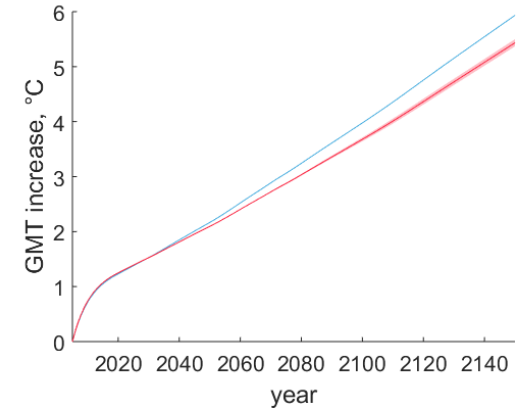

(a) Global mean temperature increase

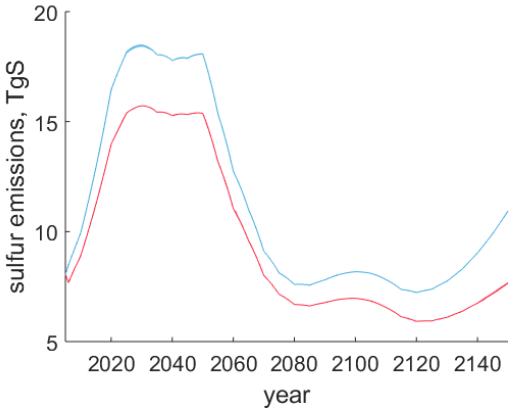

(b) India's sulfur emissions

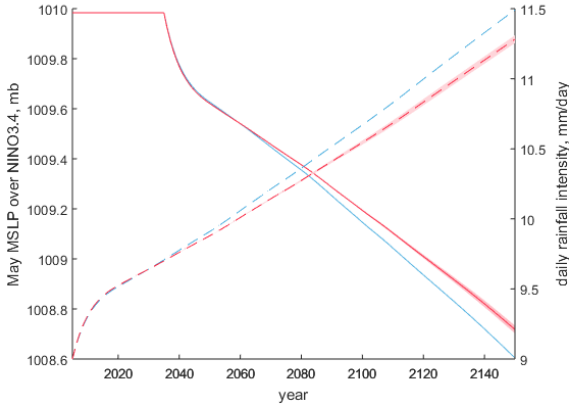

(c) May MSLP over NINO3.4 (left axis, solid lines) and daily rainfall intensity $\bar{P}_t^{wet}$, mm/day (right axis, dashed lines)

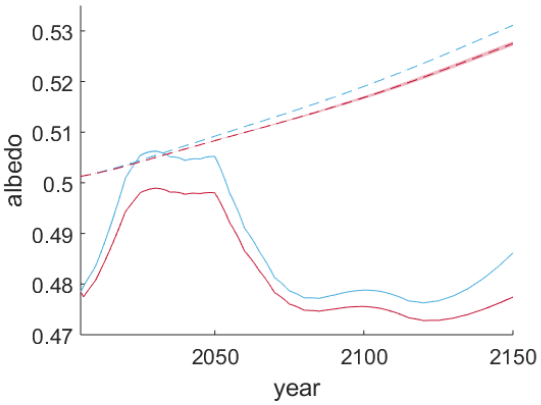

(d) Critical albedo $A_t^{pl,crit}$ (dashed line) and current albedo A_t^{pl} (solid line)

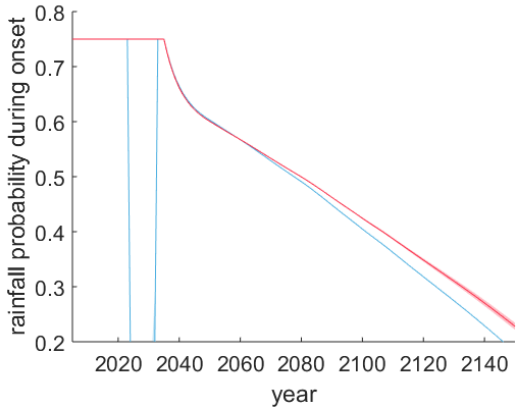

(e) Rainfall probability during monsoon onset

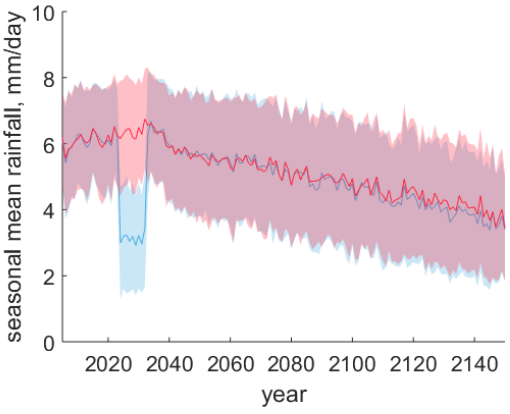

(f) Seasonal mean ISM rainfall $\bar{P}_t$, mm/day

Fig. 3.B.1 Evolution of selected climate variables under mitigation (red) and no-mitigation (blue) policies.

References

[1] Agrawala, S., Bosello, F., Carraro, C., de Cian, E., Lanzi, E., 2011. Adapting to climate change: Costs, benefits, and modelling approaches. International Review of Environmental and Resource Economics 5 (3), 245–284. URL http://dx.doi.org/10.1561/101.00000043

[2] Bahn, O., Leach, A., 2008. The secondary benefits of climate change mitigation: an overlapping generations approach. Computational Management Science 5 (3), 233–257.

[3] Belaia, M., Glanemann, N., 2017. Can india prevent summer monsoon extremes? An integrated assessment of climate change and environmental policies. Chapter 2.

[4] Bretschger, L., Valente, S., 2011. Climate change and uneven development. The Scandinavian Journal of Economics 113 (4), 825–845. URL http://dx.doi.org/10.1111/j.1467-9442.2011.01676.x

[5] Center for Science and Environment, 2015.

[6] de Bruin, K. C., Dellink, R. B., Tol, R. S. J., 2009. Ad-dice: an implementation of adaptation in the dice model. Climatic Change 95 (1), 63–81. URL http://dx.doi.org/10.1007/s10584-008-9535-5

[7] Dumas, P., Ha-Duong, M., 2013. Optimal growth with adaptation to climate change. Climatic Change 117 (4), 691–710. URL http://dx.doi.org/10.1007/s10584-012-0601-7

[8] Fankhauser, S., Smith, J. B., Tol, R. S., 1999. Weathering climate change: some simple rules to guide adaptation decisions. Ecological Economics 30 (1), 67 – 78. URL http://www.sciencedirect.com/science/article/pii/S0921800998001177

[9] Feichter, J., Kjellstrom, E., Rodhe, H., Dentener, F., Lelieveldi, J., Roelofs, G.-J., 1996. Simulation of the tropospheric sulfur cycle in a global climate model. Atmospheric Environment 30, 1693–1707.

[10] Fisher-Vanden, K., Wing, I. S., Lanzi, E., Popp, D., 2013. Modeling climate change feedbacks and adaptation responses: recent approaches and shortcomings. Climatic Change 117 (3), 481–495. URL http://EconPapers.repec.org/RePEc:spr:climat:v:117:y:2013:i:3:p:481-495

[11] Gadgil, S., Gadgil, S., 2006. The indian monsoon, gdp and agriculture. Economic and political weekly 41 (47).

[12] GAMS Development Corporation, 2013. General algebraic modeling system (gams) release 24.2.1. Washington, DC, USA.

[13] Halley, E., 1686. An historical account of the trade winds, and monsoons, observable in the seas between and near the tropicks, with an attempt to assign the phisical cause of the said winds. Philosophical Transactions 26, 153–168.

[14] IEA, I. E. A., 2015. India Energy Outlook: World Energy Outlook Special Report.

[15] Ikefuji, M., Magnus, J. R., Sakamoto, H., 2014. The effect of health benefits on climate change mitigation policies. Climatic Change 126 (1-2), 229–243.

[16] IPCC, 2014. IPCC Summary for policymakers. In: Climate Change 2014: Impacts, Adaptation, and Vulnerability. Part A: Global and Sectoral Aspects. Contribution of Working Group II to the Fifth Assessment Report of the Intergovernmental Panel on Climate ChIPCC. Cambridge University Press, Cambridge, United Kingdom and New York, NY, USA.

[17] Johns, T. C., Carnell, R. E., Crossley, J. F., Gregory, J. M., Mitchell, J. F. B., Senior, C. A., Tett, S. F. B., Wood, R. A., 1997. The second hadley centre coupled oceanatmosphere gcm: model description, spinup and validation. Climate Dynamics 13 (2), 103–134. URL http://dx.doi.org/10.1007/s003820050155

[18] lse, November 2015. India's approach to adaptation: A good start but lacks a strong long-term focus. Commentary. URL http://www.lse.ac.uk/GranthamInstitute/news/indias-approach-to-adaptation-a-good-start-but-lacks-a-strong-long-term-focus/

[19] Manne, A., Mendelsohn, R., Richels, R., 1995. MERGE : A model for evaluating regional and global effects of GHG reduction policies. Energy Policy 23 (1), 17–34.

[20] Margulis, S., Narain, U., 2010. The costs to developing countries of adapting to climate change : new methods and estimates - the global report of the economics of adaptation to climate change study. Tech. rep., Washington, DC: World Bank.

[21] Mas-Colell, A., Whinston, M., Green, J., 1995. Microeconomic Theory. Oxford University Press. URL http://EconPapers.repec.org/RePEc:oxp:obooks:9780195102680

[22] Matus, K., Yang, T., Paltsev, S., Reilly, J., Nam, K.-M., 2008. Toward integrated assessment of environmental change: air pollution health effects in the usa. Climatic Change 88 (1), 59–92. URL http://dx.doi.org/10.1007/s10584-006-9185-4

[23] McCarl, B. A., Meeraus, A., Eijk, P. V. D., Bussieck, M., Dirkse, S., Steacy, P., Nelissen, F., 2011. McCarl GAMS User Guide. GAMS Development Corporation.

[24] McMichael, A., Campbell-Lendrum, D., Kovats, S., Edwards, S., Wilkinson, P., Wilson, T., Nicholls, R., Hales, S., Tanser, F., Sueur, D., Schlesinger, M., Andronova, N., 2004. Comparative Quantification of Health Risks: Global and Regional Burden of Disease Due to Selected Major Risk Factors. World Health Organization, Geneva, Ch. Global climate change, pp. 1543–1649.

[25] Millner, A., Dietz, S., 006 2015. Adaptation to climate change and economic growth in developing countries. Environment and Development Economics 20 (3), 380–406. URL https://www.cambridge.org/core/article/div-class-title-adaptation-to-climate-change-and-economic-9DBF93B2C0535E2EF05088B2B88F6C84

[26] Nordhaus, W. D., Boyer, J., 2000. Warming the World: Economic Models of Global Warming. MIT Press, Cambridge Mass.

[27] OECD, 2012. Looking to 2060: Long-term global growth prospects. In: OECD Economic Policy Papers. OECD publishing.

[28] Olivier, J. G., Janssens-Maenhout, G., Muntean, M., Peters, J. A., 2016. Trends in global co2 emissions: 2016 report. Tech. rep., PBL Netherlands Environmental Assessment Agency.

[29] Panda, A., 2009. Assessing vulnerability to climate change in india. Economic and Political Weekly 44 (16), 105–107. URL http://www.jstor.org/stable/40279163

[30] Patt, A. G., van Vuuren, D. P., Berkhout, F., Aaheim, A., Hof, A. F., Isaac, M., Mechler, R., 2010. Adaptation in integrated assessment modeling: where do we stand? Climatic Change 99 (3), 383–402. URL http://dx.doi.org/10.1007/s10584-009-9687-y

[31] Sankovski, A., Barbour, W., Pepper, W., 2000. Quantification of the IS99 emission scenario storylines using the atmospheric stabilization framework.

Technological Forecasting and Social Change 63 (2–3), 263 – 287. URL http://www.sciencedirect.com/science/article/pii/S0040162599001006

[32] Schewe, J., Levermann, A., 2012. A statistically predictive model for future monsoon failure in india. Environmental Research Letters 7, 1–9.

[33] Smit, B., Burton, I., Klein, R., Street, R., 1999. The science of adaptation: A framework for assessment. Mitigation and Adaptation Strategies for Global Change 4 (3), 199–213. URL http://dx.doi.org/10.1023/A:1009652531101

[34] The World Bank, 2017. Employment in agriculture.

[35] The World Bank, 2017. Urban population.

[36] The World Bank, 2017. World bank national accounts data, and oecd national accounts data files. gdp per capita (current usd). URL http://data.worldbank.org/indicator/NY.GDP.PCAP.CD

[37] Tol, R. S., Fankhauser, S., 1998. On the representation of impact in integrated assessment models of climate change. Environmental Modeling and Assessment 3 (1), 63–74.

[38] UNFCC, 2017. The paris agreement. United Nations Framework Convention on Climate Change. URL http://unfccc.int/paris_agreement/items/9485.php

[39] United Nations, 2017. World Economic Situation and Prospects 2017. URL http://www.refworld.org/docid/587f35e24.html[accessed22February2017]

[40] Van Vuuren, D. P., Alfsen, K. H., 2006. Ppp versus mer: Searching for answers in a multi-dimensional debate. Climatic Change 75 (1), 47–57. URL http://dx.doi.org/10.1007/s10584-005-9045-7

[41] Vecchi, G. A., Soden, B. J., Wittenberg, A. T., Held, I. M., Leetmaa, A., Harrison, M. J., May 2006. Weakening of tropical pacific atmospheric circulation due to anthropogenic forcing. Nature 441 (7089), 73–76. URL http://dx.doi.org/10.1038/nature04744

[42] WRI, 2015. Aqueduct global flood analyzer. URL http://www.wri.org/floods

[43] Yatsenko, Y., Hritonenko, N., Brechet, T., 2014. Modeling of environmental adaptation versus pollution mitigation. Math. Model. Nat. Phenom. 9 (4), 227–237. URL http://dx.doi.org/10.1051/mmnp/20149414

[44] Zickfeld, K., 2004. Modeling large-scale singular climate events for integrated assessment. Ph.D. thesis, University Postdam.

[45] Zickfeld, K., Knopf, B., Petoukhov, V., Schellnhuber, H. J., 2005. Is the Indian summer monsoon stable against global change? Geophysical Research Letters 32 (15), n/a.

Acknowledgements

First and foremost, I would like to express my sincere and deep gratitude to my supervisor Michael Funke. He was exceptional in his support. I'm grateful to him for getting me seriously interested in the economics of climate change. This would not have been possible without his dedication, his excellent supervision and encouragement.

I also want to thank Hartmut Graßl and Uwe Schneider for continuously providing help and excellent advice throughout the work on this thesis.

My Ph.D. benefited from fruitful discussions with Frank Ackerman, Irina Bakalova, Victor Brovkin, Manita Chouksey, Rob Dellink, Johannes Emmerling, Rohit Ghosh, Hermann Held, Chao Li, Mohammad Mohammadi, Elnaz Roshan, Jacob Schewe, and Alessandro Tavoni.

I also received fantastic support from the International Max Planck Research School on Earth System Modelling. A special thank you to Antje Weitz and Cornelia Kampmann for making sure that we can focus on the research.

My friends and co-Ph.D. students and colleagues at the University of Hamburg and the International Max Planck Research School on Earth System Modelling provided the much needed change from academic work. I would like to acknowledge Antonia Arsova, Bhuiyan S. M. Ebna Hai, Boris Blagov, Jörg Burdanowitz, Eduardo Chamarro, Xi Chen, Yu-Fu Chen, Sercan Eraslan, Maria Gadova, Nicole Glanemann, Hasin T. Tasfia, Julius Loermann, Ivan Lozev, Peter V. Mihailovsky, Irina Petrova, Katja Seizinger, Martin Tschöke, Adrian Wende, and Zhou Siwen.

Finally, but most importantly, I want to thank my family for the support throughout the years of this thesis.